Technical Report Documentation Page

1. Report No.	2. Government Accession No.	3. Recipient's Catalog No.
FHWA/TX-91/1121-2F		

4. Title and Subtitle	5. Report Date
IDENTIFYING AND CORRECTING RUT-SUSCEPTIBLE ASPHALT MIXTURES	February, 1991
	6. Performing Organization Code
7. Author(s)	
Dario Perdomo and Joe W. Button	8. Performing Organization Report Code
	Research Report 1121-2F
9. Performing Organization Name and Address Texas Transportation Institute The Texas A&M University System College Station, TX 77843	10. Work Unit No. (TRAIS)
	11. Contract or Grant No.
12. Sponsoring Agency Name and Address Texas Department of Transportation, Transportation Planning Division P.O. Box 5051 Austin, Texas 78763	Study No. 2-8-87/91-1121
	13. Type of Report and Period Covered September 1987 Final - February 1991
15. Supplementary Notes Research performed in cooperation with DOT, FHWA. Research Study Title: Investigation of Rutting in Asphalt Concrete Pavements	14. Sponsoring Agency Code

16. Abstract

A field evaluation of Texas highway pavements was conducted to provide evidence that sand-size aggregate particles have a significant influence on rutting. A laboratory investigation was performed in order to (1) quantify the influence on resistance to rutting when rounded, smooth, sand-sized aggregate particles are replaced by rough, angular, porous particles while other aggregates and the total gradation remain unchanged, (2) evaluate the ability of certain test procedures to differentiate between rut-susceptible and rut-resistant mixtures, (3) develop a new rutting model for predicting pavement performance which incorporates characteristics of the aggregate, and (4) examine fractal dimension analysis as a method of quantifying aggregate angularity and surface texture.

Octahedral shear stress theory was employed to compare the rutting potential of asphalt concrete mixes containing low quality sand-size particles (rounded, smooth, non-absorptive) and high quality sand-size particles (rough, angular, absorptive). Five mixtures with varying amounts of the different aggregates were tested.

A state-of-the-art theoretical approach was developed in which hyperbolic equations are introduced to model the compressive creep and recovery compliances. The new compliance equations are further developed into a rutting prediction model. The aggregate's role in the permanent deformation behavior of the mixture is assessed by means of a novel parameter termed "p" value.

A new technique, known as fractal dimension analysis, offers a great deal of potential in providing a direct quantitative measure of aggregate angularity and surface texture which has heretofore been impossible.

A combination of the new theoretical approach, the long-term laboratory performance of the mix, and the octahedral shear stress analysis is recommended as the preferred approach to evaluate the influence of sand-sized aggregate particles on permanent deformation in asphalt concrete mixtures.

17. Key Words	18. Distribution Statement
Asphalt concrete pavements, rutting, mix design, rutting model, aggregate, permanent deformation.	No restrictions. This document is available to the public through the the National Technical Information Service, 5285 Port Royal Road, Springfield, Virginia 22161

19. Security Classif. (of this report)	20. Security Classif. (of this page)	21. No. of pages	22. Price
Unclassified	Unclassified	164	

Form DOT F 1700.7

IDENTIFYING AND CORRECTING RUT-SUSCEPTIBLE ASPHALT MIXTURES

by

Dario Perdomo
Research Assistant

and

Joe W. Button
Associate Research Engineer

Research Report 1121-2F
Research Study 2-8-87/91-1121

Sponsored by
Texas Department of Transportation
U.S. Department of Transportation
Federal Highway Administration

Texas Transportation Institute
Texas A&M University
College Station, Texas 77843

February, 1991

METRIC (SI*) CONVERSION FACTORS

APPROXIMATE CONVERSIONS TO SI UNITS

Symbol	When You Know	Multiply By	To Find	Symbol
LENGTH				
in	inches	2.54	centimetres	cm
ft	feet	0.3048	metres	m
yd	yards	0.914	metres	m
mi	miles	1.61	kilometres	km
AREA				
in^2	square inches	645.2	centimetres squared	cm^2
ft^2	square feet	0.0929	metres squared	m^2
yd^2	square yards	0.836	metres squared	m^2
mi^2	square miles	2.59	kilometres squared	km^2
ac	acres	0.395	hectares	ha
MASS (weight)				
oz	ounces	28.35	grams	g
lb	pounds	0.454	kilograms	kg
T	short tons (2000 lb)	0.907	megagrams	Mg
VOLUME				
fl oz	fluid ounces	29.57	millilitres	mL
gal	gallons	3.785	litres	L
ft^3	cubic feet	0.0328	metres cubed	m^3
yd^3	cubic yards	0.0765	metres cubed	m^3

NOTE: Volumes greater than 1000 L shall be shown in m^3.

TEMPERATURE (exact)

°F	Fahrenheit temperature	5/9 (after subtracting 32)	Celsius temperature	°C

APPROXIMATE CONVERSIONS TO SI UNITS

Symbol	When You Know	Multiply By	To Find	Symbol
LENGTH				
mm	millimetres	0.039	inches	in
m	metres	3.28	feet	ft
m	metres	1.09	yards	yd
km	kilometres	0.621	miles	mi
AREA				
mm^2	millimetres squared	0.0016	square inches	in^2
m^2	metres squared	10.764	square feet	ft^2
km^2	kilometres squared	0.39	square miles	mi^2
ha	hectores (10 000 m^2)	2.53	acres	ac
MASS (weight)				
g	grams	0.0353	ounces	oz
kg	kilograms	2.205	pounds	lb
Mg	megagrams (1 000 kg)	1.103	short tons	T
VOLUME				
mL	millilitres	0.034	fluid ounces	fl oz
L	litres	0.264	gallons	gal
m^3	metres cubed	35.315	cubic feet	ft^3
m^3	metres cubed	1.308	cubic yards	yd^3

TEMPERATURE (exact)

°C	Celsius temperature	9/5 (then add 32)	Fahrenheit temperature	°F

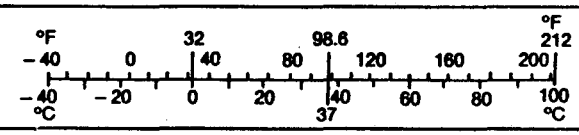

These factors conform to the requirement of FHWA Order 5190.1A.

* SI is the symbol for the International System of Measurements

IMPLEMENTATION STATEMENT

Findings from this field and laboratory investigation of rutting in asphalt concrete mixtures indicates that new laboratory procedures to test and analyze mixtures and new methods to predict rutting are warranted. An unconfined uniaxial compression and recovery test was used to provide data necessary to compute a novel term called "p" value. A hyperbolic theoretical model was developed that provides a near perfect predictor of actual creep and recovery performance of asphalt mixtures. A new permanent deformation prediction model was developed which is believed to be much more representative of actual field performance than other existing models. It is based on mixture properties; whereas, most existing models are based on binder properties alone. Study 455 has incorporated this model into the Texas Flexible Pavement System to provide for more realistic prediction of rutting from laboratory tests.

Fractal dimension analysis proved to be a powerful yet very practical technique for objectively measuring the particle shape and surface texture of coarse aggregates. This finding is significant because, heretofore, there has been no laboratory procedure to directly measure aggregate shape or surface texture. This method needs to be further developed into a useful analytical tool. A number of techniques are presented herein that can be used to improve fractal analysis of both coarse and fine aggregates.

To minimize excessive rutting under heavy traffic, the use of natural sand with rounded particle shapes and smooth surface textures in asphalt concrete mixtures should be limited to an amount not greater than 10 percent to 15 percent depending on the quality of the sand and the character of the traffic.

Density is the governing factor during construction of asphalt concrete pavements. On occasion, it appears that the asphalt content is allowed to exceed the optimum design value in order to achieve the required density. This practice should be exercised with extreme caution.

Fine-grained, dense-graded (near the maximum density gradation) mixtures that contain high amounts of natural, rounded sand and low voids in the mineral aggregate (VMA) are very sensitive to binder content. A slight increase in binder content above the optimum value will cause the mix to become tender, unstable, and subject to rutting. A minimum VMA specification should, therefore, be implemented. Data is available to

estimate an appropriate minimum VMA for the various Texas Department of Transportation (Tx DOT) aggregate gradations when the gyratory shear compactor is used to prepare specimens.

DISCLAIMER

The contents of this report reflect the views of the authors who are responsible for the opinions, findings, and conclusions presented herein. The contents do not necessarily reflect the official views or policies of the Federal Highway Administration. This report does not constitute a standard, specification, or regulation,

There is no invention or discovery conceived or first actually reduced to practice in the course of or under this contract, including any art, method, process, machine, manufacture, design or composition of matter, or any new and useful improvement thereof, or any variety of plant which is or may be patentable under the patent laws of the United States of America or any foreign country.

TABLE OF CONTENTS

TABLE OF CONTENTS (continued)

LIST OF FIGURES

LIST OF FIGURES (continued)

LIST OF FIGURES (continued)

LIST OF FIGURES (continued)

LIST OF FIGURES (continued)

LIST OF FIGURES (continued)

LIST OF TABLES

CHAPTER I
INTRODUCTION

Many roadways are prematurely experiencing high levels of rutting due to steady increases in magnitudes of loading and volume of traffic. This brings into question the ability of existing materials specifications to prevent these permanent deformation failures from occurring.

Background

Sand-size aggregate particles play a very important role in the rutting performance of asphalt concrete mixtures. Many advantages of using crushed sand-size particles in place of natural (uncrushed particles) in asphalt concrete are well known and have been documented in the literature (1, 2, 3, 4, 5, 6, 7).

In asphalt concrete mixtures, aggregate particles usually comprise between 90 percent and 95 percent by weight of the total mix. Furthermore, aggregate particles are (or should be) primarily responsible for the load-carrying capacity of the asphalt mixture. Therefore, considerable attention has been given to the physical characteristics of the aggregate.

A review of current knowledge (8, 9, 10, 11, 12, 13) concerning the influence of sand-size particles on rutting in asphalt pavements reveals that the major factors involved are:

1. Particle shape,
2. Particle surface texture, and
3. Percentage of natural sand allowed in the mix.

Rounded, non-porous, uncrushed particles are more susceptible to rutting while angular, slightly porous, crushed particles provide mixtures with greater resistance to rutting. Having particularly high percentages of rounded, porous, uncrushed particles in a mixture accentuates the permanent deformation problem.

Most mixtures contain a certain percentage of naturally occurring sand. This sand adds workability to the mixture and, due to its wide-spread availability, it is economical to use. However, natural sands are generally rounded and non-porous due to their depositional history and mineralogy. Finding a threshold percentage for the maximum amount of natural sand that should be allowed in a rut-resistant mixture was one of the objectives of this research study.

Review of current research concerning laboratory evaluation of permanent deformation potential in a mixture has revealed that the most commonly used test configurations are uniaxial and triaxial, both employing either static or cyclic loading patterns (14, 15, 16). The triaxial cyclic test seems to be the best approach since it can more closely reproduce the in situ pavement conditions, including general stress states.

In the case of the influence of aggregate on rutting, laboratory tests have been used only to compare different asphalt mixtures in order to establish relative performance. A breakthrough in this research study was the development of a theoretical approach, supported by a specific laboratory test, which analyzes the influence of sand-size particles on permanent deformation potential. This theoretical approach uses a hyperbolic model to fit the creep and recovery compliances.

Purpose and Scope

The primary objective of this research study was to investigate the influence that sand-size aggregate particles have on permanent deformation in asphalt concrete mixtures through a comprehensive field and laboatory evaluation. An allied objective of equal importance was to develop the best methodology by which to evaluate aggregate effects on deformation potential. Several procedures were evaluated based on their ability to establish and assess the role of the aggregate in rutting potential. The areas investigated include the hyperbolic creep and recovery models, octahedral shear stress theory, cyclic permanent deformation, and image processing analysis.

Organization

This report is organized into eight chapters and four appendices. This chapter (Chapter I) is an introduction to the problem with a brief discussion of the background information related to the influence of natural sand on permanent deformation and a description of the objectives.

Chapter II discusses findings from the literature review, in which a survey of related information was conducted to determine possible laboratory tests and theoretical approaches that can analyze the influence of aggregate on permanent deformation.

Chapter III presents the field evaluation. This chapter deals with the

analysis of selected pavements that were undergoing various levels of deformation distress, and some that were free of deformation related distress. In the analysis, laboratory testing techniques were used on cores obtained from various pavements in order to isolate the primary contributors to permanent deformation. The effect of sand-size particles on field performance was carefully analyzed in this chapter.

Chapter IV presents the comprehensive laboratory investigation. The test program, consisting of two phases, was conducted to: (1) quantify the influence on resistance to rutting when natural sand is replaced or partially replaced by manufactured sand (crushed limestone), (2) evaluate the ability of selected test procedures to identify good rutting resistant mixtures, and (3) evaluate the sensitivity of mixtures to asphalt content, air void content, and temperature. The test procedures included in the first phase are: indirect tension, Hveem stability, Marshall stability, unconfined direct compression, long-term static creep, and long-term cyclic creep. The second phase included the evaluation of the triaxial cyclic test. Conclusions obtained from the analysis and comparison of the results are also discussed in this chapter.

Chapter V explains the state-of-the-art theoretical approach, in which new hyperbolic models are introduced for both the compressive creep and recovery compliances. In these models, the aggregate's role in the permanent deformation potential of a mixture is assessed by means of the "p-value". The new compliance equations are further developed into a rutting model.

Chapter VI introduces the application of an image processing technique called fractal analysis for the quantification of texture of aggregate particles. The texture of both types of aggregate particles used in the laboratory program (Chapter IV) is characterized using this method. Results from the analysis and methods to improve the process are discussed.

Chapter VII discusses the octahedral shear stress approach for evaluating the potential to rutting of an asphalt concrete mix. In particular, typical pavement structures containing natural sand are analyzed and compared using this method.

Chapter VIII examines several factors regarding Texas DOT specifications, test methods, and construction practices that may influence rutting.

Finally, Chapter IX presents conclusions concerning the influence of sand-size particles on rutting potential and recommendations for how to evaluate rutting potential using state-of-the-art test procedures and analysis techniques.

This report includes four appendices. Appendix A includes some of the sample preparation and testing techniques. Appendix B presents results from the comprehensive laboratory test program. Appendix C presents results from the state-of-the-art theoretical approach.

Importance of Work

The findings of this research study should result in a better and more comprehensive understanding of the influence of sand-size aggregate particles on permanent deformation potential since it covers both field and laboratory performance of the asphalt mixtures. The new theory will make contributions toward visualizing and understanding how important it is to consider aggregate characteristics in theoretical predictions of permanent deformation in asphalt concrete pavements.

CHAPTER II
LITERATURE REVIEW

Aggregate particles comprise between 90 percent and 95 percent by total weight of an asphalt concrete mixture. In Texas, sand-size particles, in particular, often comprise around 40 percent by total weight of the mixture. Considerable attention has been given to the physical characteristics of the aggregate since it is the major factor responsible for the load-carrying capacity of an asphalt concrete mixture. Advantages of using crushed sand-size particles and major physical factors of sand-size particles affecting rutting have already been mentioned in the introduction of the report. This literature review concentrates on testing techniques and theoretical approaches that possess the ability to analyze the influence of aggregate on rutting. The Study 1121 interim report includes a comprehensive literature review of the major causes of rutting and solutions to reduce rutting, many of which are now being adopted by several state highway agencies.

Permanent Deformation Testing

Lai and Anderson (17) agreed on using periodic loading tests when evaluating permanent deformation in asphalt concrete pavements primarily because they simulate actual pavement loading patterns.

Freeman and Carpenter (18) discussed the use of the triaxial compressive test, using a constant rate of strain, and analyzed the results by means of octahedral shear stress theory. Ameri-Gaznon and Little (19) further developed the concept of the octahedral shear stress ratio and analyzed several pavement structures. The octahedral shear stress ratio was used as a tool to estimate the rutting potential of the mixture.

Brown and Bell (20) used the triaxial test because the stress conditions on the axis of symmetry of a wheel load can be modeled with this test, except for those in the tension zone of the asphalt concrete layer.

Monismith and Tayelabi (16) suggested the creep test as a useful tool in the prediction of rutting potential and described a modified testing methodology based on their experience. They also used the triaxial repeated loading test, where a cyclic haversine load was applied to the specimens under different confining pressures.

In general, the creep and cyclic loading tests, with and without confining pressure, appear to be the most accepted laboratory tests used in the analysis of permanent deformation. The shear strength test (used in the analysis of octahedral shear stress) is also becoming an accepted procedure for evaluating rutting potential.

This research study evaluated a comprehensive range of laboratory tests, including all the tests mentioned above. The best procedures for evaluating the influence of sand-size aggregate particles on permanent deformation were then selected based on their ability to distinguish performance between different mixtures and estimate rutting potential.

Theoretical Approaches

Among the wide range of theoretical analyses reviewed (14, 17, 18, 19, 21, 22, 23, 24, 25), none of them included the aggregate's physical characteristics as a contributing factor in the prediction of permanent deformation or evaluation of rutting potential. A major accomplishment of this research study was the development of a model for predicting rutting that considers the contribution of the aggregate. Octahedral shear stress theory was also used to evaluate rutting potential because it was found to be a unique and novel technique.

CHAPTER III
FIELD INVESTIGATION

The field investigation (26) was performed in order to provide a better understanding of the primary contributors to rutting, to quantify them, and to study the influence of sand-size particles on rutting in real pavements.

Field sites were confined to the State of Texas and limited to pavements that were no more than two years old (with one exception) and experiencing rutting greater than 0.4 inches. Rutted and unrutted (or less rutted) pavements composed of the same materials (whenever possible) were studied.

Description of Test Pavements

Rutting pavements in Districts 4, 8, 10, 11, and 17 were selected for investigation (Figure 3.1). Pavements were selected only if rutting appeared to be occurring in the asphalt concrete surface layer; that is, rutting in an untreated base or subgrade was not considered in the study. A visual condition survey of each pavement was conducted and rut depths were measured. Where possible, mixture design data, typical sections, and a sampling of daily construction reports were obtained. A summary of the test pavements is given in Table 3.1. Two sets of cores were collected from sites near Sweetwater, Fairfield, and Centerville, which represented high and low levels of rutting (Table 3.1). All cores were collected from the travel lanes. Environmental data is included in Table 3.2. A total of ten sites (including rutted and unrutted pavements) were analyzed.

Sampling and Testing Program

Five cores distributed across the pavement in and between the wheelpaths (Figure 3.2) were drilled in order to ascertain the profile of the transverse cross section of the pavement. Cores were drilled in accordance with this scheme at each of five different locations at any particular field site. The cores were taken to the laboratory where the surface layer portions were carefully separated by sawing and later tested in accordance with Figure 3.3.

In some instances, the surface layer of the asphalt concrete pavement was found to be less than 1-inch thick. Mixture testing (Figure 3.3) of these cores was not performed due to the unreliability in test results on

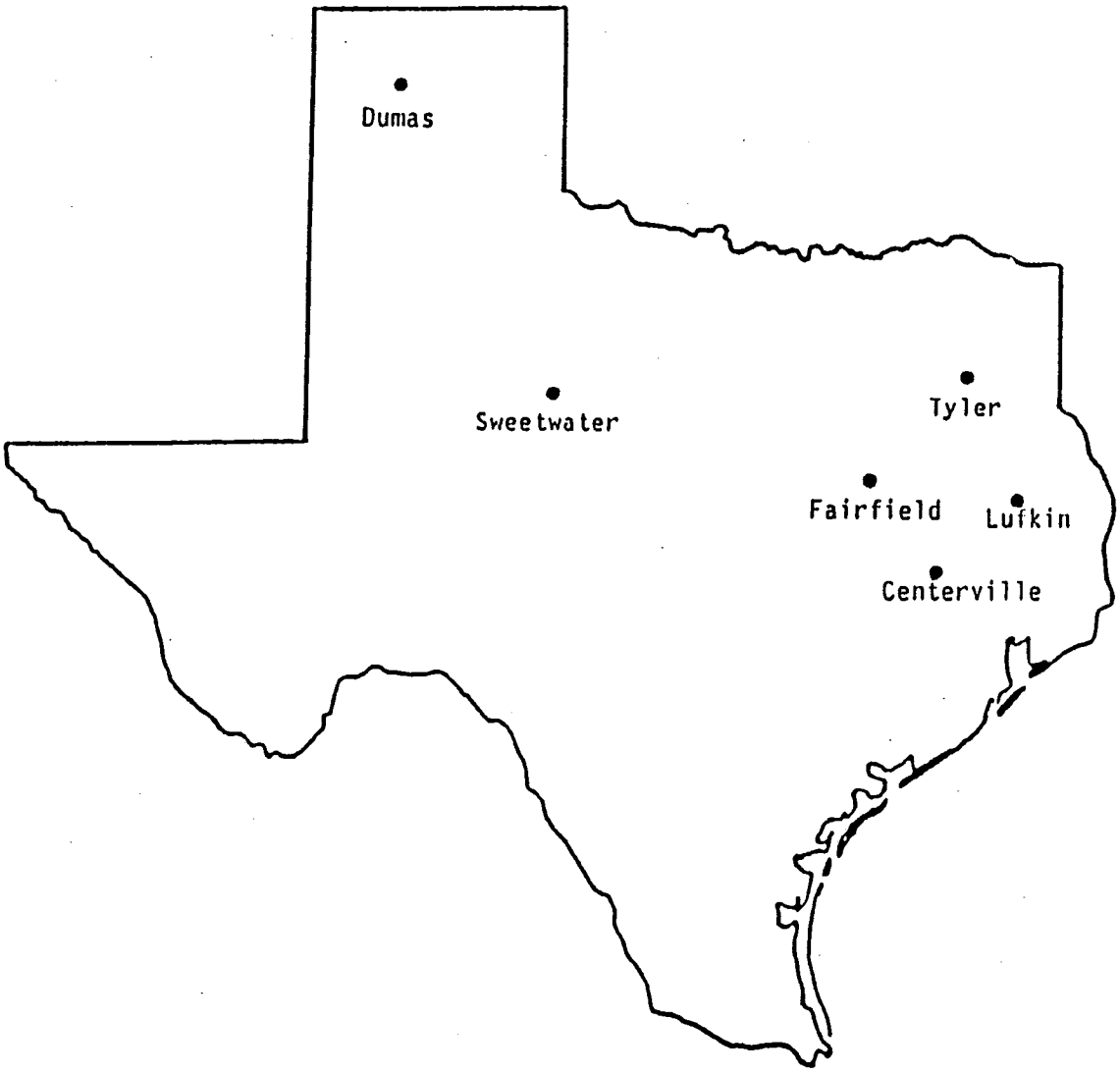

Figure 3.1. Location of field test sites for rutting pavements.

Table 3.1. Summary of rutting pavements evaluated.

	Location					
	Sweetwater	Fairfield	Centerville	Tyler	Lufkin	Dumas
District No.	8	17	17	10	11	4
Highway No.	IH 20	IH 45	IH 45	IH 20	US 59	US 287
Existing Pavement						
Layer 1 (Top)	2 1/2" Ty D	3/4" Ty D	3/4" Ty D	1 1/2" Ty D	3" Ty D	
Layer 2	8 1/2" Recycle	3.75"Ty C	4.5" Ty C	2" Ty B	Surf Trt.	
Layer 3	Lime Trt Base	Asp. Rub.	Asp. Rub.	Fabric	Conc. Pvt.	
Layer 4	Subgrade	8" CRCP	8" CRCP	8" CRCP	Subgrade	
Date of last const.	Sept 84	Sept 85	Oct 85	July 81	Nov 85	July 85
Date Cored	Mar 87	April 87	April 87	Sept 87	Dec 87	Nov 86
Rut Depth, in. (site 1)	0.72	0.22	0.55	0.73	0.75	0.41
Rut Depth, in. (site 2)	0.21	0.52	0.16	-	-	-

Table 3.2. Climatological summary for rutting pavement test sites.

Item	Sweetwater	Fairfield/ Centerville	Dumas	Lufkin	Tyler
Climate	Semiarid, mild winter, lower humidity and hot summers	Subtropical with mild winter and hot humid summers	Short but severe winters, warm summer days, cool nights, low humidity	Humid, mild winters and hot summers	Humid, mild winters and hot summers
Temperature(°F)					
Mean*/Record Max	95/111	96/111	92/109	94/108	94/108
Mean*/Record Min	31/-9	35/-3	19/-18	38/-2	33/2
No. Days/Year 20° and above	96	101	72	103	83
No. Days/Year 32° and below	55	45	129	35	57
Frost Penetration, in.	3	<3	>3	<3	<3
Precipitation(in.)					
Mean Annual Precip.	23	39	19	42	43
Mean Annual Ice/Snow	0.8	0.8	16.2	0.8	1.9
Mean Heating °days	2620	2150	3750	1930	2330

*Mean Daily minimum and maximum temperatures for a given month.

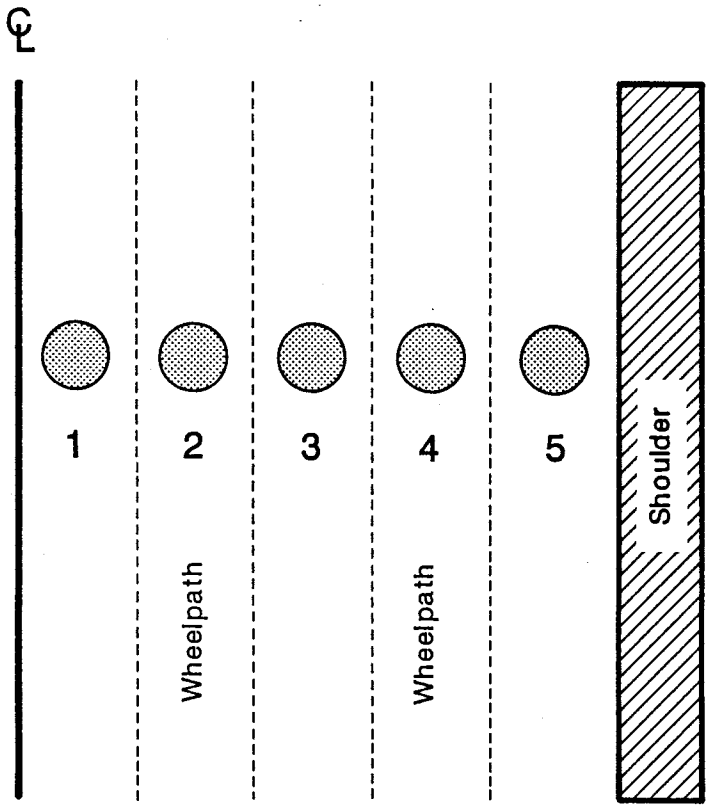

Figure 3.2. Distribution of cores across the pavement.

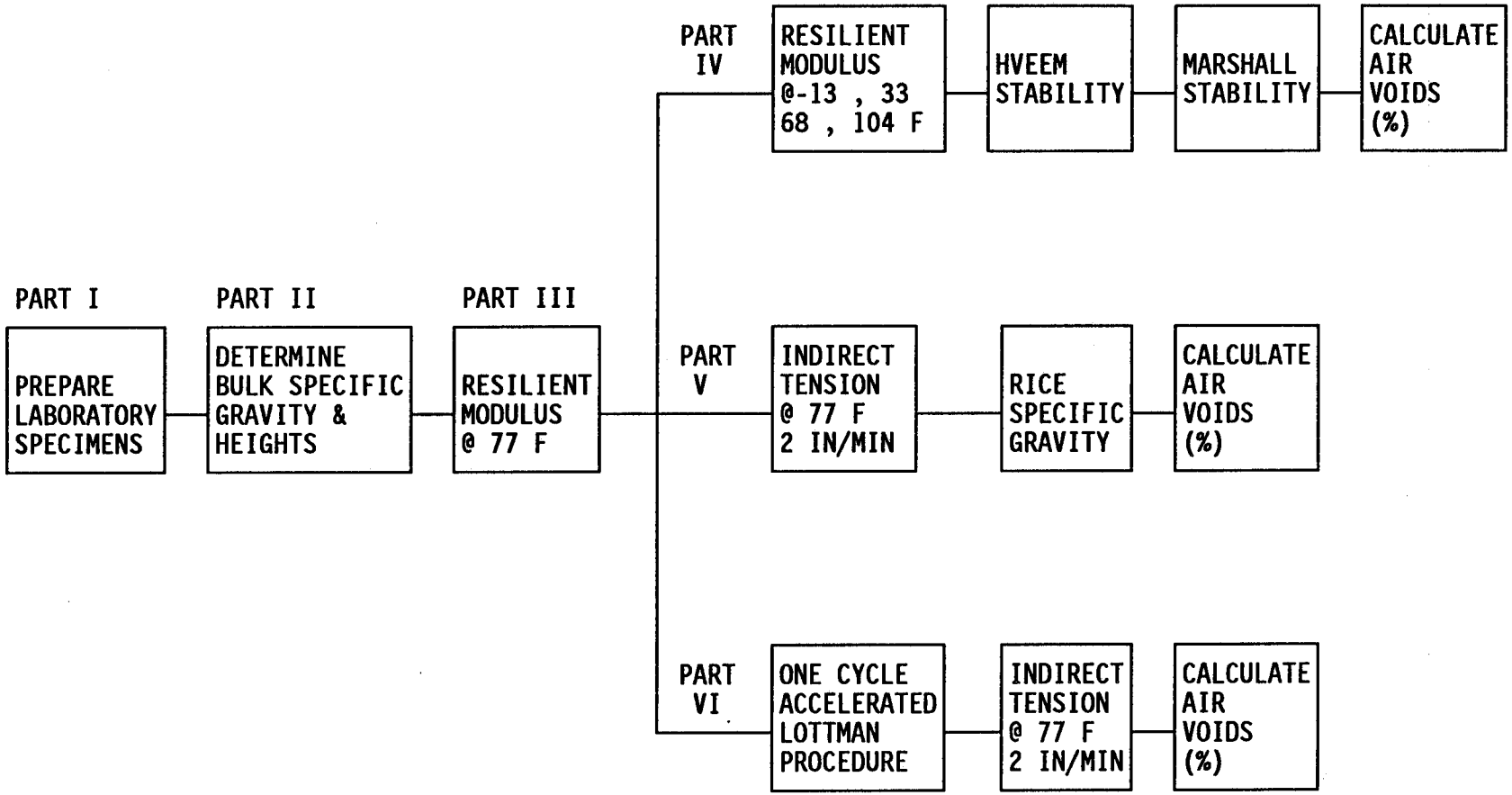

Figure 3.3. Laboratory test program.

layers this thin. In these cases, two steps were followed:

1. The top surface layer was tested for air void content, asphalt content, asphalt viscosity, aggregate gradation, and aggregate classification.
2. Mixture testing (Figure 3.3) was performed on the subsurface layer.

Test Results

Laboratory test results are described in the following subsections for each of the pavement sites analyzed. Test results were separated by location. Mixture properties were analyzed and compared.

Sweetwater. In Sweetwater, the asphalt pavement at site 1 exhibited more premature rutting (Table 3.1) than the pavement at site 2 primarily because the average asphalt content extracted from the cores in site 1 was much higher (0.7 percent more) than the average asphalt content found in the cores from site 2 (Table 3.3). With the interaction of these three major factors, a considerable rutting susceptibility was produced in the mixture.

Another important factor to consider is that the aggregate gradation curves (Figures 3.4 and 3.5), for both sites, are very close to the maximum density line. This means that the gradations are very dense and, therefore, very sensitive to asphalt content. Mixtures with this type of aggregate gradation may become unstable with a slight excess of asphalt.

Although Hveem and Marshall stability yielded higher average values for site 2 (Table 3.5), other material properties like VMA and resilient modulus were quite similar for both sites. Air voids were found to be considerably low (Table 3.6) for both sites. Although the sand content was quite low (12 percent), the sand particles were found to be very rounded, smooth, and nonporous, for both sites (Table 3.4). Most of the minus number 200 material came from the limestone crusher screenings which should aid in toughening the mix.

Fairfield. The Fairfield pavement at site 1 exhibited less rutting than the pavement at site 2 (Table 3.1) even though the base mix at site 1 contained 0.6 percent more asphalt, on the average, than the base mix at site 2 (Table 3.3). A possible contributing factor to the difference in rutting is that the viscosity of the asphalt extracted from the base mix at site 1 is twice the viscosity of the asphalt extracted from the base mix at site 2 (Table 3.3). The effect on the mix performance by the asphalt is likely accentuated by the character (rounded, smooth, and nonporous) and

Table 3.3. Data for asphalts extracted from pavement cores.

	Sweetwater Surface		Sweetwater Base	Fairfield		Centerville		Tyler		Lufkin	Dumas
Site No.	1	2	1	1	2	1	2	Base	Surf	1	1
Penetration											
77°F,100gm,5sec	37	36	31	27	44	27	36	32	72	56	65
39.2°F,200gm,60sec	10	11	3	13	15	5	3	-	-	21	19
Viscosity, poise											
140°F	2230	2330	4290	10,710	5170	6150	4210	4700	2520	4170	1800
275°F	3.20	3.30	4.24	5.63	3.61	5.05	4.26	5.19	-	4.90	5.39
Asphalt Content, percent	5.3	4.6	5.3	5.3	4.7	5.6	5.0	5.0	8.7	9.5	7.0
Design Asphalt Content	5.0	5.0	5.0	4.9	4.9	5.1	5.1	5.0	8.1	8.5	Unknown

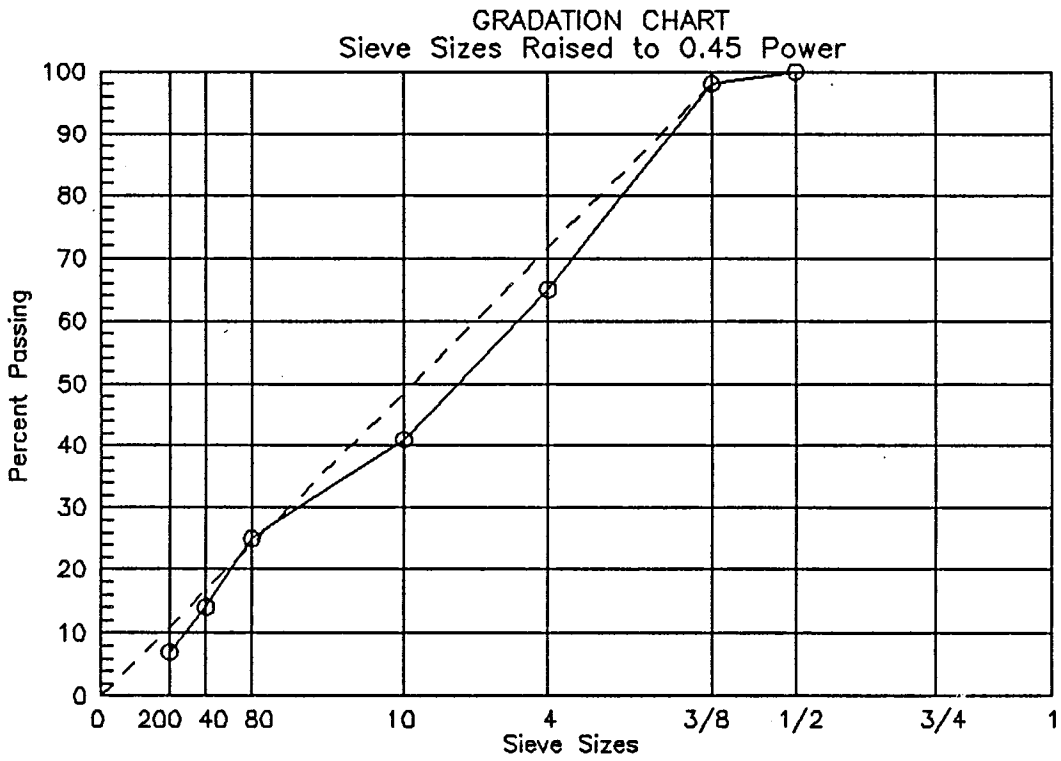

Figure 3.4. Gradation of aggregate from extracted cores - Sweetwater, site 1.

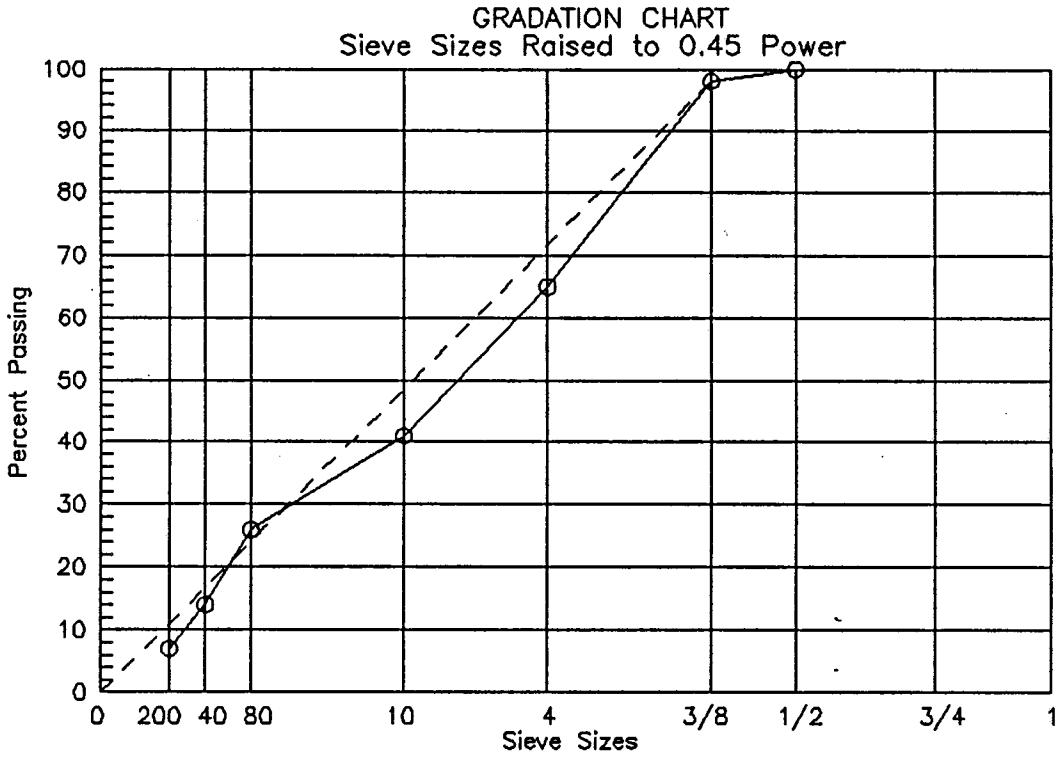

Figure 3.5. Gradation of aggregate from extracted cores - Sweetwater, site 2.

Table 3.4. Aggregate gradations and physical characteristics for all sites analyzed.

Pavement Location	Aggregate Type	Aggregate Blend	Particle Shape +#40	Particle Shape -#40	Particle Texture +#40	Particle Texture -#40	Porosity +#40	Porosity -#40
Sweetwater (surface)	• Limestone - 59% Martin Source	62% -3/8"+#4, 30% -#4+#10	Angular to Subangular	Angular to Subangular	Rough to Smooth	Smooth	Porous	Nonporous
	• Screenings - 29% Martin Source	13% -#4+#10, 49% -#10+#40, 24% -#80+#200, 14% -#200						
	• Sand - 12% Strain & Sons	5% -#10+#40, 62% -#40+#80 29% -#80+#200, 4% -#200						
Sweetwater (base)	• Recycle Mix - 61%	49% -1 1/4"+#4, 29% -#4+#10 22% -#10	Angular to Subangular	Subangular to Rounded	Rough	Smooth	Porous	Nonporous
	• Aggregate - 30% (Martin)	57% -1 1/4"+7/8" 39% -7/8"+34, 4% -#4						
	• Martin Base - 9%							
Fairfield (surface)	• Type D Rock - 60% D.P. Frost	97% +#10	-	-	-	-	-	-
	• Screenings - 30% D.P. Frost	14% +#10, 48% -#40						
	• Field Sand - 10% Bohler Field	100% -#40						

Table 3.4. Continued.

Pavement Location	Aggregate Type	Aggregate Blend	Particle Shape +#40	Particle Shape -#40	Particle Texture +#40	Particle Texture -#40	Porosity +#40	Porosity -#40
Fairfield (base)	• Type C Rock - 30% D.P. Frost • Gravel - 30% Gifford Hill • Screenings - 30% D.P. Frost • Field Sand - 10% Bohler Field	17% -5/8", 67% -3/8", 14% -#4 53% -#4, 44% -#10 42% -#40, 25% -#80, 19% -#200 69% -#80, 26% -#200	Angular to Subangular	Angular to Subangular	Rough to Smooth	Smooth	Porous and Nonporous	Nonporous
Centerville (surface)	• Type D Rock - 74% Crushed Sandstone • Fines - 26% East Texas Stone	87% +#10 3% +#10, 33% -#40	-	-	-	-	-	-
Centerville (base)	• Grade 3 Rock - 25% • Type D Rock - 40% • Screenings - 21% East Texas Stone • Field Sand - 14% Harris	87% -5/8", 11% -3/8" +#4 52% -3/8" +#4, 33% -#4 +#10 28% -#10 +#40, 42% -#40 +#80, 20% -#80 +#200 46% -#40 +#80, 33% -#80 +#200, 13% -#200	Angular to Subangular	Angular to Subangular	Rough	Smooth	Porous	Nonporous

Table 3.4. Continued.

Pavement Location	Aggregate Type	Aggregate Blend	Particle Shape +#40	Particle Shape -#40	Particle Texture +#40	Particle Texture -#40	Porosity +#40	Porosity -#40
Tyler	Base • Coarse Crushed Limestone(Stewart Bridgeport) • Medium Crushed Limestone(Stewart Bridgeport) • Field Sand(Lone Star Gas - local) • Field Sand(Fair Pit - local)		Angular to Subangular	Angular to Subangular	Rough to Smooth	Rough to Smooth	Porous	Nonporous
	Surface • Lightweight - 50% (TXI Streetman) • Concrete Sand - 15% (Norton Sand & Gravel) • Field Sand - 18% (J. Fair - local) • Field Sand - 17% (Lone Star Gas)		Subrounded to Rounded	Angular to Subangular	Rough to Smooth	Smooth	Porous	Nonporous
Lufkin	• Lightweight - 62% Aggregate • O & I Sand - 27% • Elliot Sand - 11%	71% -3/8"+#4, 24% -#4+#10 13% -#10+#40, 68% -#40+#80 70% -#40+#80, 17% -#80+#200, 10% -#200	Subangular	Angular	Rough	Smooth	Porous	Porous and Nonporous
Dumas	-	-	Subangular	Subangular	Rough	Smooth	Porous	Nonporous

Table 3.5. Mixture properties of pavement cores.

Location	VMA, percent[1]	Resilient Modulus, psi x 10^3 13°F[2]	33°F[2]	68°F[2]	77°F[1]	104°F[2]	Hveem Stab[2]	Marshall Stab, lbs[2]	Marshall Flow, 0.01"[2]
Sweetwater - 1	13.6[3]	1850	1396	489	344	37	8	650	17
Sweetwater - 2[4]	12.8[3]	2015	1364	601	551	63	20	850	15
Sweetwater - base	-	2000	1620	1040	729	114	17	1700	17
Fairfield - 1[4]	18.9	2110	1540	930	910	250	45	1450	16
Fairfield - 2	15.2	1940	1330	780	750	230	36	1500	16
Centerville - 1	16.1	2080	1650	804	560	84	44	3000	11
Centerville - 2[4]	14.5	1880	1650	880	680	140	44	2700	13
Tyler - base	17.5	2820	2220	1280	940	170	43	3700	9
Tyler - surface	22.1	1430	900	420	300	57	44	2600	13
Lufkin	16.0	1490	860	230	170	23	32	960	11
Dumas	22.0[3]	1600	1060	360	250	35	24	1900	16

[1]Average of 25 values(in wheelpath and outside wheelpath)
[2]Average of 6 values (3 in wheelpath, 3 outside wheelpath)
[3]Based on estimated value of bulk specific gravity of aggregate of 2.65
[4]Less rutted than other site near same location

Table 3.6. Summary of air voids in and outside wheelpaths.

Pavement Location	Air Voids Content, percent					
	Adjacent to Centerline	Wheelpath	Between Wheelpath	Wheelpath	Adjacent to Shoulder	Average
Sweetwater - site 1	2.5	1.6	1.7	1.2	1.5	1.7
Sweetwater - site 2	1.8	0.9	3.1	0.9	1.5	1.6
Sweetwater (base)	1.1	1.2	0.2	1.0	2.5	1.2
Fairfield - site 1	8.1	6.5	7.5	6.6	6.8	7.1
Fairfield - site 2	4.8	4.1	5.7	5.4	5.8	5.2
Centerville - site 1	2.4	1.3	1.2	1.0	1.9	1.6
Centerville - site 2	3.9	1.1	1.0	2.1	2.0	2.0
Tyler - base	4.3	2.5	3.3	3.0	3.8	3.4
Tyler - surface	2.1	2.8	2.7	2.9	2.7	2.6
Lufkin	3.3	2.8	3.7	3.5	4.0	3.5
Dumas	9.9	4.1	6.9	4.7	6.5	6.4

quantity (40 percent) of natural aggregate used in the 4-inch base.

Other important factors in the Fairfield mixtures are the high air void contents (Table 3.6) and dense gradations (Figures 3.6 and 3.7) in the base material at both sites. Hveem stability yielded a higher average value for the base mix at site 1. It is important to note that, in this case, the surface layer could not be meaningfully tested in the laboratory because it was less than one inch thick.

Centerville. In Centerville, the asphalt pavement at site 1 exhibited more rutting (Table 3.1) than the pavement at site 2. This can be explained by the interaction of the following factors:

1. The average asphalt content extracted from the cores of site 1 is higher (0.6 percent more) than the average asphalt content obtained from the cores of site 2 (Table 3.3).
2. The sand-size particles found at both sites are rounded, smooth, and nonporous (Table 3.4) making the mix sensitive to binder content.
3. The gradations are on the fine side of the specification and exhibit a large hump in the curve at the number 40 sieve for both sites, indicating a critical mixture that becomes readily unstable with a slight excess of fluids (Figures 3.8 and 3.9).

Another factor to mention is that the air void profile (Table 3.6) indicates that the Centerville pavement was probably compacted below the normally specified levels during construction. Thus the higher binder content of site 1 is the critical factor differentiating the performance between the two sites.

Tyler. This pavement was placed as a fabric test section (27) in 1981 at a very high-traffic area of IH 20. Rutting leveled off for four years and then, in the spring of 1987, it began to increase dramatically (Figure 3.10). The surface required milling and overlaying by July of 1987.

It seems that the most important factor that contributed to rutting in this particular site was the amount and character of the natural aggregate. The surface mix contained 50 percent natural sand and gravel composed of rounded, smooth, and nonporous aggregate particles. The surface mix was also gap graded, exhibiting a notable hump in the gradation curve at the number 40 sieve (Figure 3.11). Both the gradation and character of the aggregate particles determined the performance of the mixture.

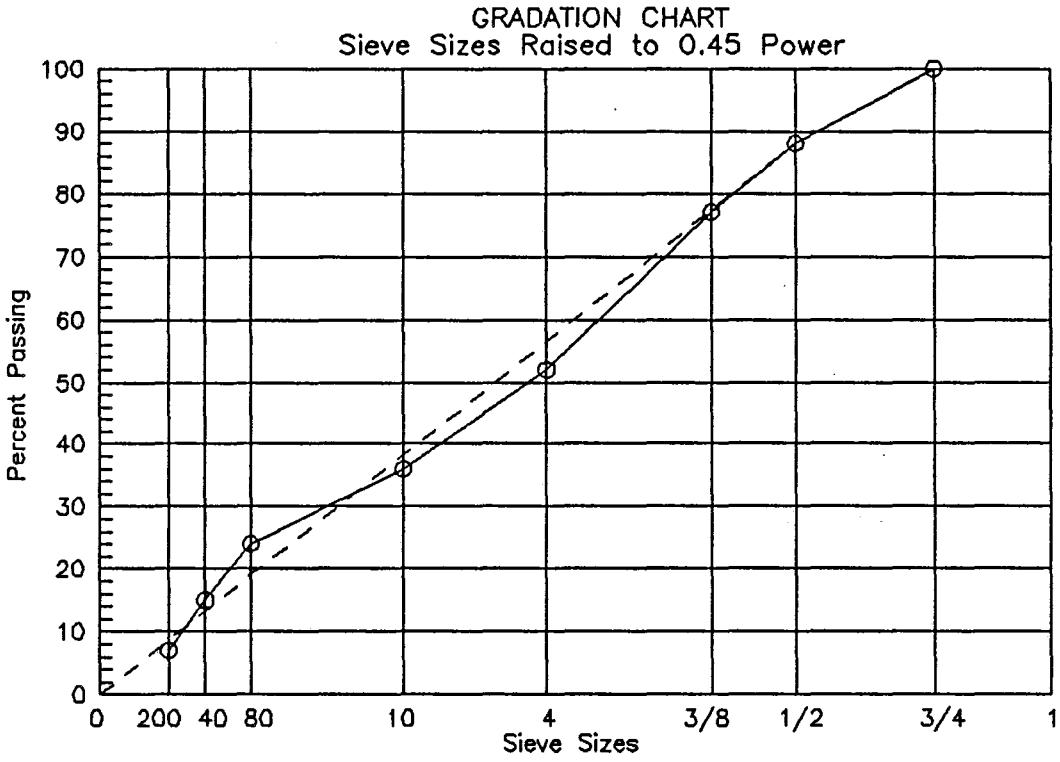

Figure 3.6. Gradation of aggregate from extracted cores - Fairfield, site 1.

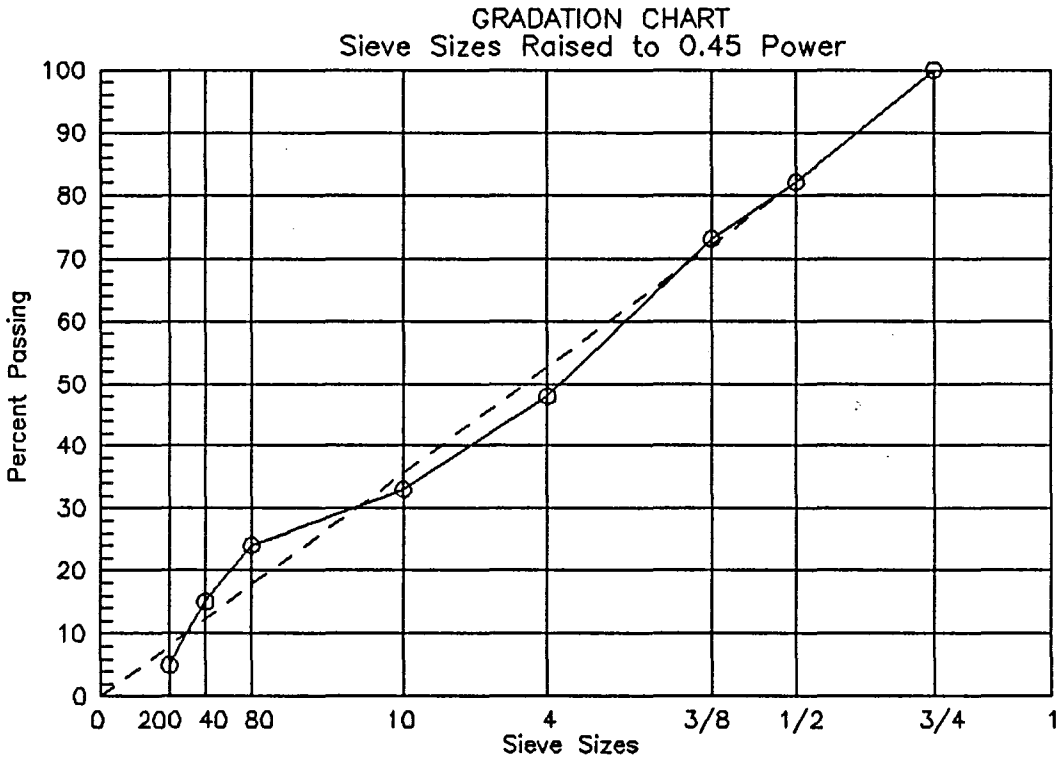

Figure 3.7. Gradation of aggregate from extracted cores - Fairfield, site 2.

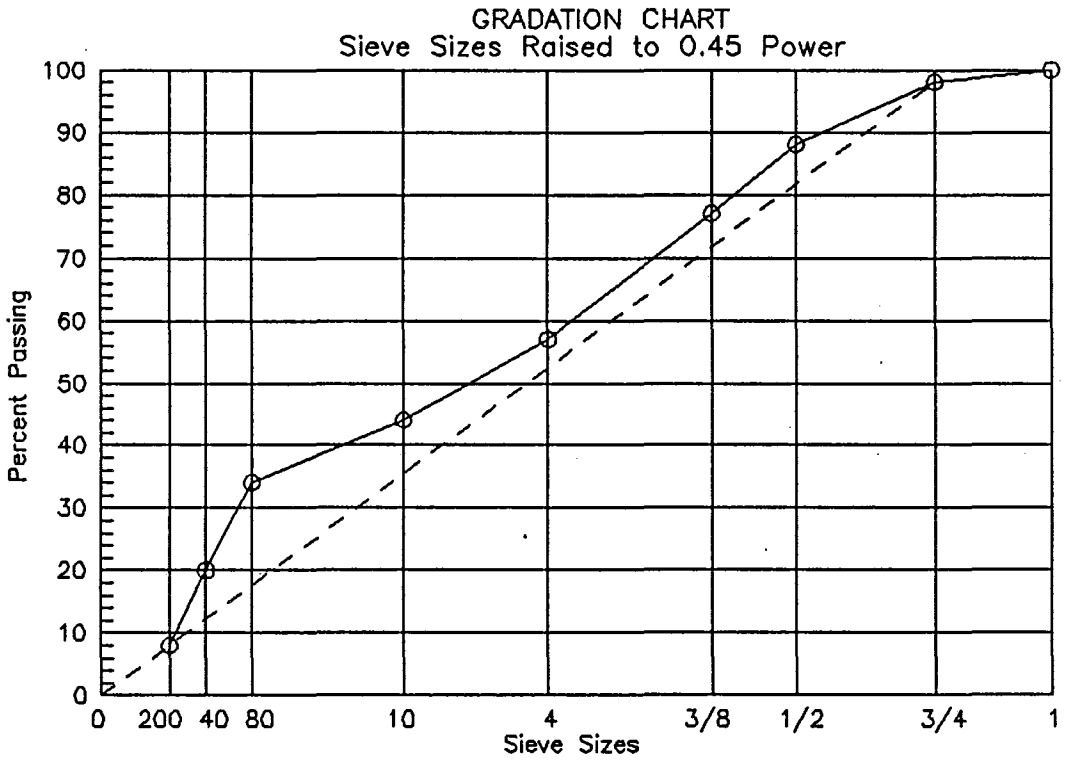

Figure 3.8. Gradation of aggregate from extracted cores - Centerville, site 1.

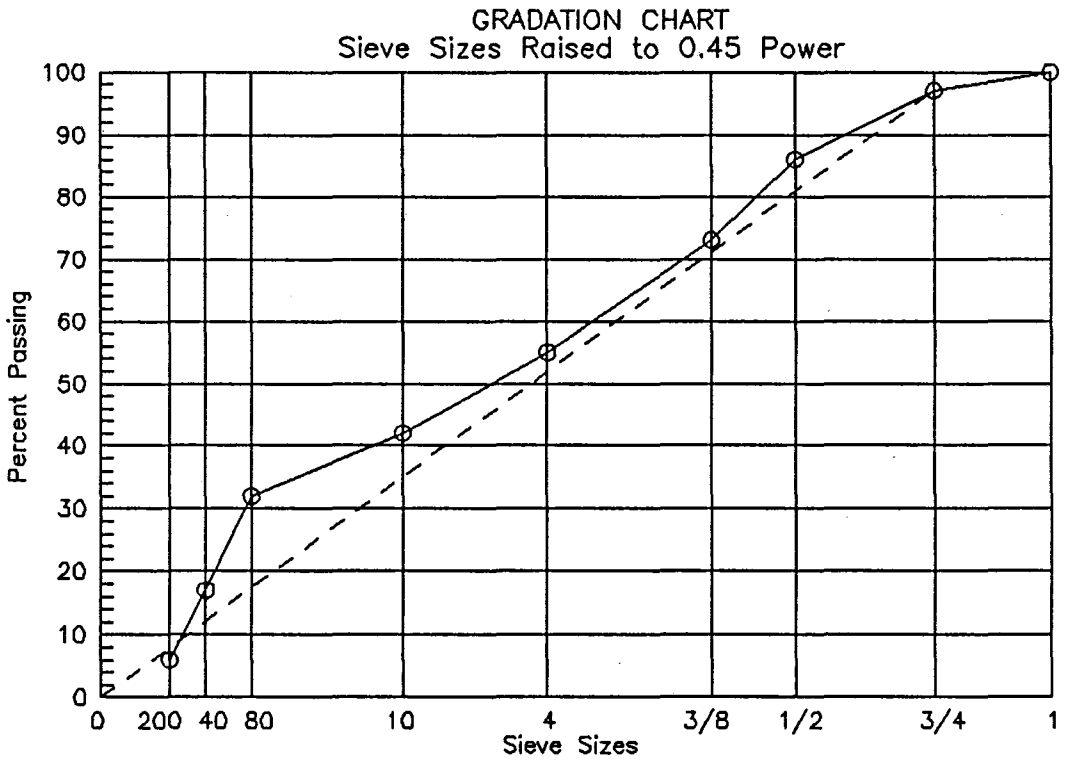

Figure 3.9. Gradation of aggregate from extracted cores - Centerville, site 2.

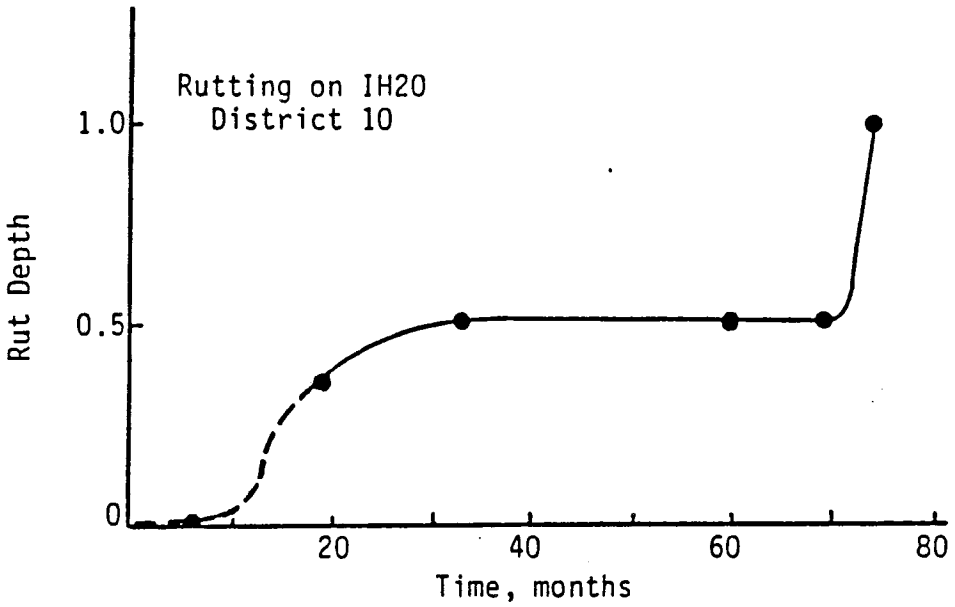

Figure 3.10. Rutting history of pavement on IH20 near Tyler, Texas.

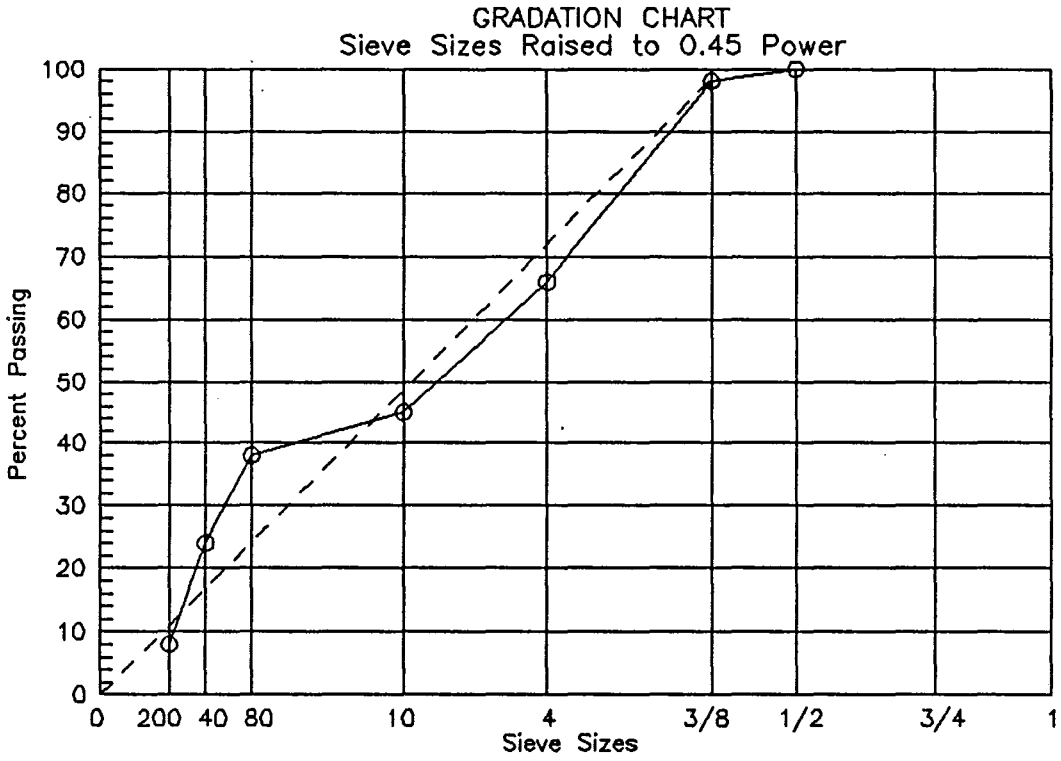

Figure 3.11. Gradation of aggregate from extracted cores - Tyler surface course.

It was also found that the surface mix contained 0.6 percent more asphalt, on the average, than the design asphalt content (Table 3.3).

Based on laboratory tests, both the base and surface mixtures indicated severe moisture susceptibility (Table 3.7); however, visual examination of the cores did not indicate that moisture had damaged the pavement layers.

Lufkin. The Lufkin mix contained acceptable air voids (Table 3.6) and voids in the mineral aggregate (VMA) above the minimum percentage (15 percent) recommended by the Asphalt Institute (28) (Table 3.5). However, this mix contained 37 percent by weight natural sand particles (Table 3.5) with an asphalt content one percent above optimum design (Table 3.3) and, as a result, exhibited relatively low stability. The coarse material in this mixture was lightweight synthetic aggregate. The aggregate grading exhibited excessive amounts (Item 340, Type D) of minus number 40 sieve size material (Figure 3.12). This may be due partially to aggregate degradation during plant operations, pavement service, and coring. The mixture also exhibited sensitivity to moisture. This combination of factors in the presence of the incessant traffic of US 59 resulted in severe rutting after two summers. This pavement was milled off in the spring of 1988 to remove ruts near 1-inch deep.

Dumas. Tests on the Dumas cores showed relatively high air voids and a mixture of low stability and poor resistance to moisture damage. Table 3.6 shows significantly lower air voids in the wheelpaths than between or outside the wheelpaths indicating inadequate compaction during construction. Figure 3.13 indicates a very dense aggregate gradation which when adequately compacted should contain relatively low air voids. Visual examination of the cores indicated stripping of asphalt from the large and intermediate size aggregate. Inadequate compaction may have provided permeable voids which enhanced stripping, which in turn contributed to rutting. The design asphalt content is not known, but the actual content appears quite high. Another factor contributing to the rutting problem could be the low viscosity of the asphalt.

Summary of Findings

Based on findings from the field investigation, the following is given to discuss the primary contributors to rutting and methods to alleviate these problems.

1. The aggregate gradations of all the rutting mixtures analyzed were

Table 3.7. Tensile properties of cores before and after Lottman freeze-thaw moisture treatment.

Location	Before Moisture Treatment				After Moisture Treatment				TSR[2]
		Tensile Properties[1]				Tensile Properties[1]			
	Average Air Void Content (%)	Tensile Strength (psi)	Strain @ Failure (in/in)	Secant Modulus (psi)	Average Air Void Content (%)	Tensile Strength (psi)	Strain @ Failure (in/in)	Secant Modulus (psi)	
Sweetwater-1	1.7	142	0.0086	78,000	1.9	151	0.0013	82,000	106
Sweetwater-2	1.2	175	0.0032	69,000	2.9	160	0.0023	64,000	91
Sweetwater-base	1.0	221	0.0031	71,000	0.2	170	0.0067	37,000	77
Fairfield-1	8.4	200	0.0015	154,000	6.3	174	0.0017	103,000	87
Fairfield-2	4.8	188	0.0013	147,000	5.9	116	0.0045	51,000	62
Centerville-1	2.8	268	0.0028	97,000	0.5	275	0.0031	92,000	103
Centerville-2	1.3	289	0.0025	132,000	1.1	181	0.0022	86,000	63
Tyler-base	2.6	251	0.0013	202,000	3.1	100	0.0021	47,000	40
Tyler-surface	3.1	175	0.0024	75,000	3.4	95	0.0050	19,000	54
Lufkin	2.2	119	0.0040	30,000	4.5	74	0.0044	18,000	62
Dumas	4.7	143	0.0017	58,000	9.9	74	0.0042	18,000	52

[1]Tensile tests were performed at 77°F and 2 inches per minute.(Average values are reported).
[2]Tensile strength ratio = (Tensile strength after / Tensile strength before) x 100.

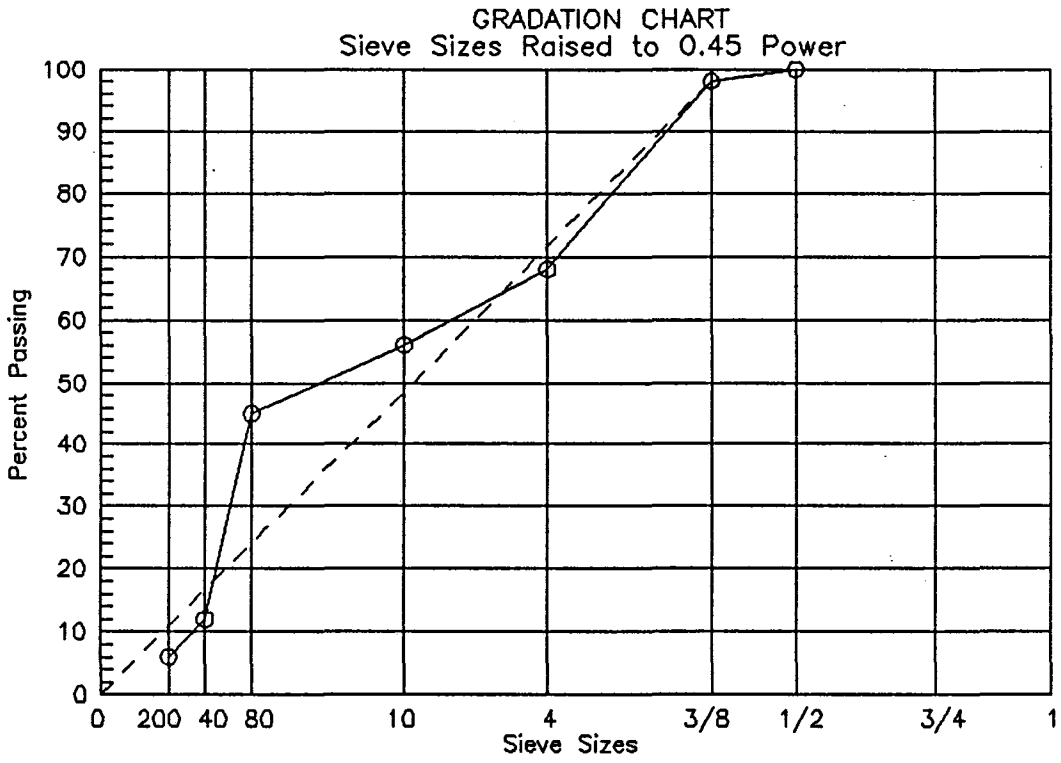

Figure 3.12. Gradation of aggregate from extracted cores - Lufkin.

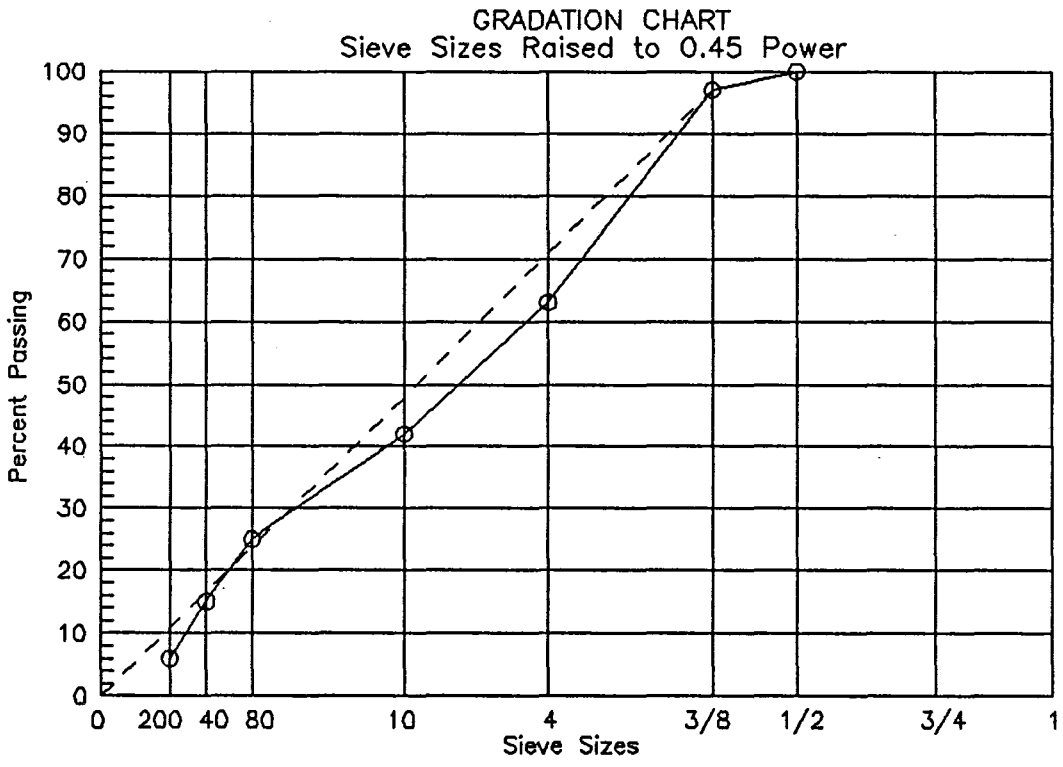

Figure 3.13. Gradation of aggregate from extracted cores - Dumas.

found to be near the theoretical gradation of maximum density or found to exhibit a hump in the gradation curve at the No. 40 sieve. The dense gradation provides little room for asphalt and both of these characteristics produce a mix that is sensitive to asphalt content. Therefore, a slight excess of asphalt will result in an unstable mixture. Subsequent compaction by traffic will reduce the air voids in the mat below some critical level then rapid failure by rutting will occur.

2. The rutting mixtures contained from 12 percent to 50 percent natural, rounded, non-porous particles (most of which were sand-sized particles). Twelve percent sand should not produce a rut-susceptible mix, however, this particular mix had a very dense gradation (low VMA) and asphalt in excess of optimum. This combination of factors produced a low stability mix which resulted in rutting. The mix with 50 percent sand exhibited excellent VMA but the high VMA was obtained because of the very fine gradation which showed a large hump at the No. 40 sieve. The fine gradation produced a mix with low shear strength which rutted under heavy traffic.
3. Binder content in the asphalt-aggregate mixture was in excess of that required by the optimum mixture design. This finding may have been a direct result of the fact that density is often the governing factor during construction of asphalt pavments. Asphalt contents may have been increased simply to achieve the required density. This action should be taken with extreme caution particularly when a mixture may be sensitive to asphalt content (i.e., low VMA, high sand content, rounded/smooth particles, small top size aggregate).

   The Item 340 specification allows the asphalt content to vary by ± 0.5 percent by weight of total mix around the optimum during field operations which is realistic, particularly when drum mix plants are used. It, therefore, behooves the engineer to design a mix with VMA high enough to accept 0.5 percent asphalt above optimum without excessive loss of stability.
4. Heavy traffic enhanced rutting when the previously discussed factors were present in an asphalt mixture. Current pavement design equations and performance data (from the AASHO Road Test,

1958-60) are based on tire pressures about 15 to 20 psi lower than actual tire pressures and based on axle loads that are routinely exceeded in actual practice. Engineers must insure that high quality aggregates of proper gradation are specified for mixes on high volume highways.

CHAPTER IV
LABORATORY INVESTIGATION

The field investigation indicated that the character and quantity of sand-size aggregate particles have a great influence on the permanent deformation performance of asphalt concrete mixtures. The literature study indicated that this problem is widespread. As a result, a comprehensive laboratory investigation, consisting of two phases, was conducted to: (1) quantify the influence on resistance to rutting when manufactured sand (crushed limestone particles) is replaced, or partially replaced, by natural, uncrushed sand, and (2) evaluate the ability of test procedures to identify the resistance of mixtures to rutting (based on their percentage of natural sand). The test procedures included in the first phase were: indirect tensile strength, Hveem stability, Marshall stability, unconfined compressive strength, long-term static creep, and long-term cyclic deformation. The second phase included the evaluation of triaxial cyclic deformation under various conditions of stress and temperature. Only laboratory prepared specimens were evaluated in the test program. In this chapter, general descriptions of the materials and tests used are given. Results and their interpretation are presented for each phase.

Materials

The asphalt used in all the asphalt concrete test specimens was Texaco AC-20 obtained from Port Neches, Texas. The asphalt properties are listed in Table 4.1. It was decided to use only one type and grade of asphalt in order to reduce the number of factors affecting the results and stay within the budget.

Crushed limestone (obtained from Brownwood, Texas) was selected as the coarse aggregate (plus No. 10 sieve). This material type is commonly used in asphalt concrete surface layers. By keeping this coarse fraction as a constant, it is possible to evaluate the effect of natural fines on permanent deformation.

The sand-size aggregate fraction is defined as the material passing the No. 10 sieve. The natural sand selected was a siliceous, subrounded, smooth

Table 4.1. Properties of asphalt.

Asphalt source:	Texaco
Grade:	AC-20
Specific gravity at 77°F	1.029
Viscosity at 140°F, P	2040
Viscosity at 275°F, cSt	398
Penetration at 77°F, 100 g, 5 s	75
Penetration at 39.2°F, 100 g, 5 s	8
Penetration at 39.2°F, 200 g, 60 s	28
Softening point, °C	51.8
Softening point, °F	125
Temperature susceptibility[1] 140°F to 275°F	-3.52
PVN[2]	-0.6
P.I.[3] from penetration at 39.2°F and 77°F	-1.0
P.I. from penetration at 77°F and softening point	+0.3

[1]Temperature susceptibility $=(\log\log\eta_2 - \log\log\eta_1)/(\log T_2 - \log T_1)$ where η = viscosity in cSt, T = absolute temperature.

[2]Determined from penetration at 77°F and viscosity at 275°F

[3]P.I. $= (20 - 500\alpha)/(1 + 50\alpha)$
$\alpha = [\log(pen_2) - \log(pen_1)]/(T_2 - T_1)$, or
$[\log 800 - \log(pen_{25°C})]/(T_{SP} - 25)$, where T = temperature, °C.

surfaced, and nonporous aggregate. The manufactured sand selected was washed limestone screenings. These particles, contrary to the natural sand particles, are angular in shape, rough in texture, and somewhat more absorbant.

An aggregate gradation (Figure 4.1) was selected based on gradations typically used in the field. The gradation was designed to meet Texas SDHPT Item 340, Type D specifications (29). The total aggregate mixture contained a blend of 60 percent coarse crushed limestone and 40 percent sand. Five different aggregate mixtures were produced by replacing different percentages of the natural field sand with manufactured sand while maintaining the same total gradation. The five mixes are as follows:

Mix 1 - 40 % natural field sand,
Mix 2 - 20 % natural sand, 20 % limestone screenings,
Mix 3 - 10 % natural sand, 30 % limestone screenings,
Mix 4 - 5 % natural sand, 35 % limestone screenings, and
Mix 5 - 0 % natural sand, 40 % limestone screenings.

All tests from phases I and II were performed on selected mixtures which are presented in Table 4.2. The mixtures tested in phase II were selected after analyzing the results from phase I. It was then determined, as will be described in the following pages, that the 40 percent natural sand mixture was highly susceptible to plastic deformation.

Samples for testing were fabricated (Appendix A) at two air void content levels in an attempt to simulate mixture performance immediately after construction (5 percent to 7 percent air voids) and after several years of consolidation under traffic (3 percent to 4 percent air voids) for a well-designed mixture.

Description of Tests

The indirect tensile strength test employs the indirect method of measuring mixture tensile properties (30). Two inch high and 4-inch diameter cylindrical specimens were loaded diametrally and monotonically until complete failure occurred. This loading configuration generates a uniform tensile stress perpendicular to and along the diametral plane. The specimens were compacted using the Texas Gyratory shear compactor, and the

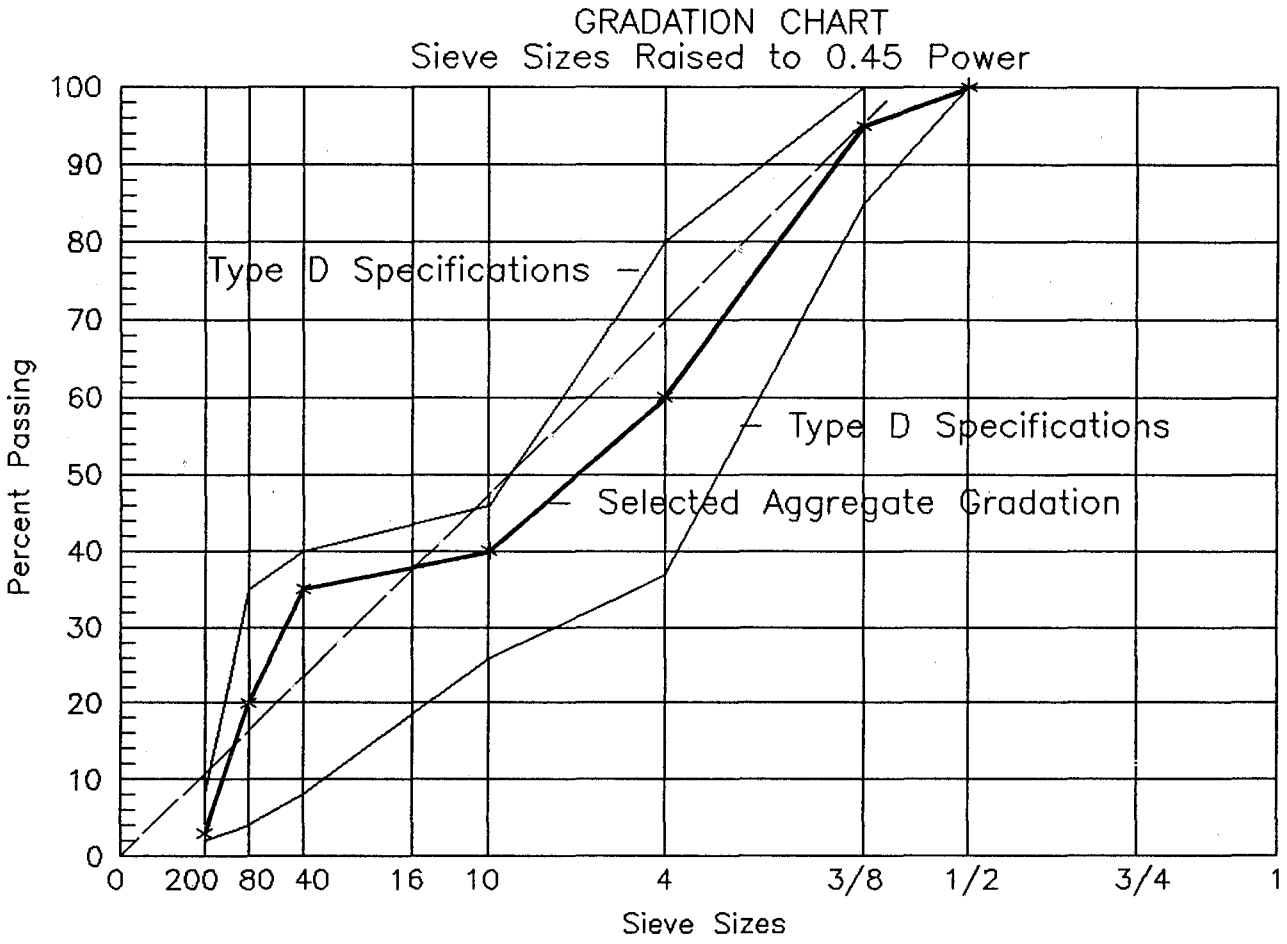

Figure 4.1. Selected aggregate gradation and Type D specifications.

Table 4.2. Tests performed on selected aggregate mixtures.

Test Performed	Percentage of Natural Sand in the Mix				
	40%	20%	10%	5%	0%
Indirect Tensile Strength	X	X			X
Hveem Stability	X	X		X	
Marshall Stability	X	X		X	
Unconfined Compression Strength	X	X	X	X	X
Long-term Static Creep	X	X	X	X	X
Long-term Cyclic Test	X	X	X	X	X
Triaxial Cyclic Test		X	X		X

tests were conducted at a temperature of 77°F and a deformation rate of 2 inches per minute.

Hveem stability tests were performed in accordance with Texas SDHPT test method Tex-208-F (31) which is a modification of ASTM D 1560.

Marshall stability tests were performed in accordance with the ASTM D 1559 method except that the specimens were prepared using the gyratory compactor.

Cylinders with 4-inch diameter by 8-inch height were fabricated using the Cox kneading compactor (Appendix A) for the unconfined compression tests, the long-term static and cyclic creep tests, and the triaxial cyclic test.

Unconfined compressive strength tests were performed on 4-inch diameter by 8-inch high cylindrical specimens at 104°F. This test is a specific case of the triaxial compression test, where the confining pressure is zero. The main purpose of the test was to determine the shear strength of the mixture.

In the long-term static creep test, cylindrical specimens were tested in axial unconfined compression at 104° F and under a 60 psi stress level (Appendix A). Vertical deformations were measured by means of linear variable differential transformers (LVDT's) (Figure 4.2). This allowed a visco-elasto-plastic characterization of the asphalt mix. Data are recorded throughout the test and plotted on a linear scale.

A long-term cyclic test was performed using the same setup as the long-term static creep test (Appendix A) wherein a repeated haversine load was applied instead of the static load. This test was also performed at 104°F. Data were recorded periodically as accumulated deformation versus number of loading cycles and plotted on a linear scale.

The triaxial cyclic test was performed utilizing the same setup and loading technique as the long-term cyclic test; however, with these tests a lateral confining pressure was applied to the specimen. Two temperatures (104° F and 122° F) were used for this test. Data were recorded as accumulated permanent deformation versus number of cycles and plotted on a linear scale.

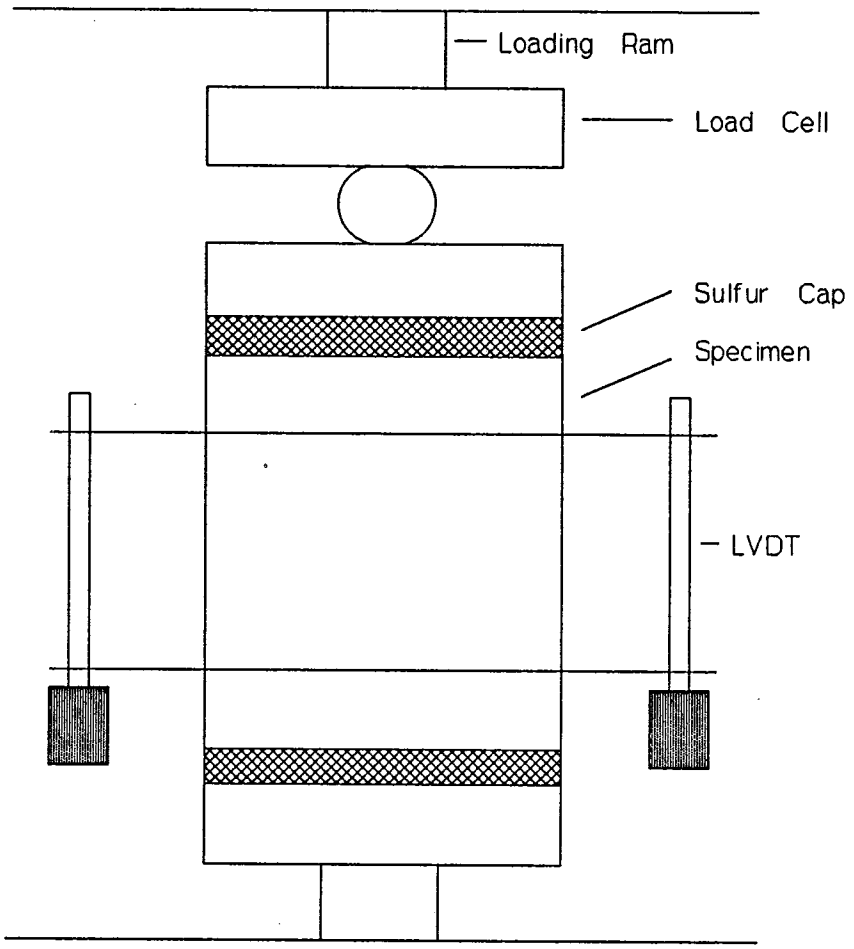

Figure 4.2. Setup for long-term static creep test.

Phase I Test Results

An indirect measure of the shape and textural characteristics of the aggregate was obtained using the particle index test. This test was originally developed by Huang (32) and has been used frequently in research following its standardization (ASTM D3398-81). Test results showed that particle index values decreased with increasing percentages of natural sand in the mixture:

MIX NO.	SAND CONTENT OF AGGREGATE MIXTURE	PARTICLE INDEX OF AGGREGATE MIXTURE
1	0	13.5
2	5	13.2
3	10	13.0
4	20	12.4
5	40	11.3

This measure of particle index can be used in comparing the performance of the different mixtures. As shown in Figure 4.3, mix quality (expressed in number of load cycles to reach 15,000 microstrain of permanent deformation) can be plotted against particle index (which indirectly represents mixture cost) for the various mixtures. It is observed, from the figure, that particle index values above 13 do not produce substantial increases in mix quality. Therefore, reducing the natural sand content of this particular mix below ten percent may have negative economic effects when considering materials cost, workability, and compactibility. This, of course, will not necessarily be true for all mixes.

The tests used to characterize the mixtures in this phase were indirect tensile strength, Hveem stability, Marshall stability, unconfined compressive strength, long-term static creep, and long-term cyclic loading test. In this phase, an asphalt concrete mixture design was performed for the mixture containing 20 percent natural sand (Table 4.3), and the optimum asphalt content obtained (5.5 percent) was used for preparing two other mixes with higher and lower natural sand contents. This was done in order to reduce the number of variables and to further isolate the effect of natural field sand. The 5.5 percent asphalt content can be thought of as an average optimum asphalt content for all the mixtures analyzed. Mixture design procedures specified by the Texas SDHPT (33) were followed.

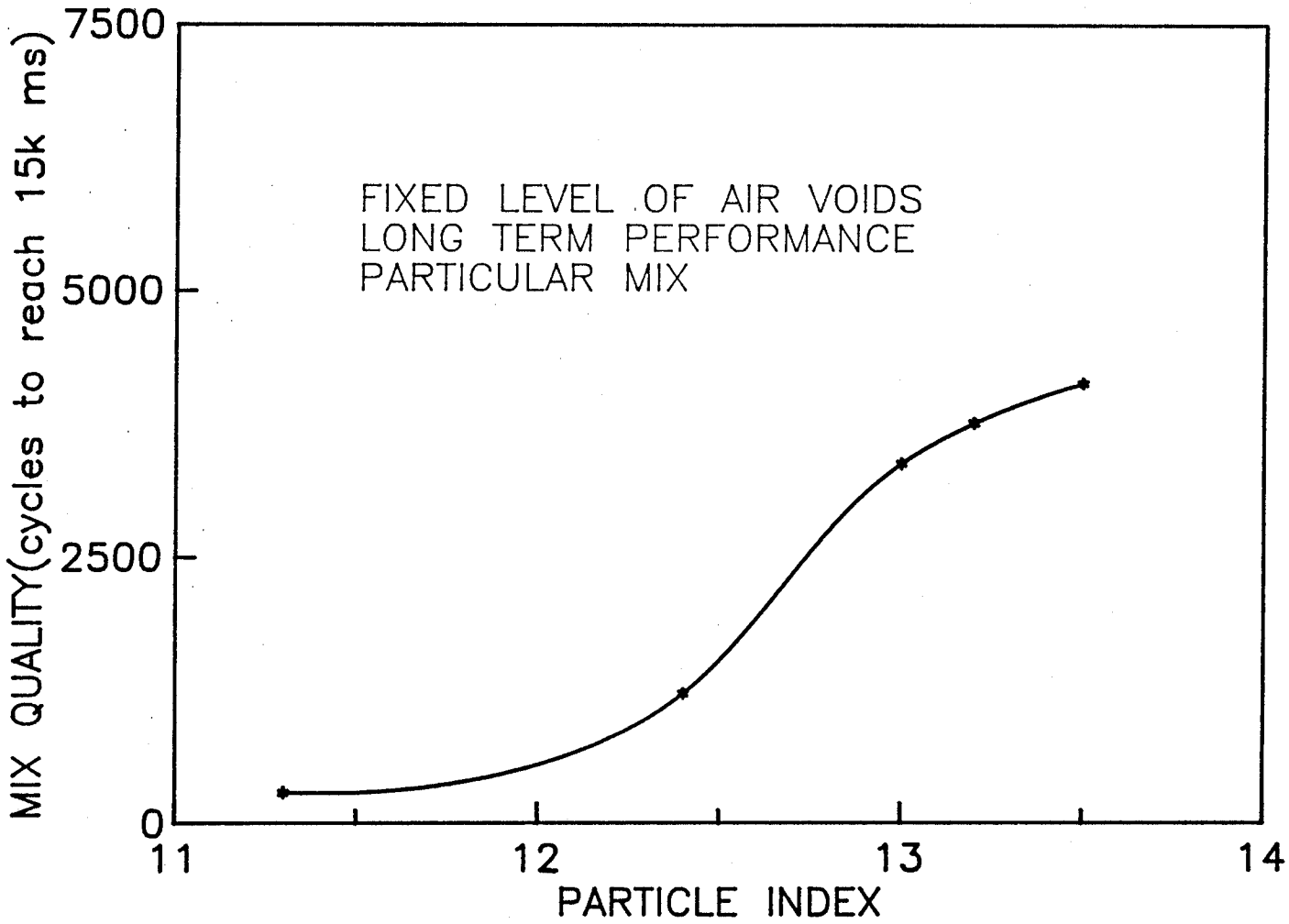

Figure 4.3. Asphalt Concrete Mixture Quality (as Measured by Resistance to Permanent Deformation) as a Function of Particle Index.

Table 4.3. Design data for mix containing 20 percent natural sand in total aggregate blend.

Mix No.	Asphalt Content, percent	Density, percent	Hveem Stability	Marshall Stability, lbs	Unit Weight, lbs/ft3
1	4.0	93.2	41.3	1715	146.8
2	4.5	93.5	42.8	2025	147.5
3	5.0	95.0	41.3	2150	148.9
4	5.5	96.7	38.7	2135	150.1
5	6.0	97.6	34.4	2040	149.5

Optimum asphalt content selected at 97 percent density: 5.5%

Results from the indirect tensile strength test are presented in Table 4.4. Tensile strength is primarily a function of the binder properties. Furthermore, with all other variables held constant, tensile strength will always vary inversely with air void content. Tensile strength and strain at failure exhibited a decrease as the proportion of manufactured sand was increased. This was due partially to the corresponding increase in air void content and the thicker asphalt films on the smoother, more rounded and less absorbent natural sand particles.

To optimize tensile strength and equalize void content, a slight increase in asphalt content would be required as the crushed limestone particles replace the natural sand particles. Varying asphalt content, however, may have caused other difficulties in interpreting these data. Therefore, the decision was made at the beginning to use one asphalt content (5.5 percent) for the three mixtures tested in this initial work. Asphalt content was varied in the second phase of this study.

Results from the Hveem stability test are presented in Figure 4.4. In this type of test, the character of the sand-size particles have a great influence on the stability of the asphalt mixture. This is primarily because the Hveem stability test is a shear strength test, where the sample is subjected to a vertical compressive load under a varying confining pressure. The stability of the sample can be represented by the general Mohr-Coulomb equation:

$$s = c + \sigma \tan \phi \qquad (4.2)$$

where: c = cohesion,
ϕ = angle of internal friction,
σ = compressive stress, and
s = shear strength.

Sample shear strength (as measured by Hveem stability) decreases as the amount of natural sand in the mixture increases (Figure 4.4), which is most likely due to a decrease in the angle of internal friction. The cohesion, on the other hand, is believed to be considerably less affected. Furthermore, it was observed from the results that the decrease in stability with increase in natural sand content is true for both low (3 percent to 4 percent) and high (5 percent to 7 percent) levels of air void content.

Table 4.4. Summary of indirect tension test results at 77°F.

Mixture Type	Low Air Void Specimens			High Air Void Specimens		
	Tensile Strength, psi	Strain @ Failure, in/in	Air Voids, percent	Tensile Strength, psi	Strain @ Failure, in/in	Air Voids, percent
40% Natural Sand	154	0.44	3.0	97	0.57	5.2
20% Natural Sand	114	0.50	4.0	94	0.51	6.9
0% Natural Sand	104	0.38	3.9	91	0.39	6.9

Each value represents an average of three tests.

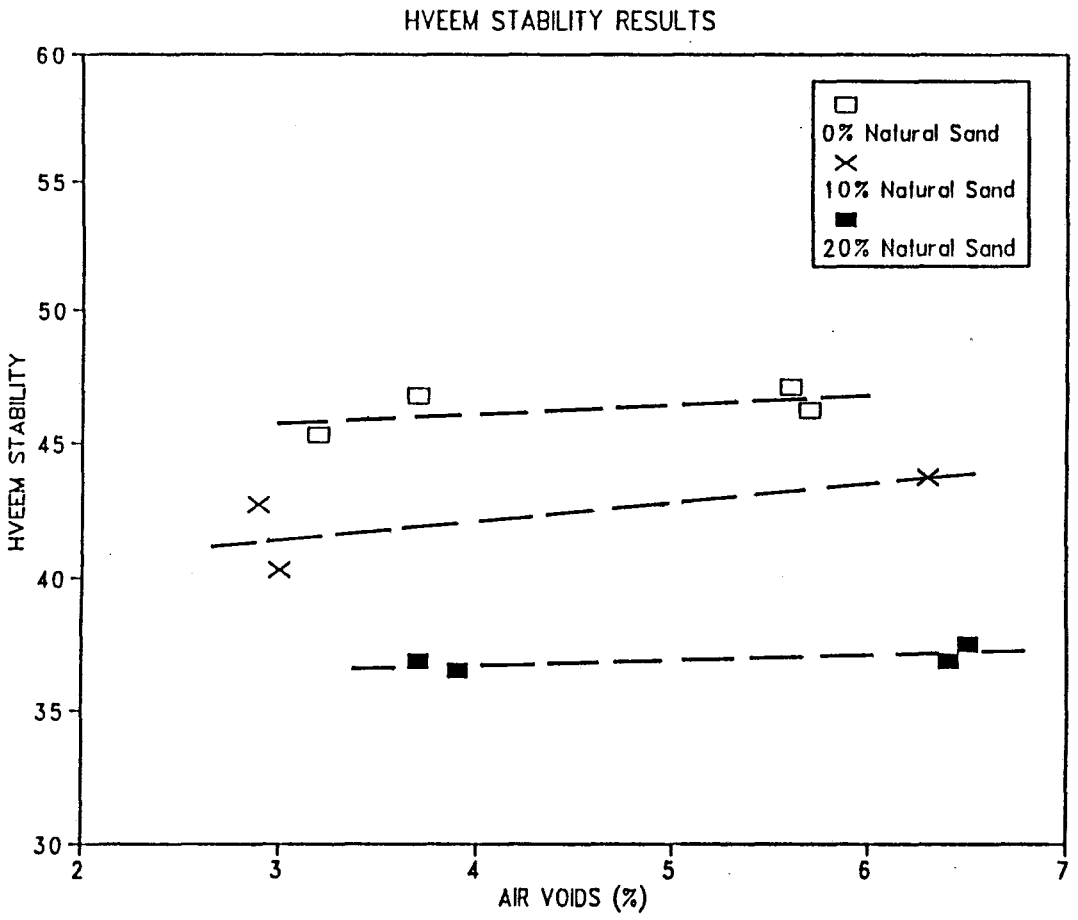

Figure 4.4. Typical Hveem stability test results (one sample per point).

Marshall stability test results are presented in Figure 4.5. These data were generally consistent with the indirect tensile strength results, which is not surprising since the Marshall stability test and the indirect tension test have similar configurations. As in the case of the indirect tension test results, the greater absorption capacity and surface area of the crushed limestone particles (resulting in decreased asphalt film thickness) seems to have contributed to a decrease in Marshall stability, acknowledging the fact that the asphalt content used in all mixes was constant. Marshall stability varied inversely with air void content.

Results from the unconfined compressive strength tests are presented in Figure 4.6. The data show that the unconfined compression (shear) strength is improved by decreasing the proportions of natural sand in the mixture. This of course, is explained by the fact that the manufactured sand (limestone screenings) has a rougher surface texture than the natural sand and, therefore, develops stronger frictional interaction forces between the aggregate particles.

Typical long-term static creep results are shown in Figures 4.7 and 4.8 for high and low air voids, respectively. All the results are shown in Figures B.1 through B.10 in Appendix B. The applied stress (60 psi) for this test was selected using a trial and error procedure (Appendix A) based on behavior after long-term loading. The test temperature (104°F) was chosen to simulate realistic critical field conditions. An analysis of the unconfined compression test results is summarized below:

1. Results in Figures 4.7 and 4.8 show that, for any duration of applied load, total deformation increases significantly as the percentage of natural sand in the mixture increases. Mixes containing 10 percent to 40 percent natural sand failed much more rapidly than mixtures containing zero percent to 5 percent natural sand.
2. Deformation upon static loading is strongly dependent on air void content. Samples having high air void contents (5 percent to 7 percent) failed much faster than samples having low air void contents (3 percent to 4 percent). Note that the low air void contents are still above the critical value (that is, air void content under which the asphalt acts as a hydrostatic fluid such

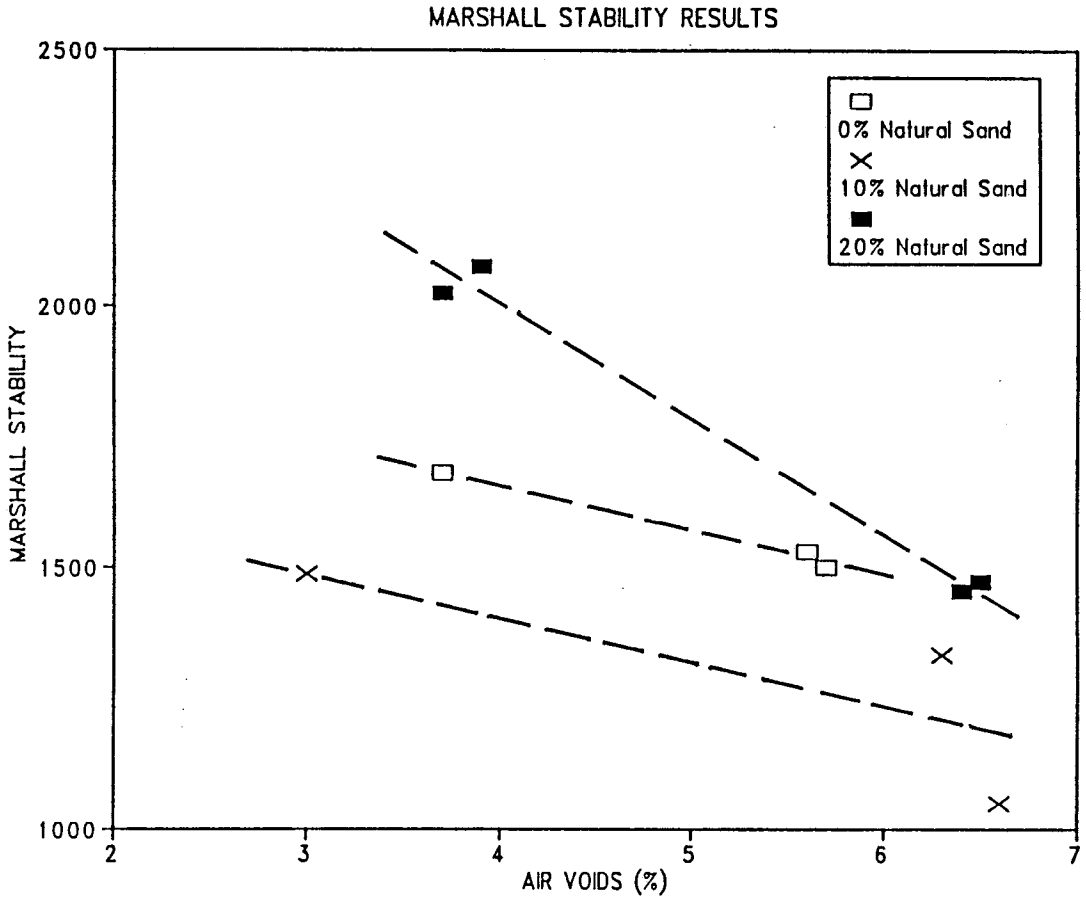

Figure 4.5. Typical Marshall stability test results (one sample per point).

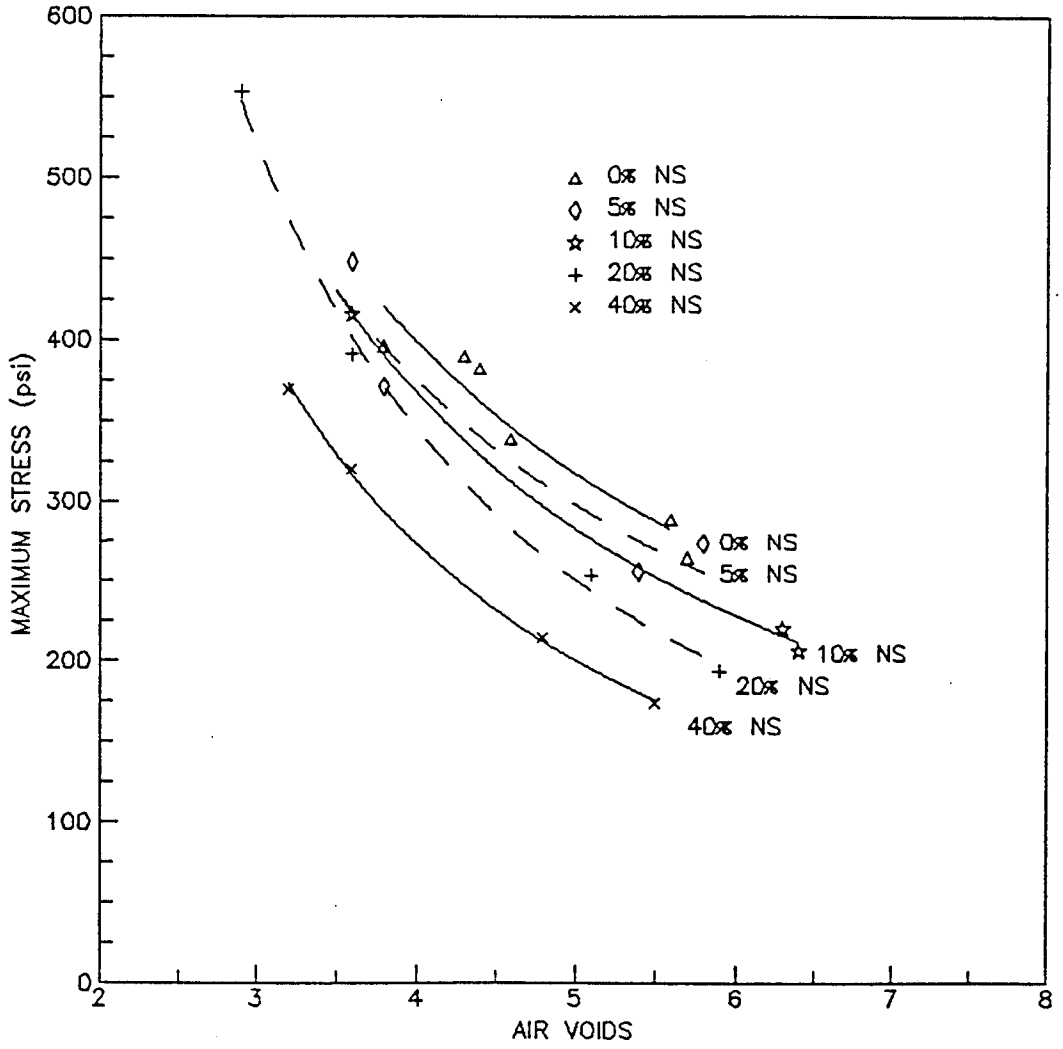

Figure 4.6. Typical unconfined compressive test results (one sample per point).

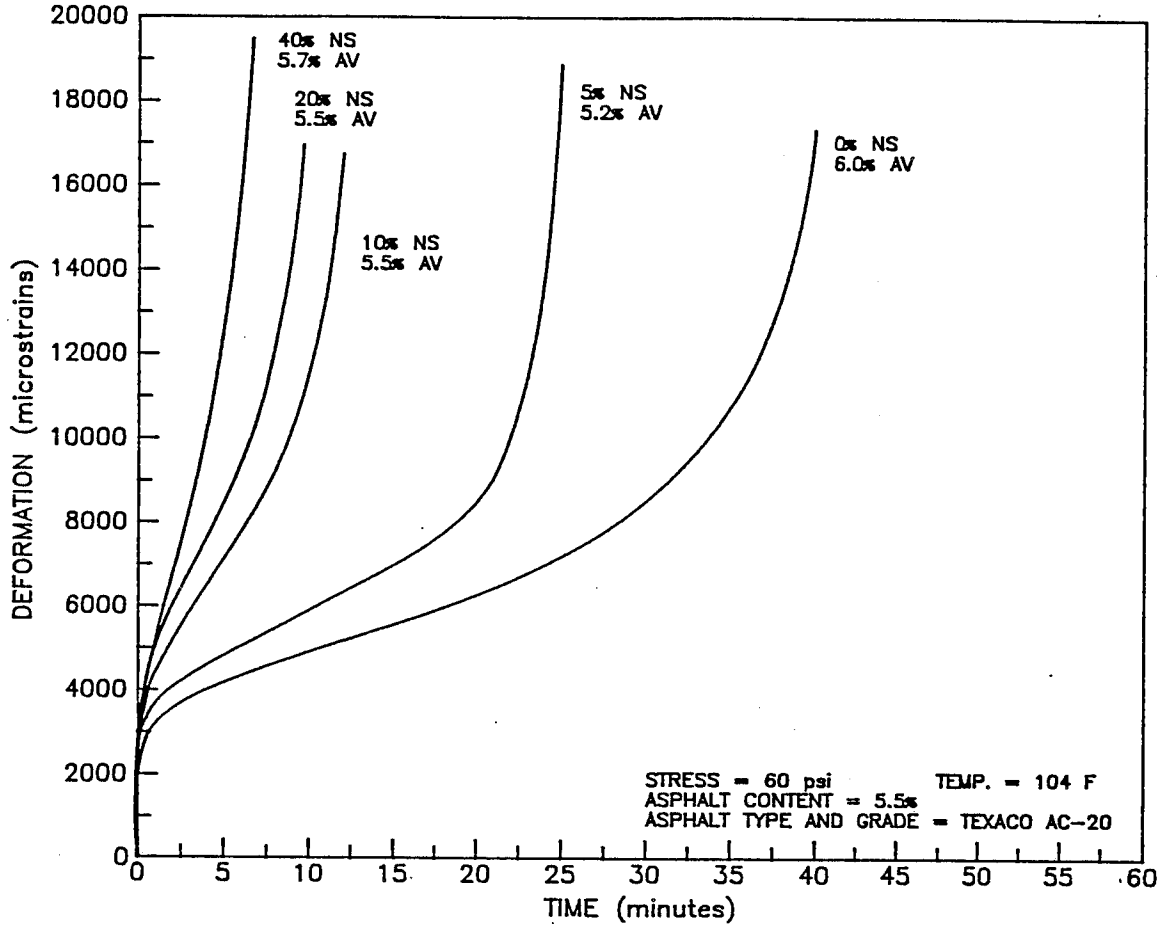

Figure 4.7. Typical relations of total deformation for the long-term static creep test at HIGH air void contents (NS = natural sand, AV = air voids).

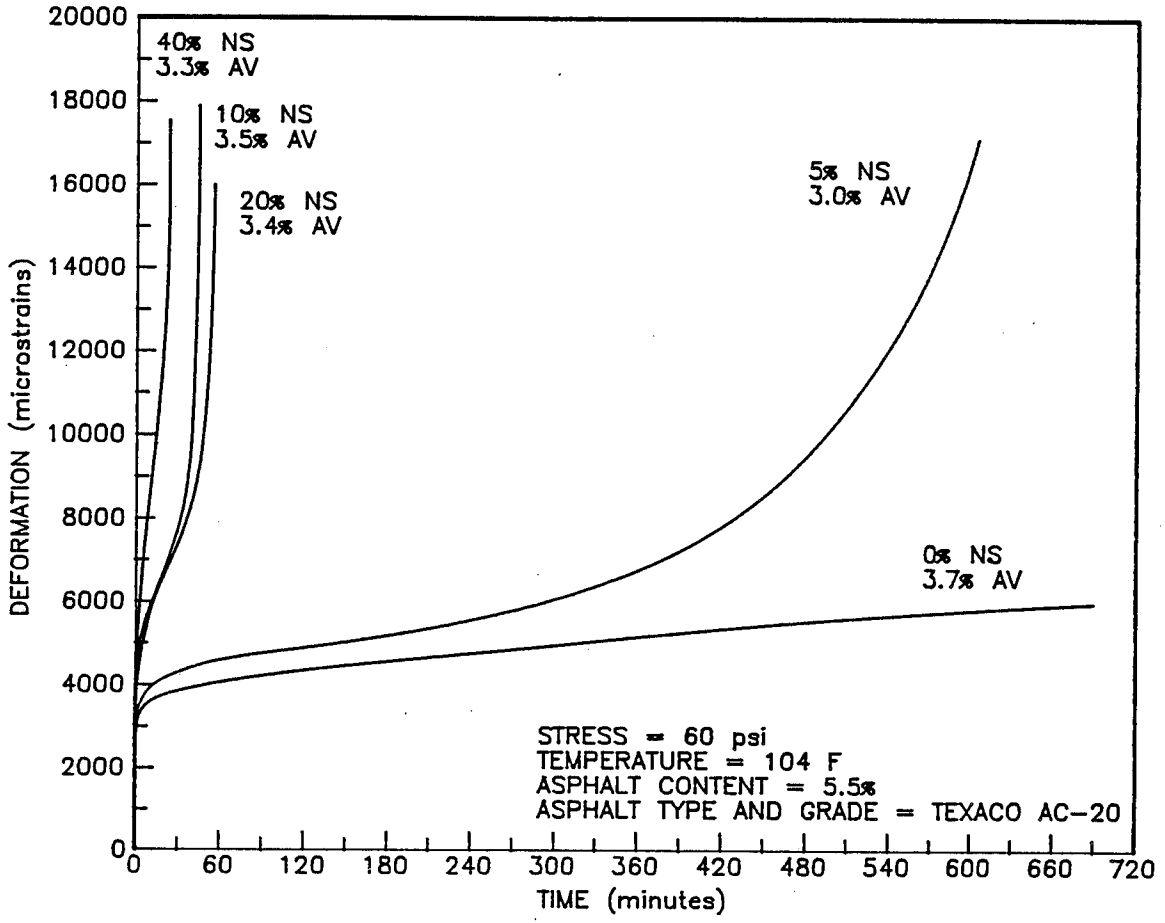

Figure 4.8. Typical relations of total deformation for the long-term static creep test at LOW air void contents (NS = natural sand, AV = air voids).

that aggregate interlock is lost and shear strength is dramatically reduced).

3. A large difference in deformation trends is observed between the mixtures containing zero and 10 percent natural sand. These data indicate that 10 percent natural sand in this mix is an excessive quantity if substantial resistance to deformation is an objective of the mixture.

Typical long-term cyclic unconfined compression test results are presented in Figures 4.9 and 4.10. All remaining test results are presented in Figures B.11 through B.20 in Appendix B. In the analysis of these results, basically the same conclusions as for the static creep test discussed above were found. Furthermore, the data indicate that larger deformations are obtained in unconfined repeated loading than in creep at comparable times of loading (e.g., 6000 repetitions at 0.1 sec per repetition would be comparable to 600 sec loading time in the creep test).

Phase II Test Results

The test used to characterize the mixtures in this phase was the triaxial cyclic test (Appendix A). Only the 20 percent, 10 percent, and zero percent natural sand mixes were analyzed in this phase. A partial factorial test matrix was developed (Figure 4.11) in order to study the effects of asphalt content and temperature among the three selected mixtures under a constant confining pressure (15 psi). The deviator stress was 60 psi as in the case of the unconfined static and cyclic tests. Optimum asphalt contents, as shown below, were used for each mixture:

MIXTURE TYPE	OPTIMUM ASPHALT CONTENT
0% natural sand	5.8%
10% natural sand	5.7%
20% natural sand	5.5%

Asphalt contents were then varied from 0.8 percent less than optimum, to 0.8 percent more than optimum, for selected mixtures (Figure 4.11).

Results from phase II are presented in Figures 4.12 through 4.18. Figures 4.12 through 4.15 show permanent deformation results when number of

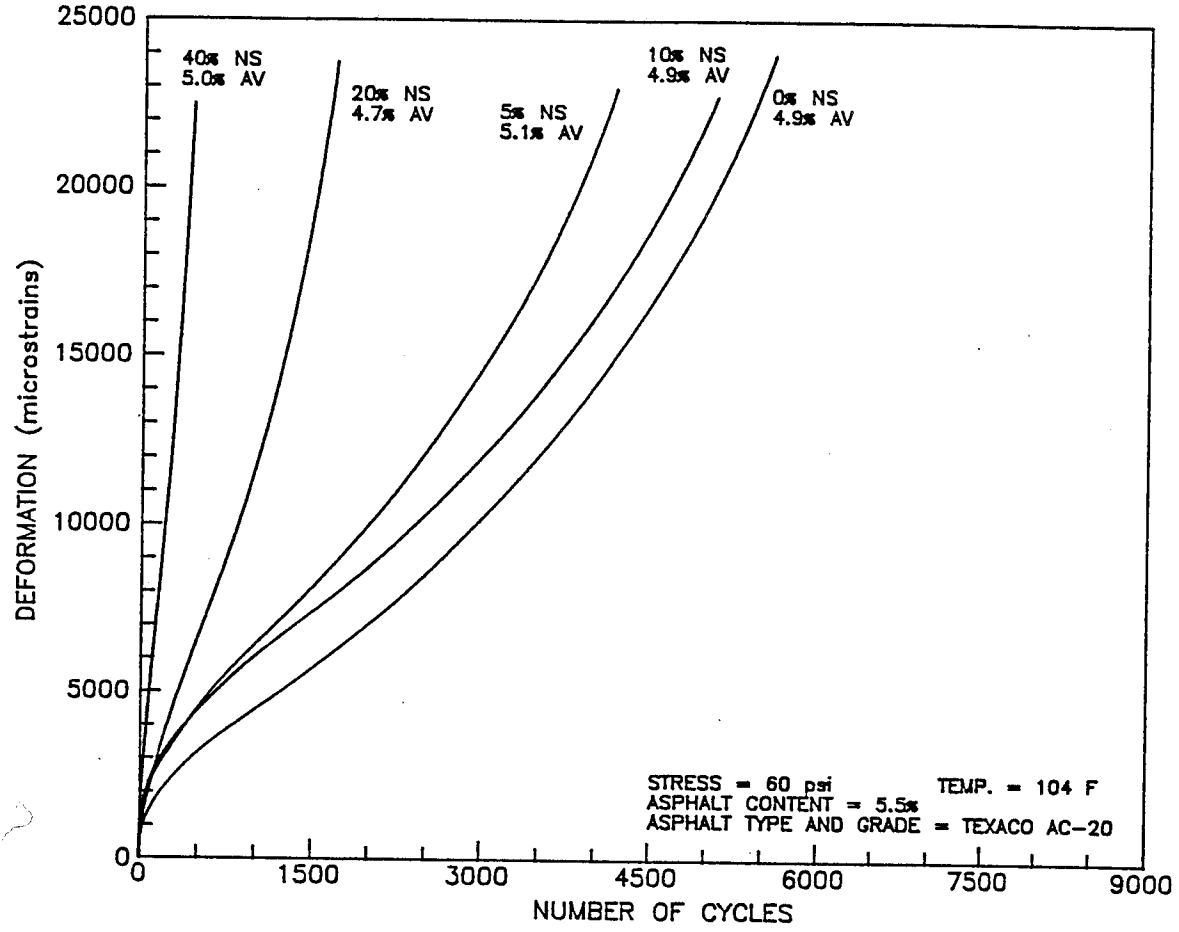

Figure 4.9. Typical relations of permanent deformation for the long-term cyclic test at HIGH air void contents (NS = natural sand, AV = air voids).

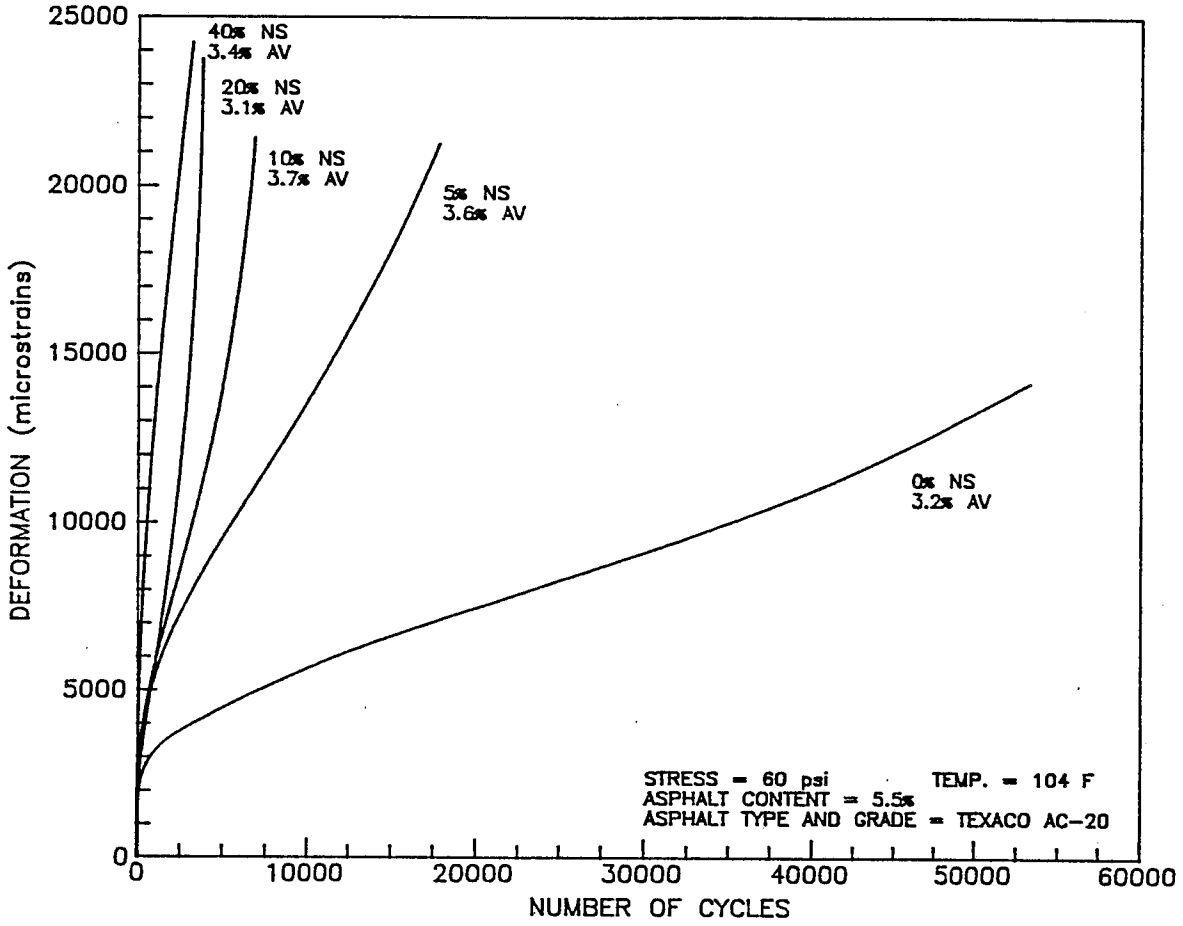

Figure 4.10. Typical relations of permanent deformation for the long-term cyclic test at LOW air void contents (NS = natural sand, AV = air voids).

AIR VOIDS	TEMP. °F	ASPHALT CONTENT	20% NATURAL SAND	10% NATURAL SAND	0% NATURAL SAND
HIGH (5-7%)	104	-0.8%	X		X
		OPT.	X	X	X
		+0.8%	X		X
	122	-0.8%			
		OPT.	X	X	X
		+0.8%			
LOW (3-4%)	104	-0.8%	X		X
		OPT.	X	X	X
		+0.8%	X		X
	122	-0.8%			
		OPT.	X	X	X
		+0.8%			

Figure 4.11. Test matrix developed for the triaxial cyclic test.

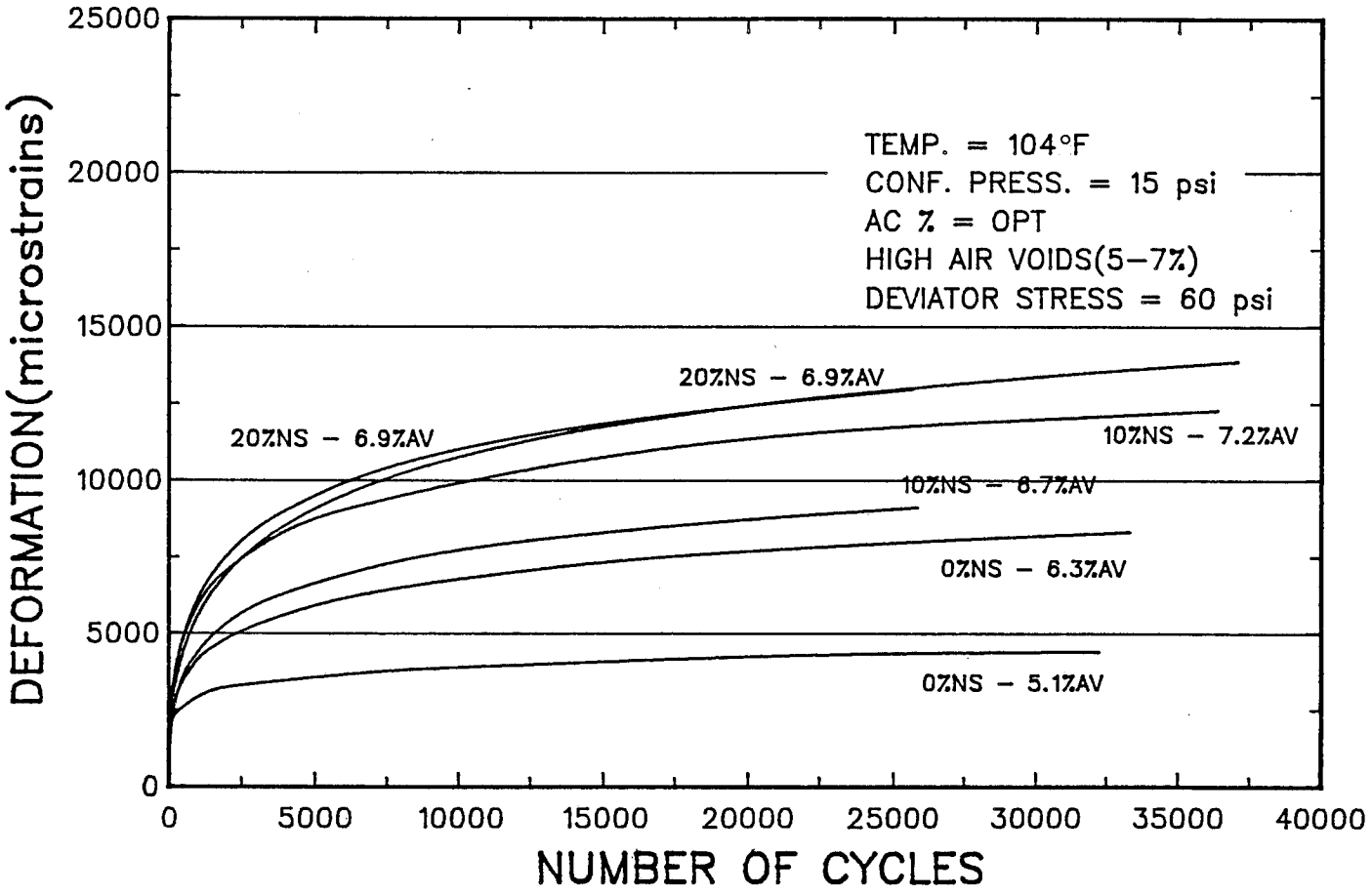

Figure 4.12. Typical relations of permanent deformation for the triaxial cyclic test at HIGH air void contents and 104°F.

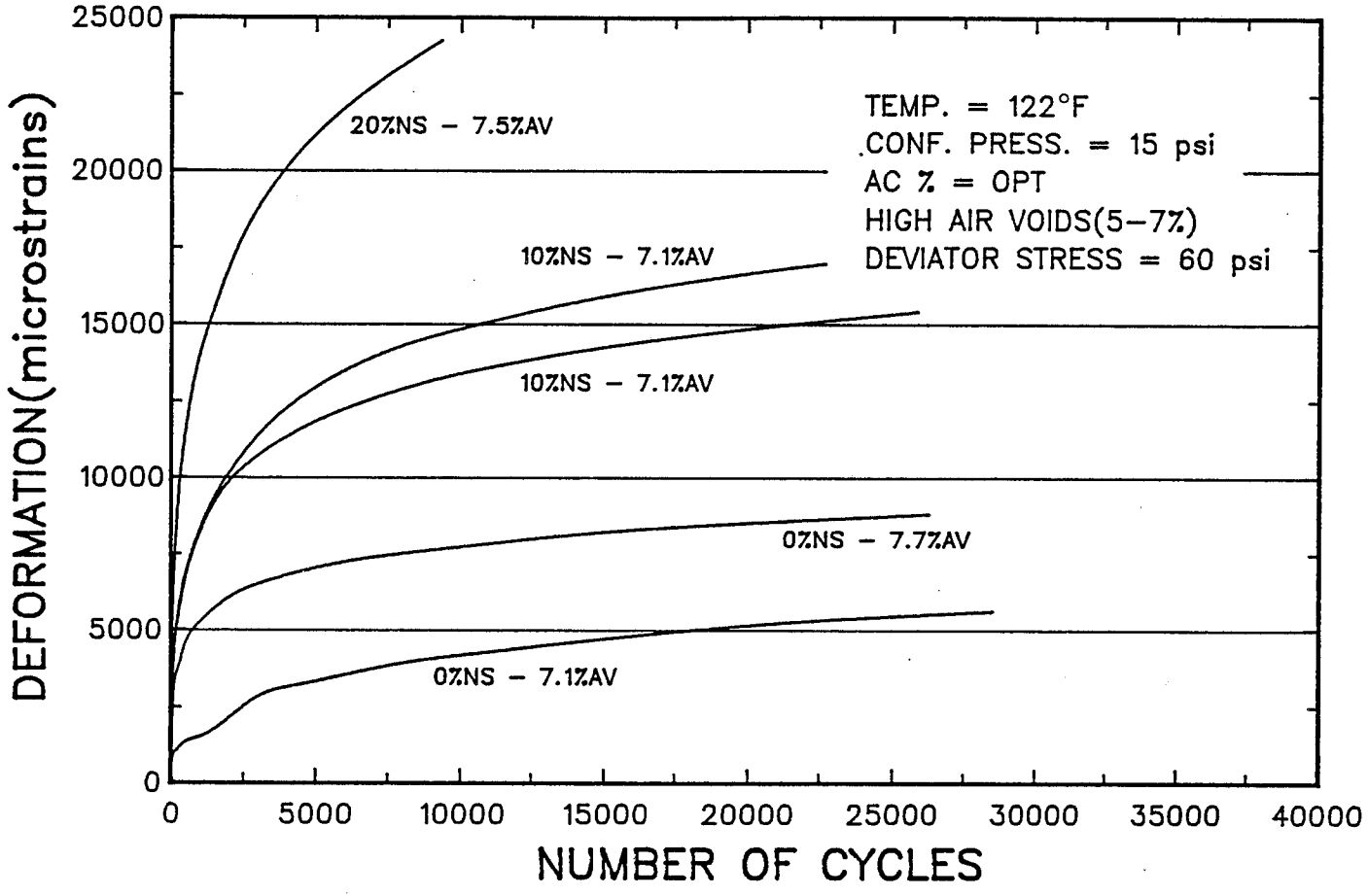

Figure 4.13. Typical relations of permanent deformation for the triaxial cyclic test at HIGH air void contents and 122°F.

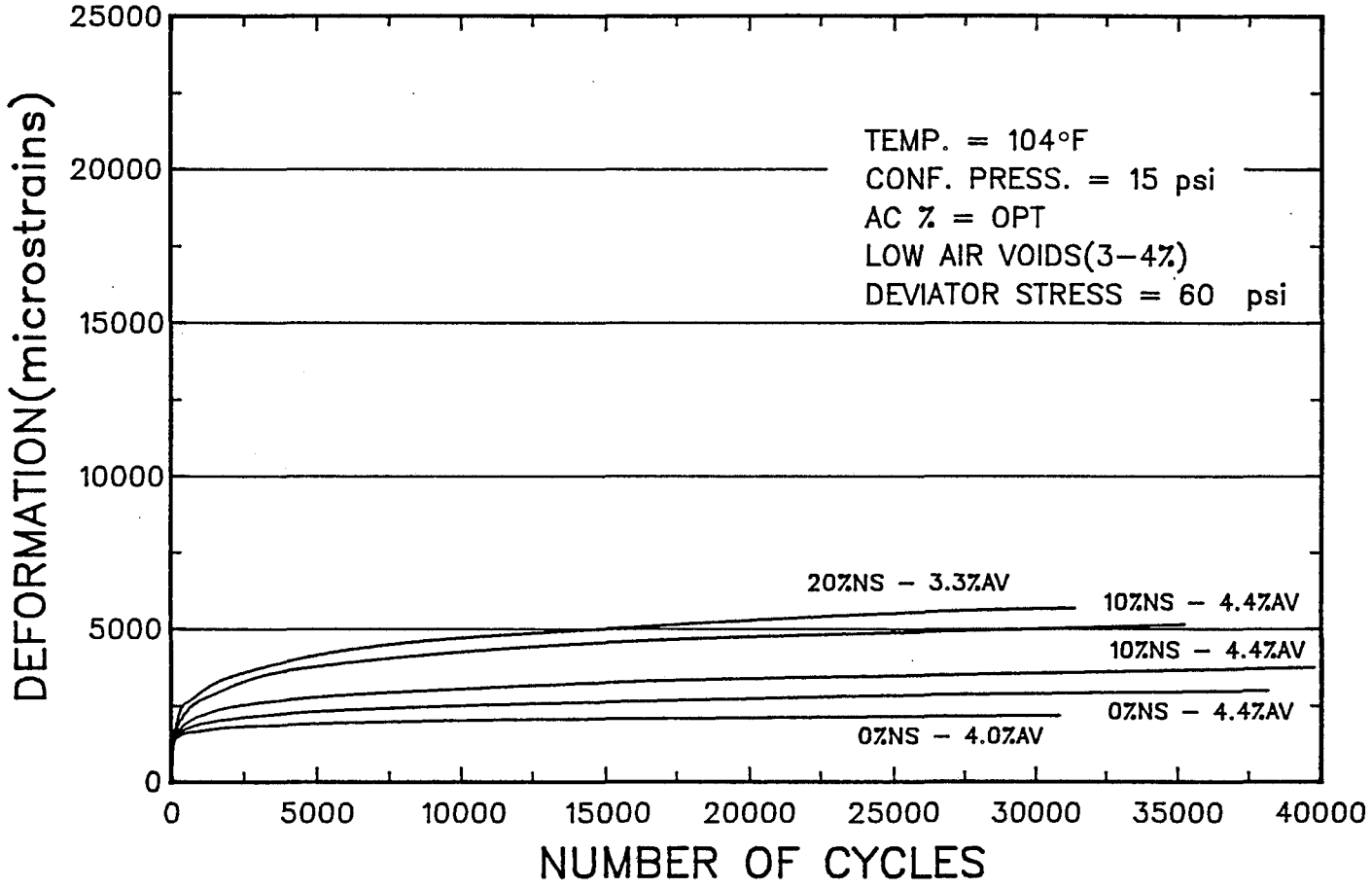

Figure 4.14. Typical relations of permanent deformation for the triaxial cyclic test at LOW air void contents and 104°F.

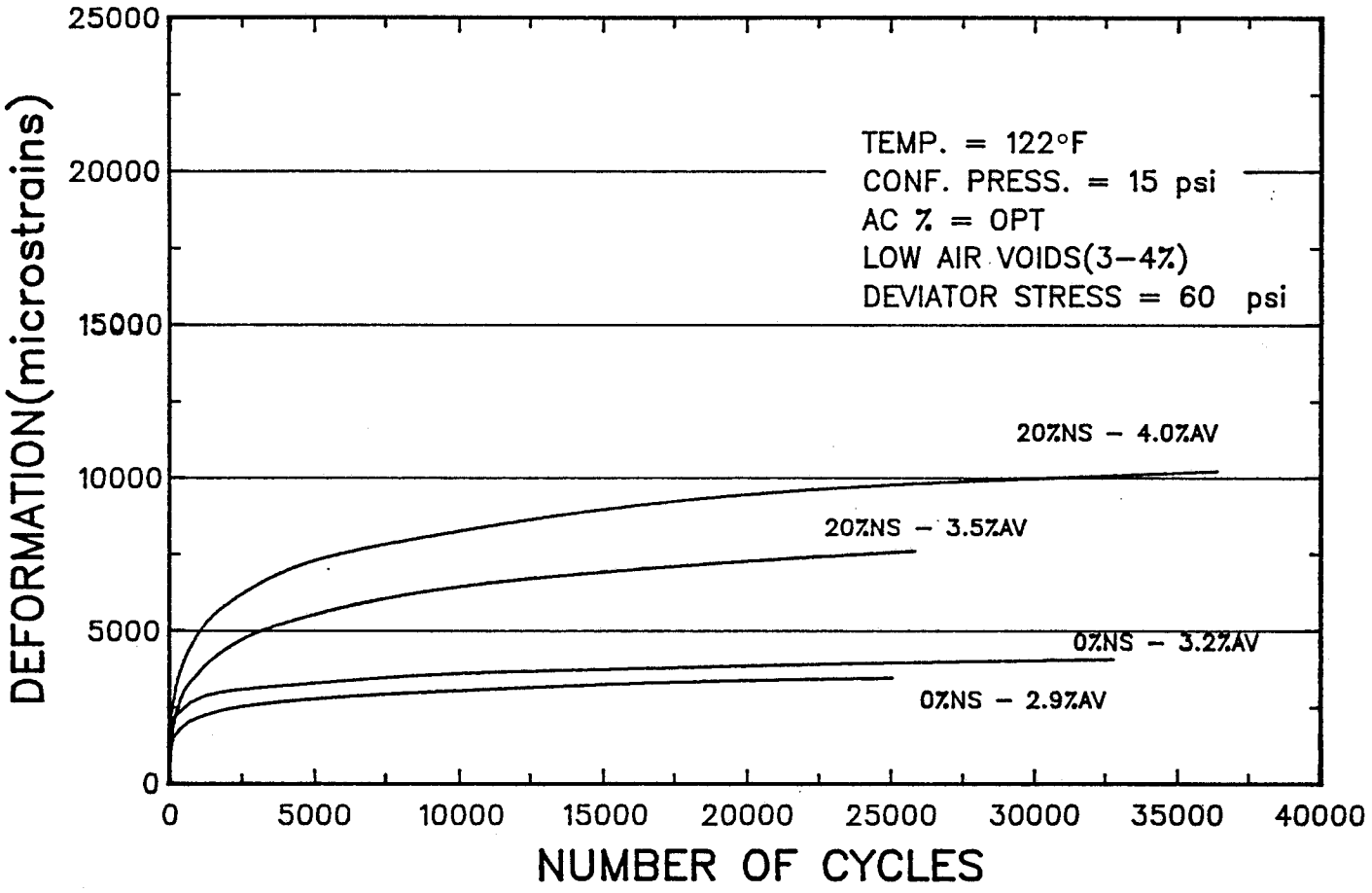

Figure 4.15. Typical relations of permanent deformation for the triaxial cyclic test at LOW air void contents and 122°F.

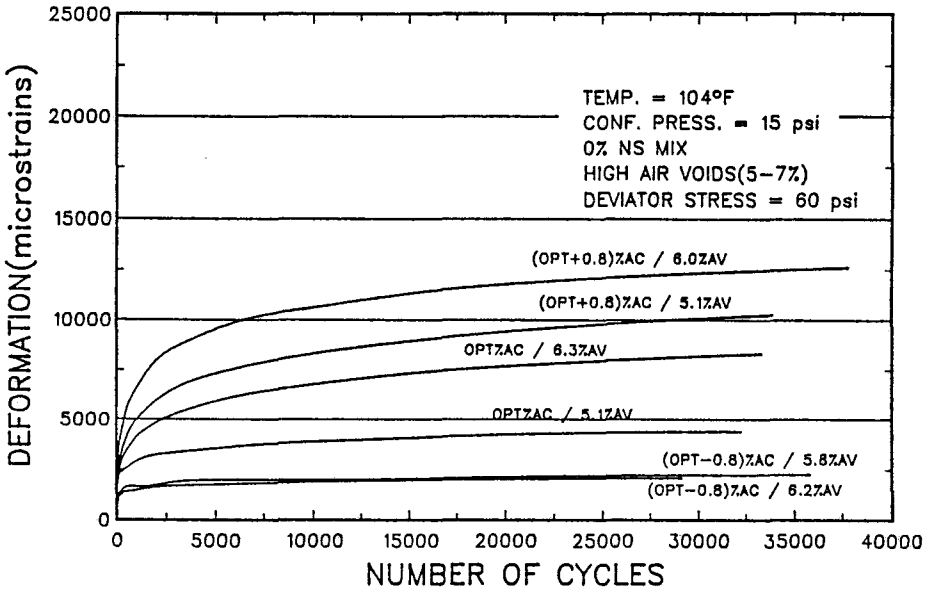

(a)

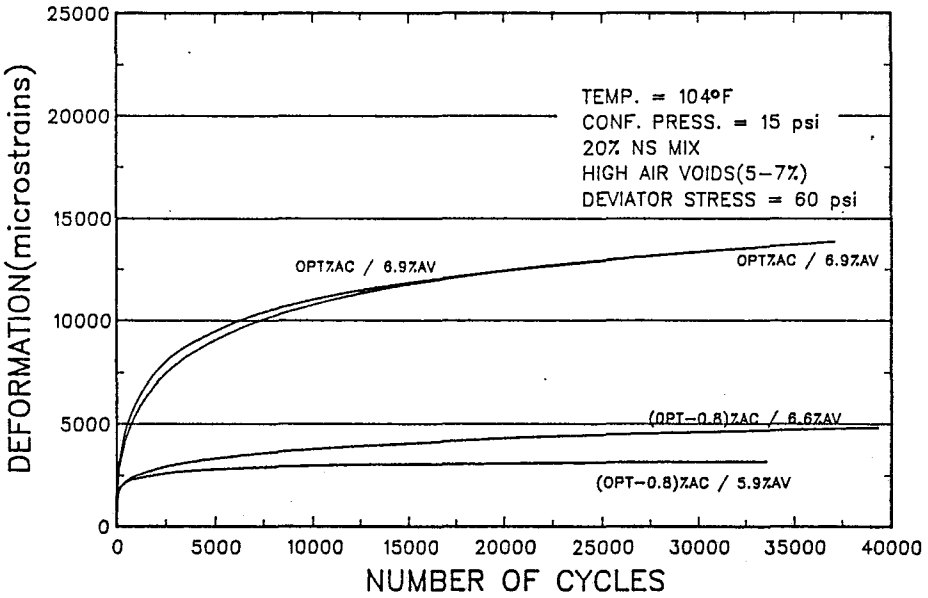

(b)

Figure 4.16. Typical effect of asphalt content on specimens tested at HIGH air void contents and 104°F for a) zero percent natural sand mixes, and b) 20 percent natural sand mixes.

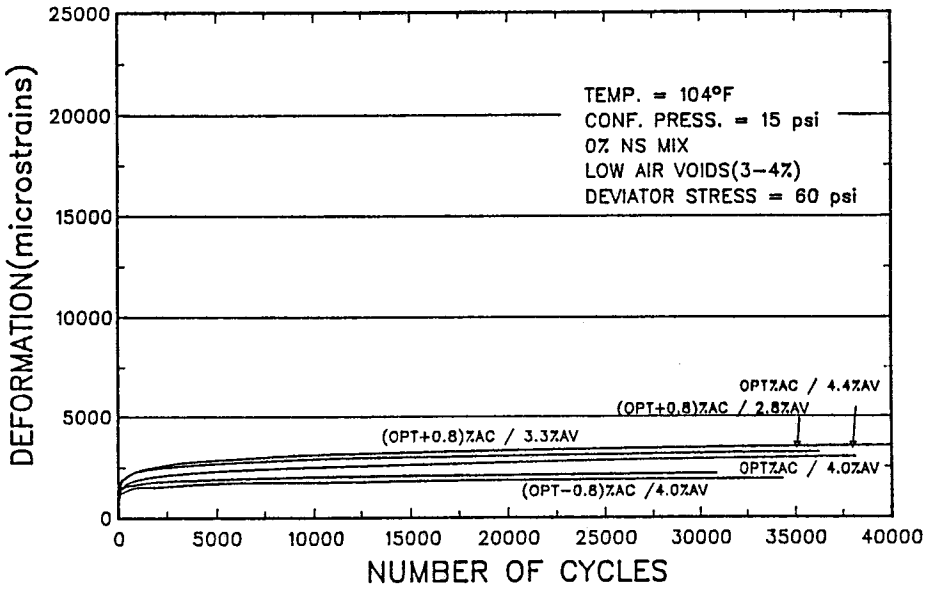

(a)

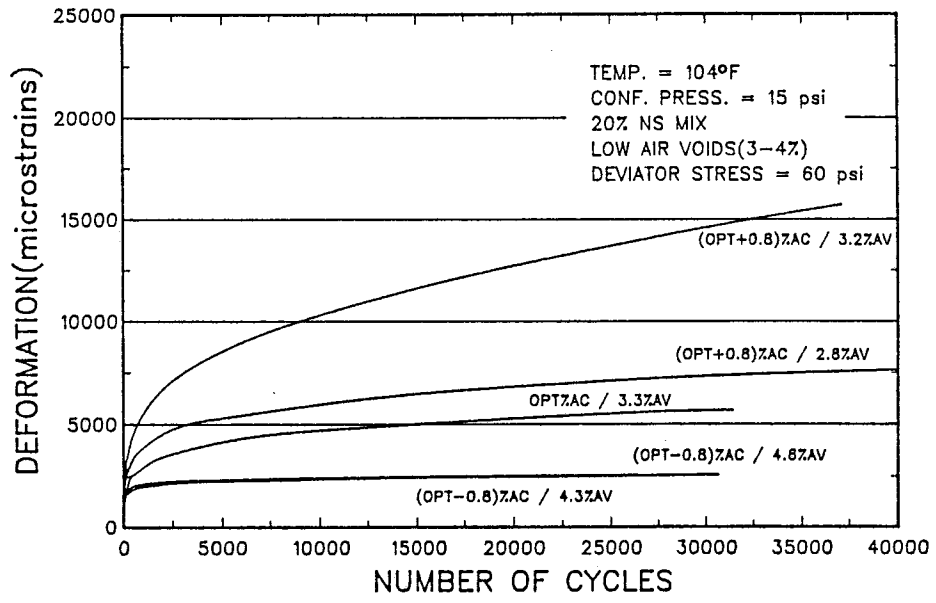

(b)

Figure 4.17. Typical effect of asphalt content on specimens tested at LOW air void contents and 104°F for a) zero percent natural sand mixes, and b) 20 percent natural sand mixes.

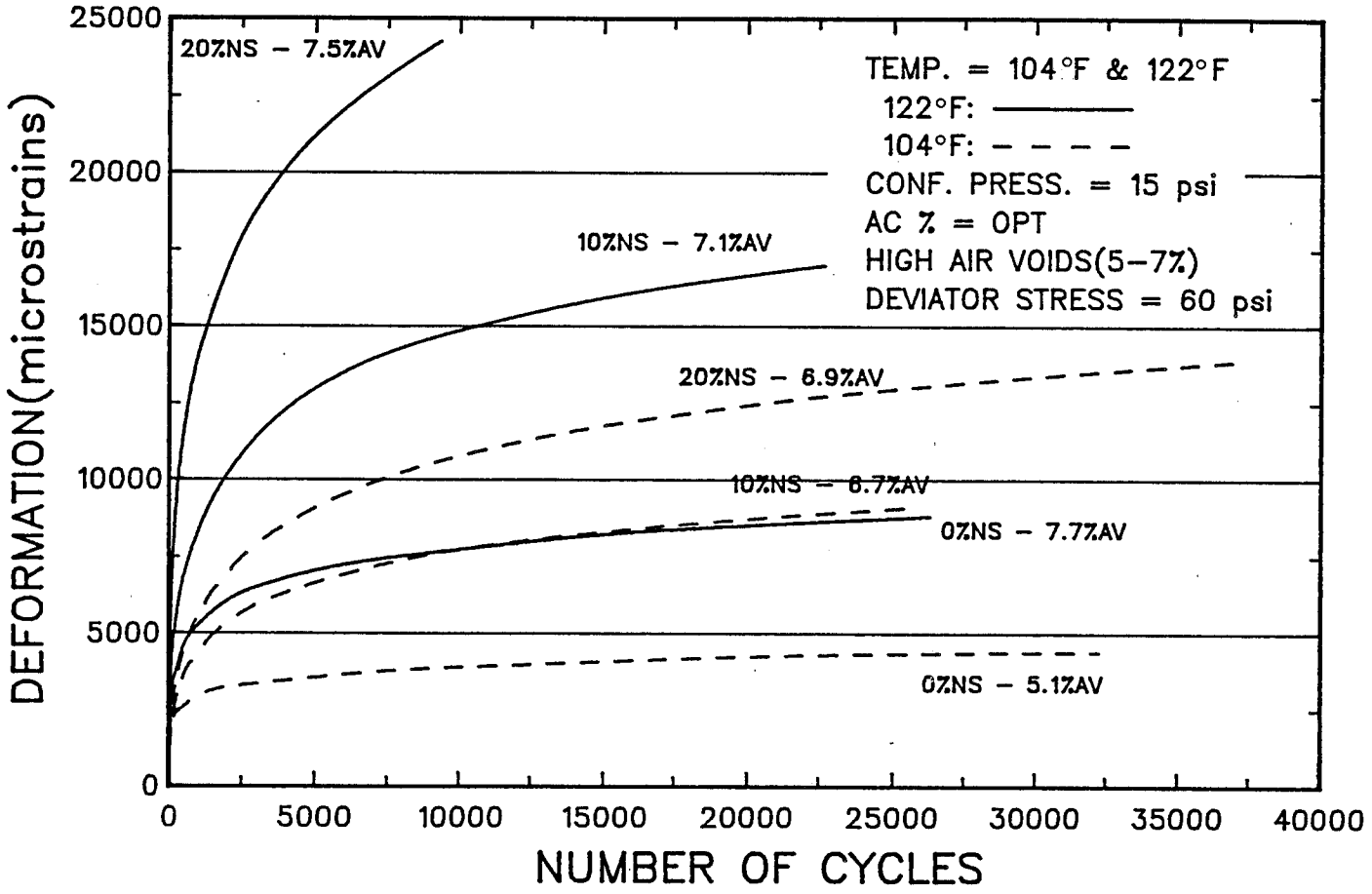

Figure 4.18. Typical effect of temperature on specimens tested at HIGH air void contents and optimum asphalt content.

load applications is varied for all mixtures at two different temperatures and two levels of air void content. Figures 4.16 and 4.17 demonstrate the effect of asphalt content at both high and low levels of air void content for tests at 104°F. Specimens containing 20 percent natural sand with optimum plus 0.8 percent asphalt content could not be fabricated using the kneading compactor because the mix was to unstable. Figure 4.18 illustrates the effect of temperature on permanent deformation for specimens prepared at the high air void content (post-construction level).

An analysis of the results from the confined compression tests is summarized below:

1. At optimum asphalt contents and high air void contents (Figures 4.12 and 4.13), the 20 percent natural sand mix is much more susceptible to permanent deformation than the zero percent natural sand mix, with the 10 percent natural sand mix lying in between. Susceptibility to permanent deformation increases dramatically with an increase in temperature from 104°F to 122°F.
2. At optimum asphalt contents and low air void contents (Figures 4.14 and 4.15) the permanent deformations of the mixes are different, but much less different than in the high air voids mixes (Figures 4.12 and 4.13).
3. At high air void contents, the 20 percent natural sand mix is much more sensitive to asphalt content than the zero percent natural sand mix (Figure 4.16). This is manifested by the fact that high air void mixes containing 20 percent natural sand with optimum plus 0.8 percent asphalt were too tender to permit fabrication of specimens. It is observed from Figure 4.16 that the increase in asphalt content (0.8 percent) produces about two-fold more variation in permament deformation in the 20 percent natural sand mix than in the zero percent natural sand mix.
4. At low air void contents, the 20 percent natural sand mix is also more sensitive to asphalt content than the zero percent natural sand mix (Figure 4.17), but the difference is less than in the high air voids case.
5. Finally, it can be deduced from Figure 4.18 that, at high air void contents, the change in permanent deformation due to changes in temperature increases with increasing percentage of natural sand

in the mixture. In other words, a 20 percent natural sand mix shows a much greater change in permanent deformation with change in temperature than does a zero percent natural sand mix.

All these findings indicate that 20 percent natural sand in this mixture is an excessive quantity for achieving low permanent deformations during long periods of cyclic loading. Furthermore, results show that asphalt mixtures containing natural (rounded) sand plastically deform much more readily than similarly graded mixtures containing only manufactured (crushed) particles. The reader is reminded that all the plus No. 4 sieve-size material in the five mixtures tested was crushed limestone.

Further, it was found that the unconfined long-term tests (static creep and cyclic), along with the triaxial cyclic test, proved to be capable of identifying permanent deformation susceptibility in mixtures containing natural sand, once the proper stress and temperature conditions are selected.

It should be pointed out that the results of these laboratory experiments were as expected. The five mixtures were designed to demonstrate the quality loss when round sand particles replace angular particles and to provide a medium to develop or investigate laboratory tests capable of identifying rut-susceptible asphalt concrete mixtures.

CHAPTER V
THEORETICAL APPROACH

The novel theoretical approach described in this chapter will ultimately become an important tool in the analysis and comparison of rut susceptible mixtures. The approach is founded on the study of the creep and recovery behavior of asphalt concrete mixtures by means of hyperbolic equations, which ideally model the deformation performance of the mixture.

In this chapter, a brief background of the most widely used permanent deformation models, along with their characteristic equations, will be presented. Subsequently, the hyperbolic equations will be thoroughly described, followed by an example with experimental data. The concept of a "p" value will be assessed at this point, along with an explanation of how the "p" value can be used to compare performance of mixtures containing different percentages of natural sand (increasing rut-susceptibility with increasing percentage of natural sand). A description of how to incorporate the equations in a rutting model will be given. Finally, important conclusions related to the theoretical approach will be ascertained.

Background

Permanent deformation in an asphalt concrete pavement layer under repeated loading has been modeled in different ways. Some of the most commonly used models are briefly described in the following paragraphs.

The VESYS model (34) uses a simple power-law equation to characterize permanent deformation:

$$\epsilon_{vp} = at^b \tag{5.1}$$

where

ϵ_{vp} = viscoplastic strain,

t = time, and

a, b = regression constants.

Other investigators (17, 35) have also used this previous approach except they incorporated additional stress-dependent terms.

Tseng and Lytton (36) developed a three-parameter exponential law for describing permanent deformation behavior. The equation describing the relationship among these three parameters is represented as follows:

$$\epsilon_a = \epsilon_o e^{(\rho/N)^\beta} \tag{5.2}$$

where

ϵ_o = strain level at zero time

ϵ_a = permanent strain,

N = number of cycles, and

ρ, β = regression constants.

This equation was derived from activation energy concepts.

In general, most investigators have agreed upon using a power-law model which, in the majority of the cases, constitutes a linear relationship when deformation and time are plotted on a log-log basis. This is not the case for the hyperbolic model developed, where the deformation increases asymptotically with time, when both are plotted on a log-log basis.

Hyperbolic Model

In the analysis of the creep and recovery compliance behavior of an asphalt mixture, a standard experimental procedure needs to be followed. The procedure chosen in this study consists of the following steps:

1. Precondition the sample (using Shell's recommendations: 1.45 psi for 30 minutes).
2. Load the sample with 14.5 psi (Shell's recommendation) for 1000 secs.
3. Unload the sample for 1000 secs.
4. Record strain vs. time data.

It has been found from actual experimental data obtained by following the procedure described above, that both creep and recovery compliance behavior of the asphalt mixture follow curves similar to the ones shown in Figures 5.1 and 5.2. Using a philosophical approach developed by Badillo (37), one can obtain equations for predicting both the creep and recovery performance of the mixture.

Philosophical Approach. Consider the creep compliance, D(t), under a constant stress for time, t. The problem is to find the infinitesimal change in compliance, dD, under an infinitesimal change in time, dt. The relation between dD and dt should produce an equation that satisfies the following philosophical principle:

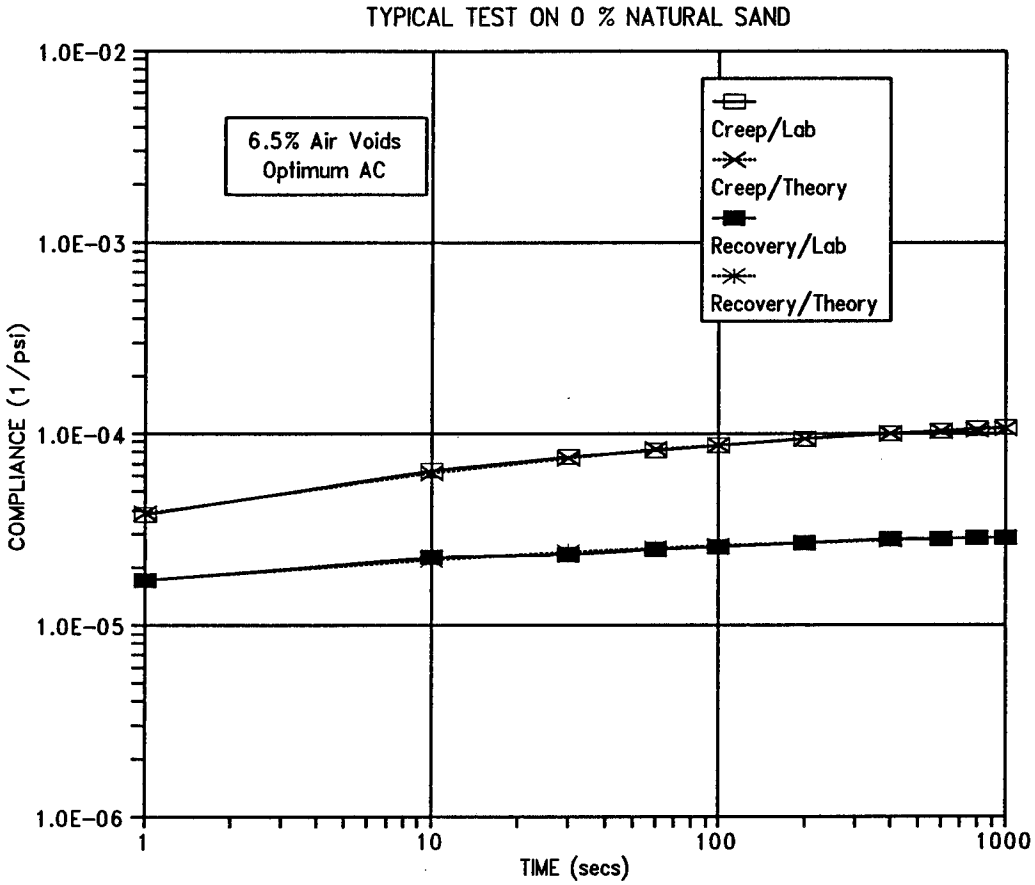

Figure 5.1. a) Logarithmic representation of typical creep and recovery behavior of a zero percent natural sand mix at high air void contents.

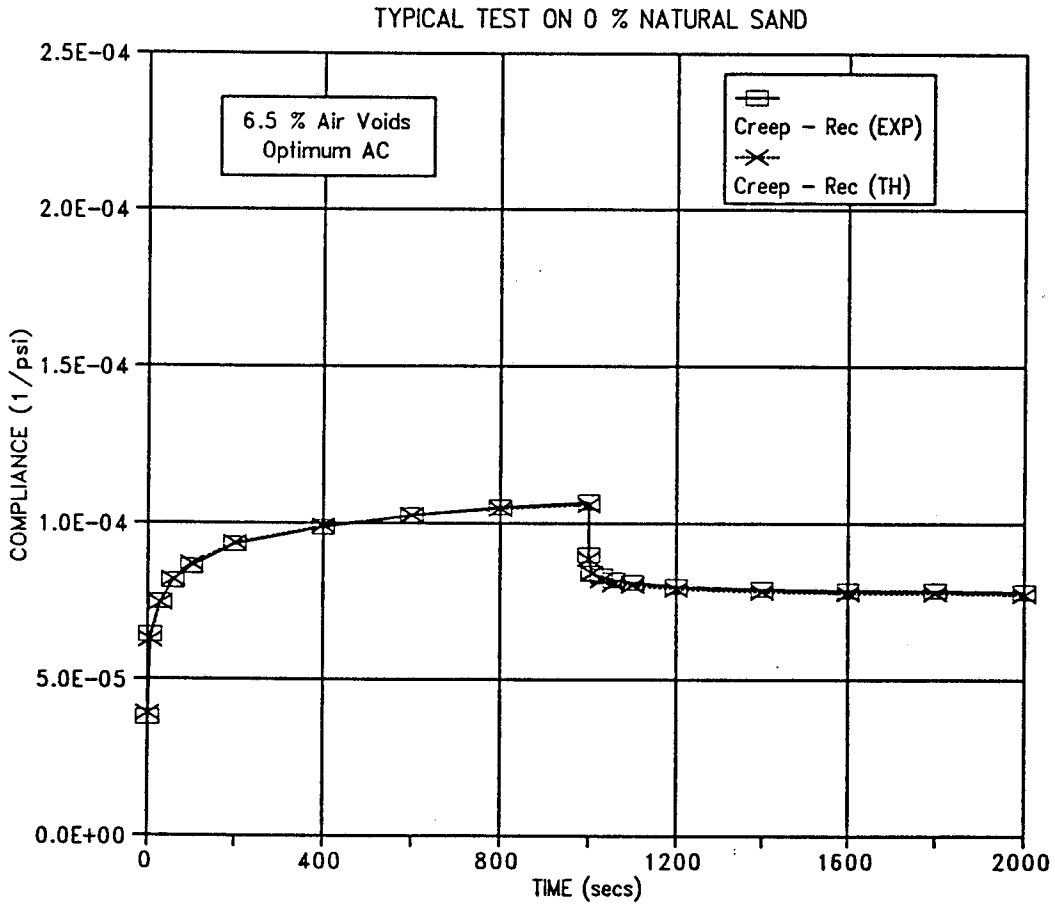

Figure 5.1. b) Linear representation of typical creep and recovery behavior of a zero percent natural sand mix at high air void contents.

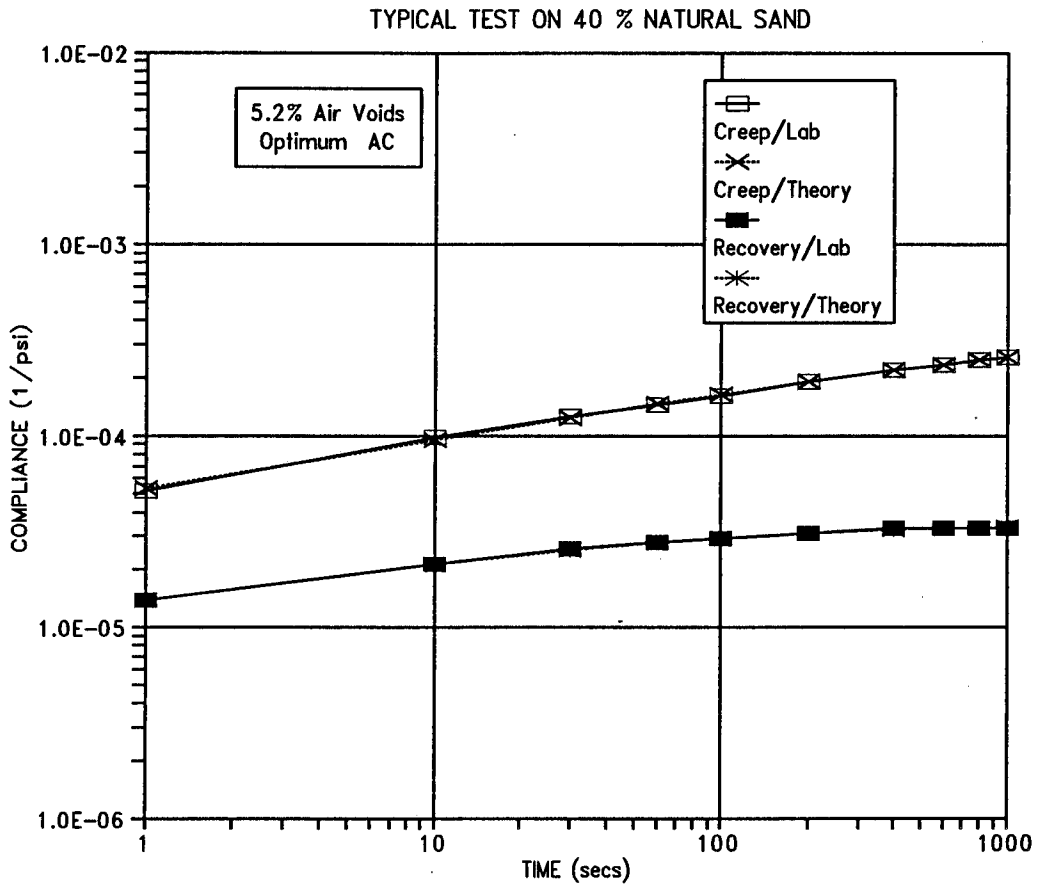

Figure 5.2. a) Logarithmic representation of typical creep and recovery behavior of a 40 percent natural sand mix at high air void contents.

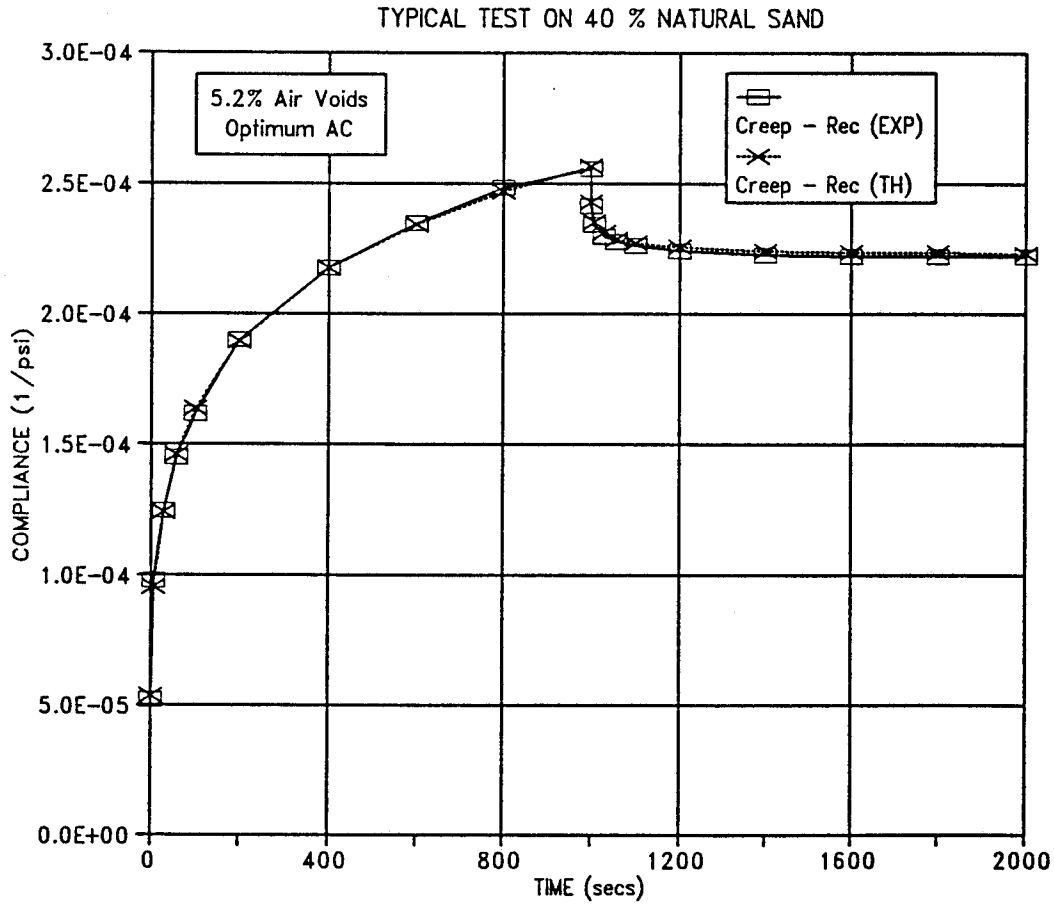

Figure 5.2. b) Linear representation of typical creep and recovery behavior of a 40 percent natural sand mix at high air void contents.

"The equation relating D(t) and t may exist only through a non-dimensional parameter and should, independently of critical points, satisfy the extreme boundary conditions, namely: D = Dm for t = ∞ and D = Do for t = 0".

The link between dD and dt can be obtained through the following steps which adhere to the philosophical approach presented here:

1. The real domain for t is complete, that is, from 0 to ∞, while the real domain for D(t) is incomplete, that is, from Do to Dm. We need to find a function, f(D), with real domain complete and straight, that is f(D) = 0 for t = 0 and f(D) = ∞ for t = ∞. The simplest form of f(D) which achieves these objectives is:

$$f(D) = \frac{1}{Dm - D} - \frac{1}{Dm - Do} \tag{5.3}$$

2. Now f(D) and t are ready to be connected. Based on the philosophical principle mentioned above, the relationship should be:

$$\frac{df(D)}{f(D)} = m \frac{dt}{t} \tag{5.4}$$

where m is a non-dimensional parameter of proportionality, called the non-linear slope factor.

Hyperbolic Equations. After introducing equation 5.3 into equation 5.4, and integrating, one can obtain the following equation which describes the creep compliance behavior of the asphalt mixture:

$$D(t) = \frac{D_o + D_m a t^m}{1 + a t^m} \tag{5.5}$$

where

D_o = initial creep compliance,
D_m = maximum creep compliance,
a = regression constant,
t = time, and
m = slope factor.

The same philosophical approach can be applied to the recovery compliance, even though it shows a different slope factor and a partial strain recovery. The equation obtained for this recovery compliance is represented as follows:

$$R(t) = \frac{R_o + R_m b t^{mp}}{1 + b t^{mp}} \qquad (5.6)$$

where

R_o = initial (elastic) recovery compliance,
R_m = maximum recovery compliance,
b = regression constant,
t = time, and
p = slope factor modifier.

In order to obtain all the unknown parameters in Equations 5.5 (D_o, D_m, a, m) and 5.6 (R_o, R_m, b, p), an optimization technique known as pattern search is used. Pattern search is a technique based on an optimization method developed by Hooke and Jeeves (38). The method consists, basically, of finding the unknown parameters that minimize the sum of the squared differences between observed data and predicted values. In this method, no derivatives are required, and a unimodal function is assumed. A better description of how the algorithm works is given by Kuester and Mize (39).

Test Results

Figures 5.1 and 5.2 show typical results for mixtures with low and high susceptibility to rutting, respectively. The mix considered highly rut susceptible is the 40 percent natural sand mix, while the mix considered to be rut resistant is the zero percent natural sand mix (both described in Chapter III). Both figures include experimental results, as well as theoretical predictions obtained by using the hyperbolic models described above. The results for the remaining cases analyzed are shown in Appendix C.

The results obtained from all the cases analyzed reveal that:

1. The hyperbolic modeling of the creep and recovery behavior produced near-perfect predictions.

2. The value of "p" defined for equation 5.6 increases as the percentage of natural sand in the asphalt mixture increases (Table 5.1).

Based on these results, one can infer that the "p" value accounts for the role of the natural sand in the permanent deformation behavior of asphalt concrete mixtures. This constitutes a novel way of characterizing the influence of the aggregate's physical nature in a permanent deformation model.

Permanent Deformation Model

In this section, a permanent deformation model is derived from equations 5.5 and 5.6.

Suppose that a load pulse of duration Δt is applied repeatedly, N times. Then, both creep and recovery equations may be used to estimate the total deformation and recovery that occurs:

$$D(N) = \frac{D_o + D_m r N^m}{1 + r N^m} \tag{5.7}$$

$$R(N) = \frac{R_o + R_m r_p N^{mp}}{1 + r_p N^{mp}} \tag{5.8}$$

where

N = number of cycles,
r = $a\,(\Delta t)^m\,\rho$,
r_p = $b\,(\Delta t)^{mp}\,\rho_p$,
t = $N\,(\Delta t)$, and
ρ, ρ_p = load pulse factors.

When the load is not a square wave, the term $(\Delta t)^m$ must be multiplied by ρ, which is a function of m and the loading wave shape, and varies between 0 and 1. For a square wave, ρ is equal to 1. The factor, ρ_p, for the recovery curve has the same meaning as ρ, and it is a function of ρ, mp, and the wave shape. For a square wave, ρ_p is also equal to 1.

Table 5.1. Mean "p" values at high air void contents.

Mix type	Mean "p" value for 3 tests
0 % natural sand	0.8
20 % natural sand	1.4
40 % natural sand	1.8

The total accumulated strain, ϵ_a, after N repetitions for a constant stress pulse, σ_o, is defined as:

$$\epsilon_a(N) = \epsilon(N) - \epsilon_r(N) = \sigma_o[D(N) - R(N)] \tag{5.9}$$

where

ϵ_r = recoverable or resilient strain.

The rate of change of the permanent strain for a given load repetition is:

$$\frac{\partial \epsilon_a(N)}{\partial N} = \sigma_o \left[\frac{\partial D(N)}{\partial N} - \frac{\partial R(N)}{\partial N}\right] \tag{5.10}$$

Replacing equations (5.7) and (5.8) in equation (5.10), and dividing by the resilient strain, ϵ_r, gives:

$$\frac{1}{\epsilon_r} \frac{\partial \epsilon_a(N)}{\partial N} = E_r D_m m N^{m-1} \, q(1 - qN^m) \, [(D_m - D_o) - (R_m - R_o)ps] \tag{5.11}$$

where

$$q = \frac{r}{1 + rN^m} \tag{5.12}$$

$$s = \frac{q_p(1 - q_p N^m)}{q(1 - qN^m)} \tag{5.13}$$

$$q_p = \frac{r_p N^{m(p-1)}}{1 + r_p N^{mp}} \tag{5.14}$$

E_r = resilient modulus

Now, recalling the permanent strain response model used in the VESYS approach (34):

$$\frac{\partial \epsilon_p}{\partial N} = \epsilon_r \cdot \mu \cdot N^{-\alpha} \tag{5.15}$$

where

μ, α = parameters determined from equation (5.11),

N = number of cycles,

ϵ_r = elastic or resilient strain, and

$\frac{\partial \epsilon_p}{\partial N}$ = rate of change of permanent strain with load repetitions.

Thus, if

$$\mu N^{-\alpha} = \frac{1}{\epsilon_r}\left[\frac{\partial \epsilon_a}{\partial N}\right]$$

then, it is apparent from equation (5.11) that

$$\alpha = 1\text{-}m \tag{5.16}$$

and

$$\mu = E_r D_m mq\ (1 - qN^m)\ [(D_m - D_o) - (R_m - R_o)ps] \tag{5.17}$$

where

$$s = \frac{q_p(1 - q_p N^m)}{q(1 - qN^m)} \tag{5.18}$$

The μ and α parameters defined in equations 5.16 and 5.17 can be easily incorporated into the Texas Flexible Pavement System (TFPS) program (40) developed at the Texas Transportation Institute in order to predict rutting. In this approach, the loading-unloading response (σ-ϵ curve) of the pavement material is modeled as in Figure 5.3. The strain response is decomposed into ϵ_e-elastic (resilient) strain, and ϵ_p-permanent strain. The total strain, ϵ_t, is the sum of $\epsilon_e + \epsilon_p$. The elastic (resilient) strain remains fairly constant during the life of the pavement except at low number of load repetitions and near failure. The change in permanent strain per load application ($\Delta\epsilon_p$) decreases with the number of load applications until the sample reaches failure, where it starts to increase dramatically (26). In general, the permanent strain is represented by equation (5.9).

From Figure 5.3 it is observed that

$$E_{lo}(N) = \frac{\sigma}{\epsilon_t(N)} = \text{modulus during loading} \tag{5.19}$$

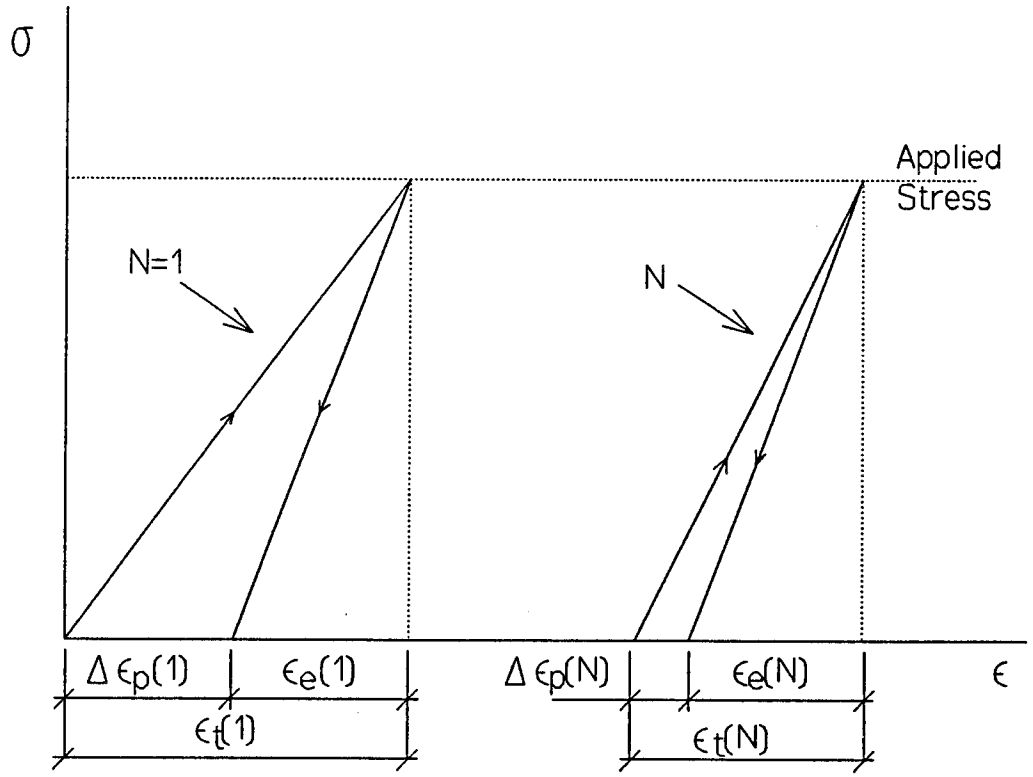

Figure 5.3. Typical loading - unloading response for an asphalt pavement material.

$$E_{un} = \frac{\sigma}{\epsilon_e} \quad = \quad \text{modulus during unloading} \tag{5.20}$$

Now, rewriting Equation 5.19 by using Equation 5.15 gives:

$$E_{lo}(N) = \frac{\sigma}{\Delta\epsilon_p(N) + \epsilon_r} = \frac{\sigma}{\frac{\partial\epsilon_p}{\partial N} + \epsilon_r} = \frac{\sigma}{\epsilon_r(1 + \mu N^{-\alpha})} = \frac{E_{un}}{1 + \mu N^{-\alpha}} \tag{5.21}$$

This equation provides a relation between $E_{lo}(N)$ and E_{un} (constant), as a function of α, μ, and N. The permanent deformation during loading is then calculated by subtracting the surface rebound, calculated while all the pavement layers are assigned the unloading moduli (E_{un}), from the surface deflection, calculated while all pavement layers are assigned the loading moduli (E_{lo}).

The influence of natural sand in this rutting model can be seen in Figure 5.4, where the loading moduli (E_{lo}), obtained from equation 5.21, is plotted against the number of cycles for both 40 percent and 0 percent natural sand typical mixes. It is observed that the loading moduli values are higher for the 0 percent natural sand mix, indicating less permanent deformation with number of cycles.

Summary

The hyperbolic model described in this chapter provides a near perfect predictor of actual creep and recovery performance of asphalt mixtures. The "p" value defined within the hyperbolic model shows a strong correlation with the percentage of natural sand in a mix, hence, it accounts for the influence that the character of the aggregate particles has on deformation behavior.

The hyperbolic models for creep and recovery can be mathematically transformed, as shown in previous pages, into a permanent deformation prediction model. Additional work is required to perform a complete calibration of the permanent deformation model developed, and to compare it with other currently used models.

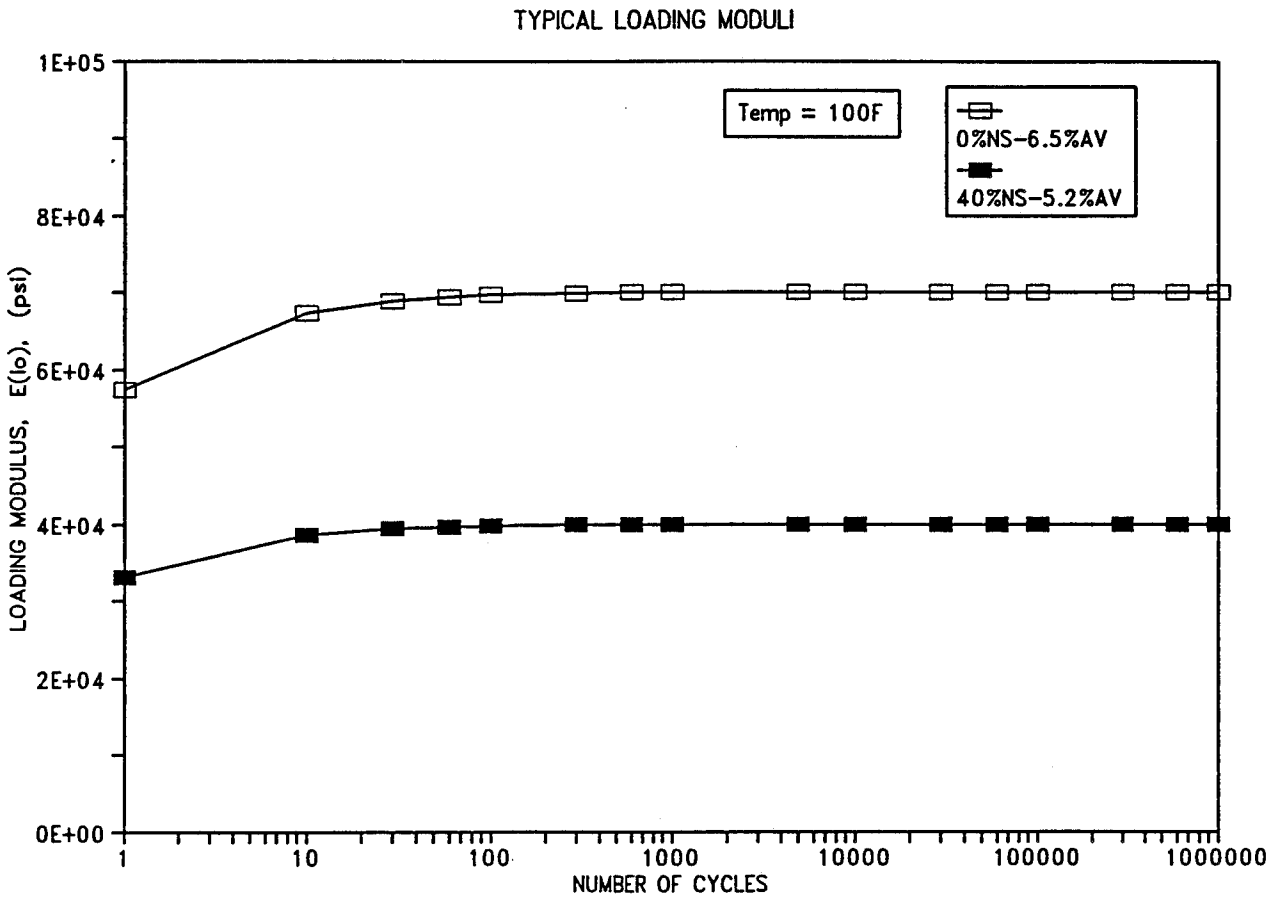

Figure 5.4. Loading modulus versus number of load applications for typical zero percent and 40 percent natural sand mixes at high air void contents.

CHAPTER VI
FRACTAL DIMENSION ANALYSIS

In nature there are many objects such as trees, mountains, clouds, rivers, and rocks, whose shapes and textures are so complex and so erratic that they are very difficult to analyze and model in an objective manner by using simple geometry. For some engineering applications, there is a need for a model that allows a high degree of erratic behavior. Irregular shapes and textures have been characterized with a high degree of success by the concept of fractals, introduced by Mandelbrot (41, 42).

Description of Fractals

Fractals are a family of mathematical functions that describe natural phenomena and shapes. As a result, the theory has begun to receive considerable attention as a method used for texture analysis and, in general, for describing natural surface shapes (41, 42, 43, 44).

The defining characteristic of fractals is that they possess a fractal dimension. The fractal dimension of a surface corresponds closely to the intuitive notion of roughness. Measurement of the two-dimensional image fractal dimension allows an estimation of the three-dimensional fractal dimension, and this three-dimensional fractal dimension relates well to the popular perception of roughness (45). Thus, the three-dimensional fractal model allows one to determine which imaged regions are observed as rough, and which appear smooth.

In order to evaluate the fractal dimension, a black-and-white digitized image of the surface in question is required. This digitized image is obtained from either a photograph or a video frame, and then analyzed by a computer program that includes the fractal mathematical functions.

The digitized video image must be black and white because the analysis of fractal dimensions is based on a gray scale. The gray levels of an image are usually plotted on a histogram. This gray-level histogram is a function that gives the frequency of occurrence of each gray level in the image (46). In other words, if the gray levels are measured from 0 to n, the value of the histogram at a particular gray level p, denoted h(p), is the number of pixels (any of the small discrete elements that together constitute an image) in the image with that gray level.

Now, for a two-dimensional gray scale image, the fractal dimension, D,

is a number representing how tightly the gray scale surface has been "folded" into three dimensions. Higher fractal dimensions are produced by abrupt, large-scale changes, while lower fractal dimensions are produced by gradual small-scale changes.

Experimental Analysis

The hypothesis, in the experimental analysis, was that images of crushed limestone aggregate had a higher fractal dimension than images of uncrushed river gravel aggregate, and that the difference between their fractal dimension was statistically significant.

Four different sets of digitized images (from black-and-white video frames) were analyzed with the help of the Mayo Foundation in Rochester, Minnesota (Since this analysis was performed, a TTI computer program that supports fractal analysis has been developed). Each set consisted of two images of the same material, each taken at a different location in the layer of aggregate. The images representing each set are shown in Figures 6.1 and 6.2. In the analysis, four different procedures were followed. First, a 400 x 400 pixel region of each digitized image was analyzed. Mean fractal dimension, D, values for the coarse river gravel is 2.34 and for the crushed limestone is 2.46. This difference seems insignificant until one realizes the maximum possible range of values is 2.0 to 3.0; then the difference becomes quite significant. From the results of this first procedure (Table 6.1), two major conclusions can be drawn:

1. For both sizes of material (coarse and fine), the crushed limestone images have a higher fractal dimension than the river gravel images of the same size.
2. The fine aggregate images have a significantly higher fractal dimension than the corresponding coarse aggregate images.

The second procedure consisted of analyzing five non-overlapping 128 x 128 pixel subregions (within the whole image) for the purpose of obtaining more statistical information. From the results of this second procedure (Table 6.2), the following conclusions can be drawn:

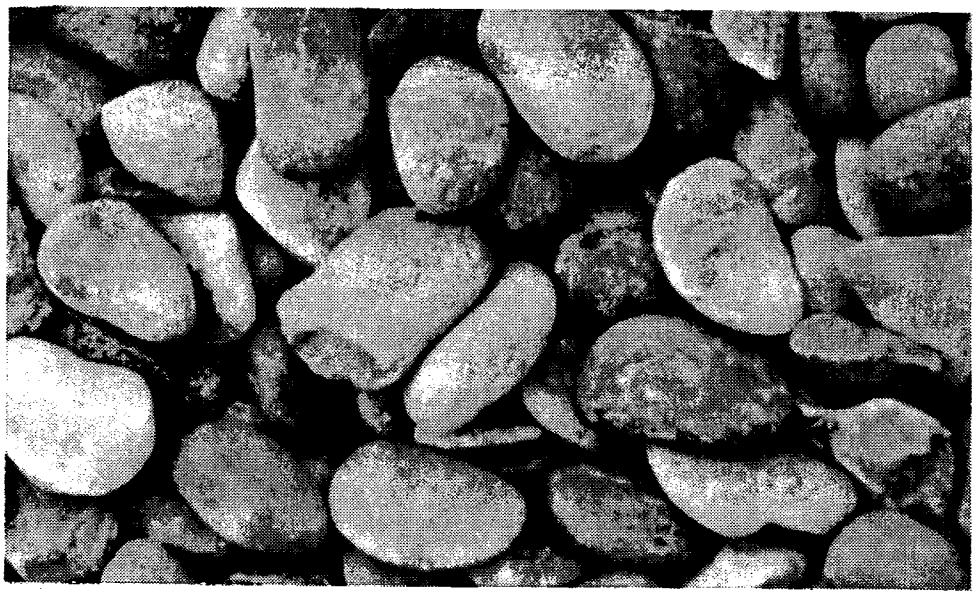

(a)

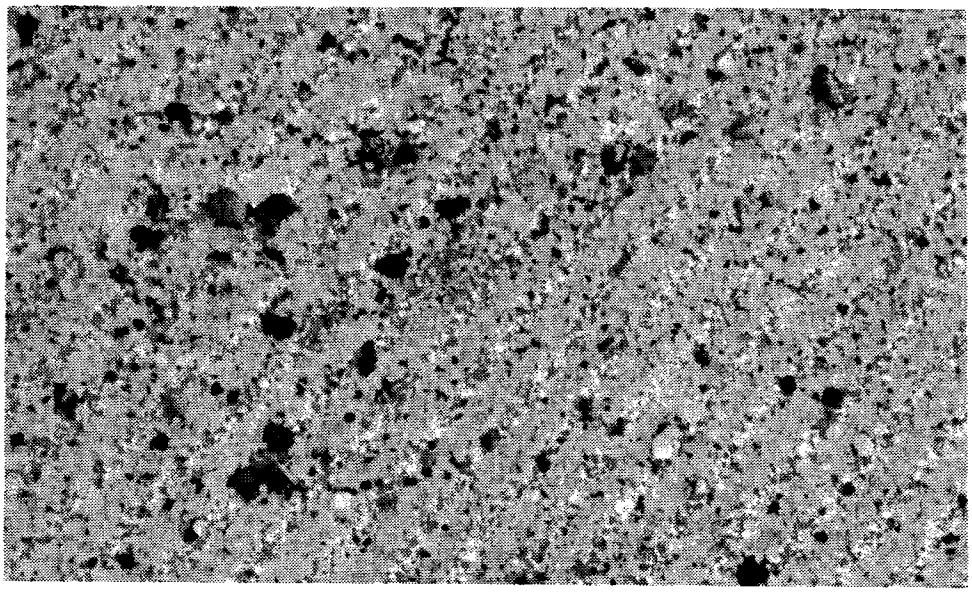

(b)

Figure 6.1. River Gravel aggregate images representing sets of (a) coarse material (b) fine material.

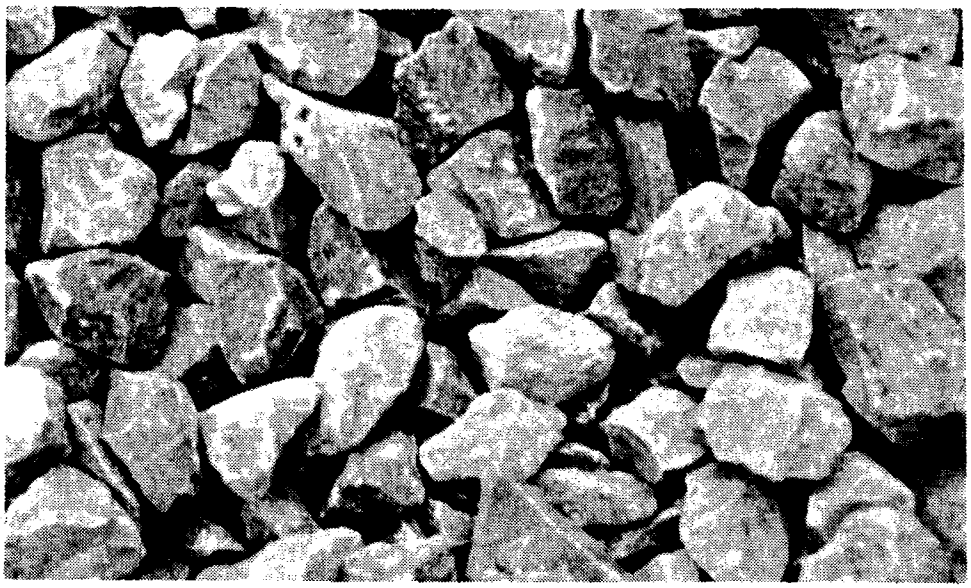

(a)

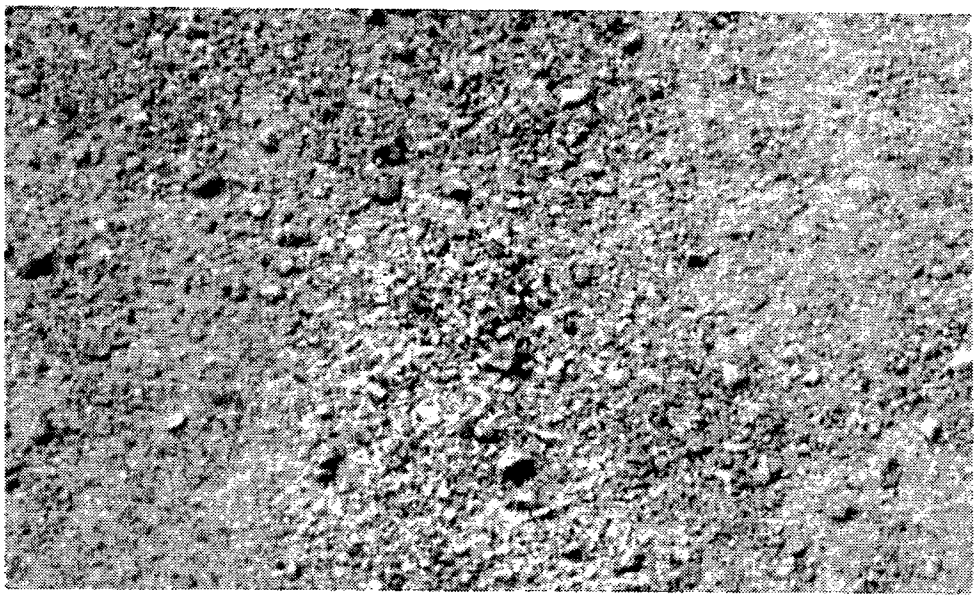

(b)

Figure 6.2. Crushed limestone aggregate images representing sets of (a) coarse materials and (b) fine material.

Table 6.1. Fractal Dimension (D) for 400 x 400 pixel regions.

AGGREGATE	IMAGE	D	MEAN	STD
Crushed Limestone (coarse)	1	2.47		
	2	2.46	2.46	.01
River Gravel (coarse)	3	2.34		
	4	2.36	2.35	.01
Crushed Limestone (fines)	5	2.69		
	6	2.72	2.70	.02
River Gravel (fines)	7	2.63		
	8	2.63	2.63	.00

Table 6.2. Fractal Dimension (Di) for five 128 x 128 pixel subregions.

AGGREGATE	IMAGE	D1	D2	D3	D4	D5	MEAN	STD
Crushed Limestone (coarse)	9	2.50	2.46	2.49	2.48	2.46	2.48	.02
	10	2.46	2.44	2.46	2.48	2.42	2.45	.02
							2.46	.02
River Gravel (coarse)	11	2.33	2.31	2.33	2.34	2.36	2.33	.02
	12	2.36	2.35	2.34	2.37	2.38	2.36	.02
							2.35	.02
Crushed Limestone (fines)	13	2.72	2.76	2.72	2.67	2.65	2.71	.04
	14	2.64	2.71	2.76	2.74	2.70	2.71	.05
							2.72	.04
River Gravel (fines)	15	2.62	2.65	2.63	2.64	2.61	2.63	.02
	16	2.68	2.68	2.63	2.55	2.56	2.62	.06
							2.63	.04

1. The mean fractal dimension of the ten 128 x 128 pixel subregions for a single aggregate type and size is very similar to the mean fractal dimension of the two 400 x 400 pixel regions for the same aggregate.
2. The fractal dimension of a 128 x 128 pixel subregion, for the coarse aggregate images, unambiguously separates crushed limestone from river gravel.
3. Although the fractal dimensions of the fine aggregate images show a significant statistical separation between crushed limestone and river gravel, there is still a quite high standard deviation within the particular images, which makes the identification of aggregate types based on fine material unreliable.

It seems that, for the fine aggregate images, the fractal analysis is extracting features from the mass (distribution of particles, contrasting colors, etc.) rather than features from the individual particles. In other words, the fine particles are too small to be analyzed using fractal analysis on standard photographs or video frames. However, based on results from the coarse aggregate particles, it may be inferred that photomicrographs of a dispersed layer of fine aggregate particles can be analyzed using fractal analysis. Therefore, this process offers potential for quantifying the angularity of sand-sized particles (or even filler-sized particles), and could also be useful in characterizing aggregate or even specifying materials to minimize rutting. It should be pointed out that there are currently no test methods capable of objectively evaluating aggregate shape and surface texture.

Additional analysis procedures consisted of applying a technique known as histogram-flattening to the coarse aggregate images, in an attempt to improve the gray-level contrast (statistical performance of the data). Histogram-flattening, better known as histogram equalization, is a very useful image processing technique. The technique consists of defining a "mapping" of gray levels, p, into gray levels, q, such that the distribution of gray levels, q, is uniform (46). This mapping compresses contrast (reduces the range of gray levels) in areas with gray levels near histogram minima and maxima and thus stretches contrast (expands the range of gray levels) for gray levels in the middle portion of the histogram. Since contrast is expanded for the majority of the image pixels, this techinque

generally improves the resolution and recognition of features in the image (i.e., angularity and texture). The results of the histogram flattened images (Tables 6.3 and 6.4) consistently follow the same conclusions drawn from Tables 6.1 and 6.2 for the coarse aggregate particles. With this new technique, the differences observed between the means are notably higher than before; thus, sensitivity of the test is enhanced.

Potential Application of Fractal Analysis

The fractal analysis technique is simple in nature and of very practical value. In this particular study, fractal analysis proved to be correlated to the character of the aggregate particles used and, therefore, it can be intrinsically related to the permanent deformation performance of the mixture. With the development of further correlations with pavement performance and other laboratory tests, fractal dimension analysis offers potential to forewarn the pavement materials specialist of aggregate that will produce rut-susceptible mixtures. It should be possible to develop an aggregate classification system to objectively measure aggregate shape and surface texture using fractal dimension analysis. Furthermore, acceptance criteria based on this procedure may be used to specify aggregate that will minimize premature rutting problems.

Summary

Fractal analysis is a very promising technique for studying the texture and shape of aggregates. The technique unambiguously identifies and ranks texture and shape of aggregates according to their fractal dimension.

Caution must be used when analyzing aggregates that present different color tones in the individual particle structure or between different particles, because fractal analysis is solely based on a gray scale (black-and-white images) and, therefore, contrasting colors will yield unrealistically high values of fractal dimension. However, this potential problem is not without possible solutions. Two suggested solutions that deserve further study include:

1. Coat aggregate particles with a very thin film of white or light gray paint or dye.
2. Apply a correction factor to the fractal dimension parameter.

Table 6.3. Fractal Dimension (D) for histogram-flattened 400 x 400 pixel regions.

AGGREGATE	IMAGE	D	MEAN	STD
Crushed Limestone (coarse)	1	2.629		
	2	2.608	2.619	.015
River Gravel (coarse)	3	2.408		
	4	2.417	2.413	.006

Table 6.4. Fractal Dimension (Di) for five histogram-flattened 128 x 128 pixel subregions.

AGGREGATE FILE	IMAGE	D1	D2	D3	D4	D5	MEAN	STD
Crushed Limestone (coarse)	9	2.676	2.617	2.682	2.612	2.624	2.642	.034
	10	2.598	2.577	2.612	2.640	2.564	2.598	.030
							2.620	.038
River Gravel (coarse)	11	2.414	2.337	2.424	2.414	2.424	2.403	.037
	12	2.401	2.414	2.403	2.444	2.447	2.422	.022
							2.412	.031

CHAPTER VII

OCTAHEDRAL SHEAR STRESS ANALYSIS

Freeman and Carpenter (18) used octahedral shear stress theory to analyze premature deformation in asphalt concrete overlays over Portland cement concrete pavements. They found that the octahedral shear stress in a pavement can indicate how close to failure a mixture will be when loaded. This indication of incipient failure was given by the ratio of actual octahedral shear stress in the pavement to the failure octahedral shear stress predicted by theory.

Ameri-Gaznon and Little (19) followed Freeman and Carpenter's work and thoroughly developed the octahedral shear stress theory for a series of typical pavement sections found across Texas. Their work is considered of great value and importance in the field of mechanistic analysis of pavement structures.

In this chapter, the octahedral shear stress theory will be used to analyze the potential for rutting of the two most widely different mixes discussed in chapter IV: the zero percent natural sand mix (low rut susceptibility) and the 40 percent natural sand mix (high rut susceptibility). Initially, a general description of the theoretical aspects pertaining to octahedral shear stress theory will be given. Subsequently, two typical pavement sections will be described and analyzed. Conclusions will be obtained from the analysis.

Theoretical Aspects

In general, the octahedral shear stress is a scalar parameter that defines the influence of nine stresses at a specific point. It is defined in a general form as:

$$\tau_{oct} = \frac{1}{3}\left[(\sigma_x - \sigma_y)^2 + (\sigma_y - \sigma_z)^2 + (\sigma_z - \sigma_x)^2 + (\tau_{xy}^2 + \tau_{yz}^2 + \tau_{zx}^2)\right]^{\frac{1}{2}} \qquad (7.1)$$

where

σ_x, σ_y, σ_z = normal stresses

τ_{xy}, τ_{yz}, τ_{zx} = shearing stresses

τ_{oct} = octahedral shear stress (invariant)

Equation (7.1) in terms of principal stresses on a plane will reduce to:

$$\tau_{oct} = \frac{1}{3}[(\sigma_1 - \sigma_2)^2 + (\sigma_2 - \sigma_3)^2 + (\sigma_1 - \sigma_3)^2]^{\frac{1}{2}} \qquad (7.2)$$

where

σ_1 = major principal stress,

σ_2 = intermediate principal stress, and

σ_3 = minor principal stress.

From Mohr-Coulomb failure theory, the equation that represents the relationship between major and minor principal stresses at failure is given by:

$$\sigma_1 = \sigma_3 \left[\frac{1 + \sin \phi}{1 - \sin \phi}\right] + 2c \left[\frac{1 + \sin \phi}{1 - \sin \phi}\right]^{\frac{1}{2}} \qquad (7.3)$$

where

σ_1, σ_3 = major and minor principal stresses,

ϕ = angle of internal friction, and

c = cohesion.

On the other hand, the octahedral normal stress is defined as:

$$\sigma_{oct} = \frac{1}{3}\,[\sigma_x + \sigma_y + \sigma_z] \qquad (7.4)$$

Equation (7.4) in terms of principal stresses on a plane reduces to:

$$\sigma_{oct} = \frac{1}{3}\,[\sigma_1 + \sigma_2 + \sigma_3] \qquad (7.5)$$

If we consider the octahedral shear strength to be obtained from triaxial compression tests ($\sigma_2 = \sigma_3$) at a specific temperature and rate of loading, equations (7.2) and (7.5) can be combined with equation (7.3) to

obtain the following general equation for octahedral shear strength:

$$\tau_{oct\ strength} = \frac{2\sqrt{2}}{3 - \sin \phi} [\sigma_{oct} \cdot \sin \phi + c \cdot \cos \phi] \quad (7.6)$$

where

σ_{oct} = octahedral normal stress,
ϕ = angle of internal friction, and
c = cohesion.

Using an appropriate computer program such as modified ILLIPAVE (47), where the pavement is modeled three-dimensionally by using a two-dimensional halfspace of a finite solid of revolution, one can obtain reasonably good information by which to evaluate the stress state within the pavement structure under any loading and pavement boundary conditions.

An indication of potential for rutting can be assessed by means of evaluating and analyzing the octahedral shear stress ratio, which is the ratio of the critical induced octahedral shear stress in the pavement layer, to the octahedral shear strength of the material, as defined by equation (7.6). A procedure for calculating this octahedral shear stress ratio can be summarized in the following steps:

1. Find τ_{oct} from the modified ILLIPAVE computer program using equation (7.1).
2. Find σ_{oct} from the modified ILLIPAVE computer program using equation (7.4).
3. Use values of the σ_{oct}, found in step 2, and appropriate ϕ and c values, obtained from triaxial compression testing, in equation (7.6) in order to obtain $\tau_{oct\ strength}$ for all σ_{oct} stresses.
4. Calculate octahedral shear stress ratios by dividing τ_{oct} from step 1 by $\tau_{oct\ strength}$ from step 3, and draw contour lines for the different values obtained. Contours of octahedral shear stress ratios will give a complete picture of the distribution of failure potential within a pavement structure.

Two Cases Analyzed

This section presents two independent comparisons of hypothetical pavements:

1. Two HMAC surface layers, one with the zero percent natural sand mix and the other with the 40 percent natural sand mix, both in a traditional pavement structure (Figure 7.1), are compared and
2. Two HMAC overlays, one with the zero percent natural sand mix and the other with the 40 percent natural sand mix, both placed on an asphalt treated base are compared (Figure 7.2).

The octahedral shear stress analysis was performed based on the following pavement boundary conditions and general assumptions:

1. In the analysis, a tire pressure of 115 psi was used with a 6,000-pound circular wheel load in order to represent high stress conditions. The Tielking tire model (48) was used to determine the contact vertical pressure distribution and the shear stress distribution to be used in the modified ILLIPAVE computer program. Figure 7.3 shows a typical stress distribution obtained from the Tielking model.
2. The surface layers in both cases were subdivided into 1-inch thick sublayers in order to incorporate the temperature gradient models derived by Li (49). The Dallas, Texas, region environment was selected as the model for this particular analysis (Figure 7.4). The temperature distributions, used in cases 1 and 2, are shown in Tables 7.1 and 7.2, respectively. Only the last four profiles from each table were used in the ILLIPAVE program because they were considered to be the most critical profiles for rutting performance (the highest temperature distributions). The highest temperature profile was labeled season 1 and subsequent profiles were labeled in order of decreasing temperature. Different modulus values were then assigned according to the temperature in each sublayer.
3. A Mohr Coulomb failure envelope was obtained for both the zero percent and 40 percent natural sand mixes at a temperature of 104°F. The values for cohesion and friction calculated from the envelopes were then used to compute octahedral shear strengths at this temperature. For the other temperatures within the pavement structure, the octahedral shear strengths were adjusted

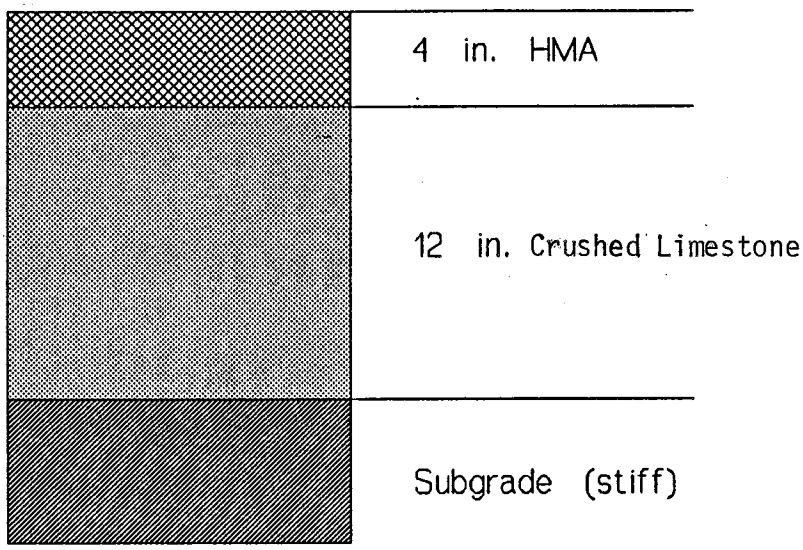

Figure 7.1. Traditional pavement structure.

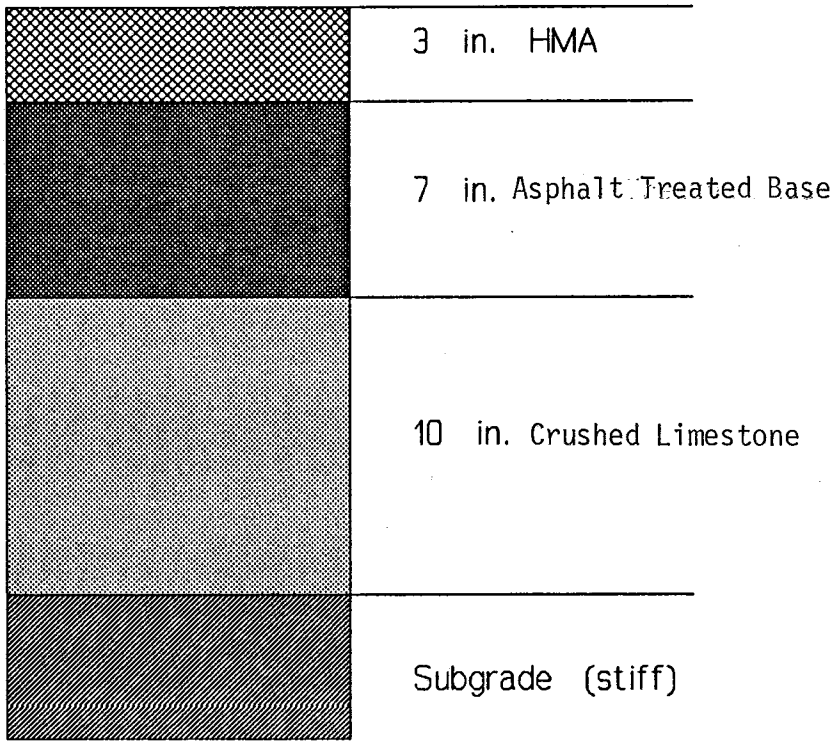

Figure 7.2. Asphalt treated base pavement structure.

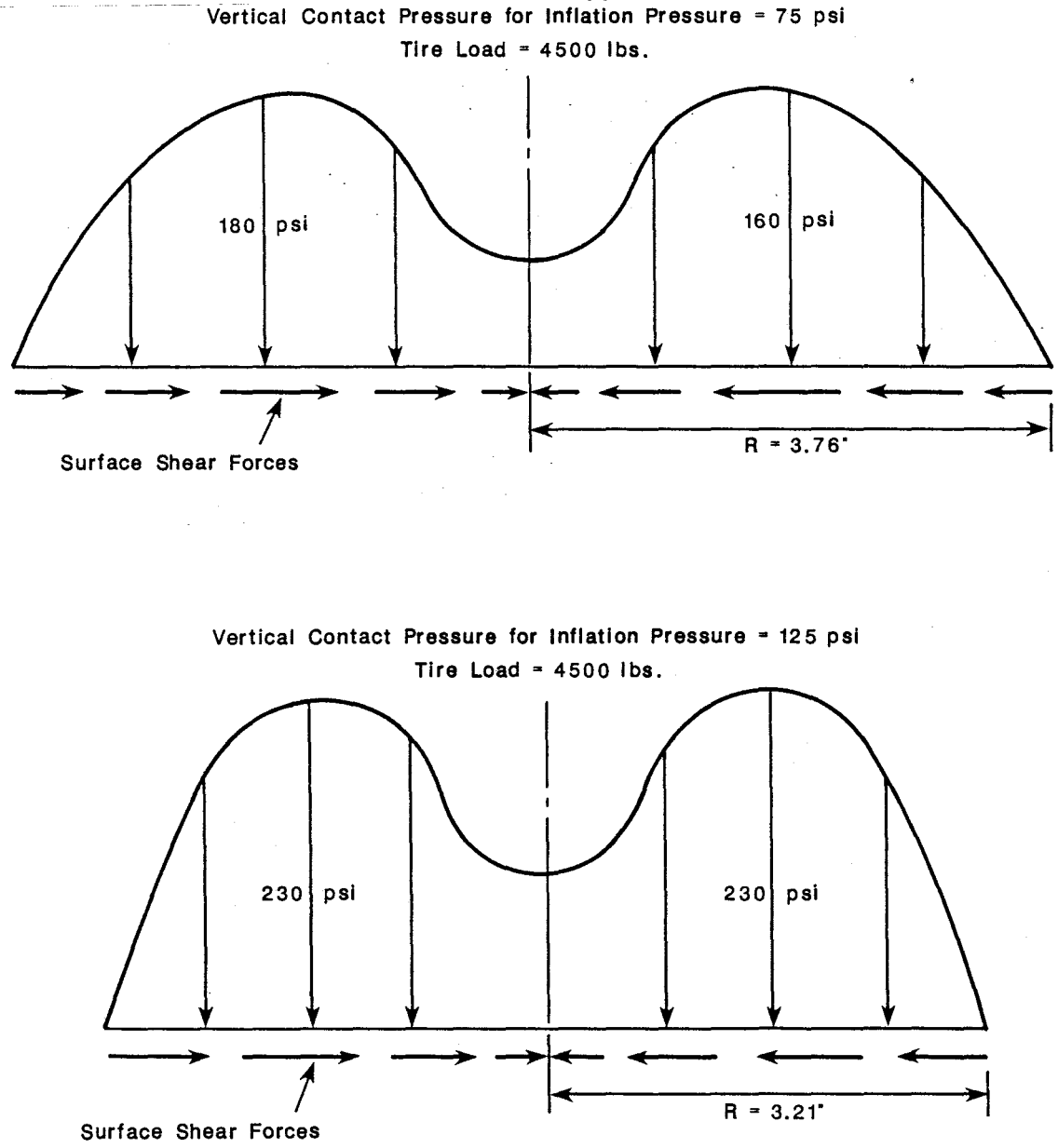

Figure 7.3. Nonlinear vertical tire pressure distribution with lateral surface forces as developed using finite element model by Tielking (after Reference 48).

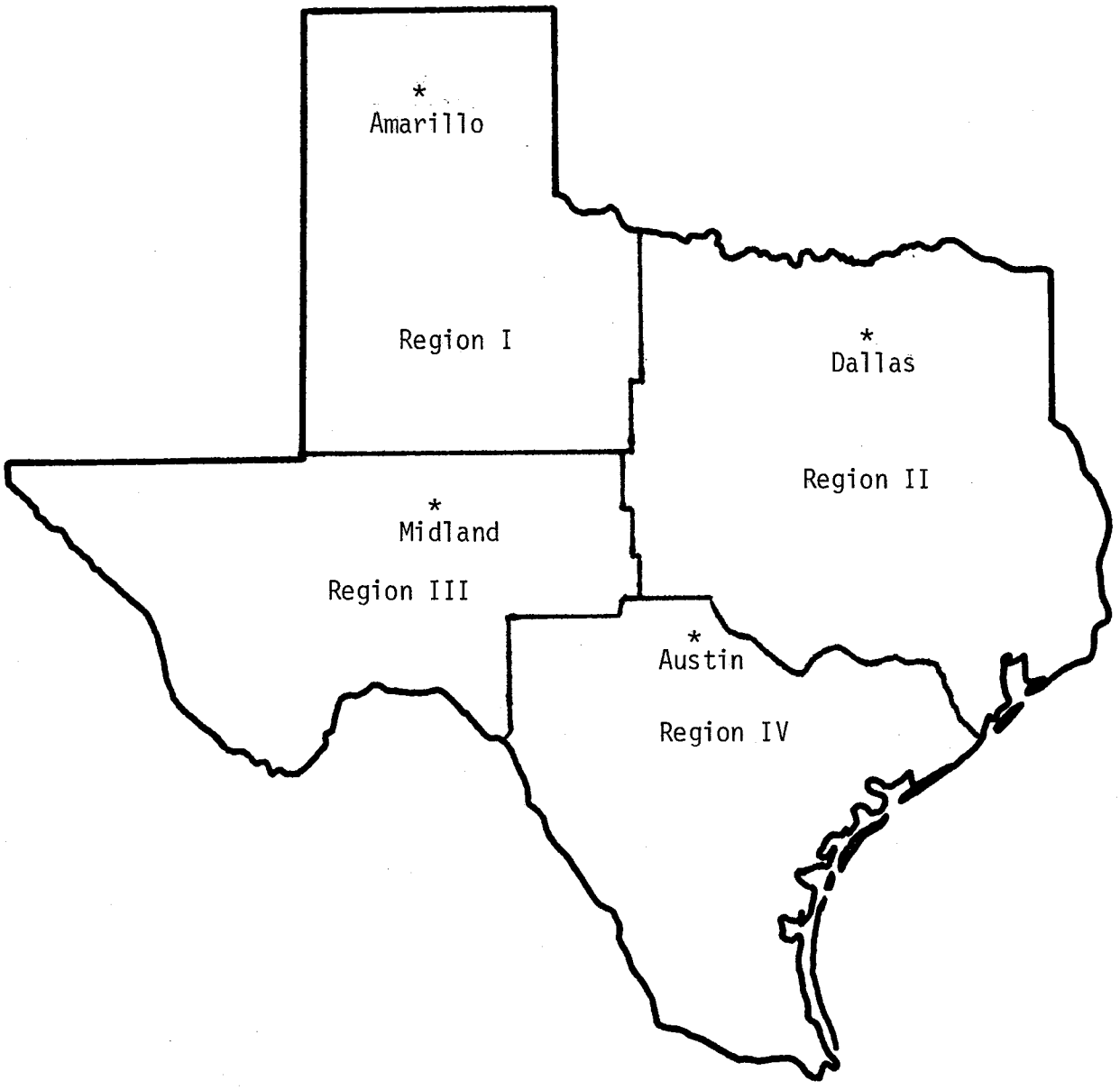

Figure 7.4. Temperature regions within Texas.

Table 7.1. Temperature distribution of 4 in. asphalt overlay (Dallas Area).

Profile No.	Season label*	Temp. (°F)	Sub-layer Temp. (°F) 1	2	3	4	% Time
1		< 75	68	70	72	73	25.58
2		75-85	79	81	82	84	25.58
3	4	85-95	90	89	88	87	15.05
4	3	95-105	100	97	94	91	14.58
5	2	105-115	110	105	101	97	12.15
6	1	115-125	118	112	107	103	6.83

* Season labels used in ILLIPAVE analysis

Table 7.2. Temperature distribution of 3 in. asphalt overlay (Dallas Area).

Profile No.	Season label*	Temp. (°F)	Sub-layer Temp. (°F) 1	2	3	% Time
1		< 75	68	70	72	25.69
2		75-85	79	81	82	25.69
3	4	85-95	90	89	88	14.93
4	3	95-105	100	97	94	14.70
5	2	105-115	110	105	101	12.15
6	1	115-125	118	112	107	6.84

* Season labels used in ILLIPAVE analysis

according to the ratio of moduli, which is considered to be a conservative approach.

4. Both pavement structures (Figures 7.1 and 7.2) were analyzed under two loading conditions: single and dual tire loading.

A series of charts were developed showing the variation of the octahedral shear stress ratio for the different mixes and cases analyzed under both single and dual tire loading conditions. Figures 7.5 through 7.12 present typical results for octahedral normal stress, octahedral shear stress, octahedral shear strength, and octahedral shear stress ratio for the pavement structure corresponding to case 1 and having a 40 percent natural sand mix as a surface layer. The figures are presented in order to illustrate the steps outlined in the procedure to calculate octahedral shear stress ratio. This procedure was described in the theoretical section of this chapter.

The octahedral shear stress ratio contours illustrate a novel way of representing failure potential within a particular pavement structure (Figures 7.8 and 7.12). Furthermore, Figures 7.13 through 7.16 contribute considerably to the overall analysis of the potential for rutting in a particular asphalt concrete mixture. The maximum octahedral shear stress ratios are plotted against resilient modulus for the first two sublayers of the asphalt concrete surface layer. The four seasons analyzed are plotted as points on the curves (S1 through S4), with a season convention given for only one of the curves (first point on the left corresponds to season 1). For the hottest season (season 1), it is observed that the potential for failure in the first inch of the surface layer is 1.6 to 1.8 times higher for a 40 percent natural sand mix than it is for a zero percent natural sand mix.

Summary

Figures 7.13 through 7.16 summarize the results obtained from the octahedral shear stress analysis. The following conclusions are drawn from the figures:

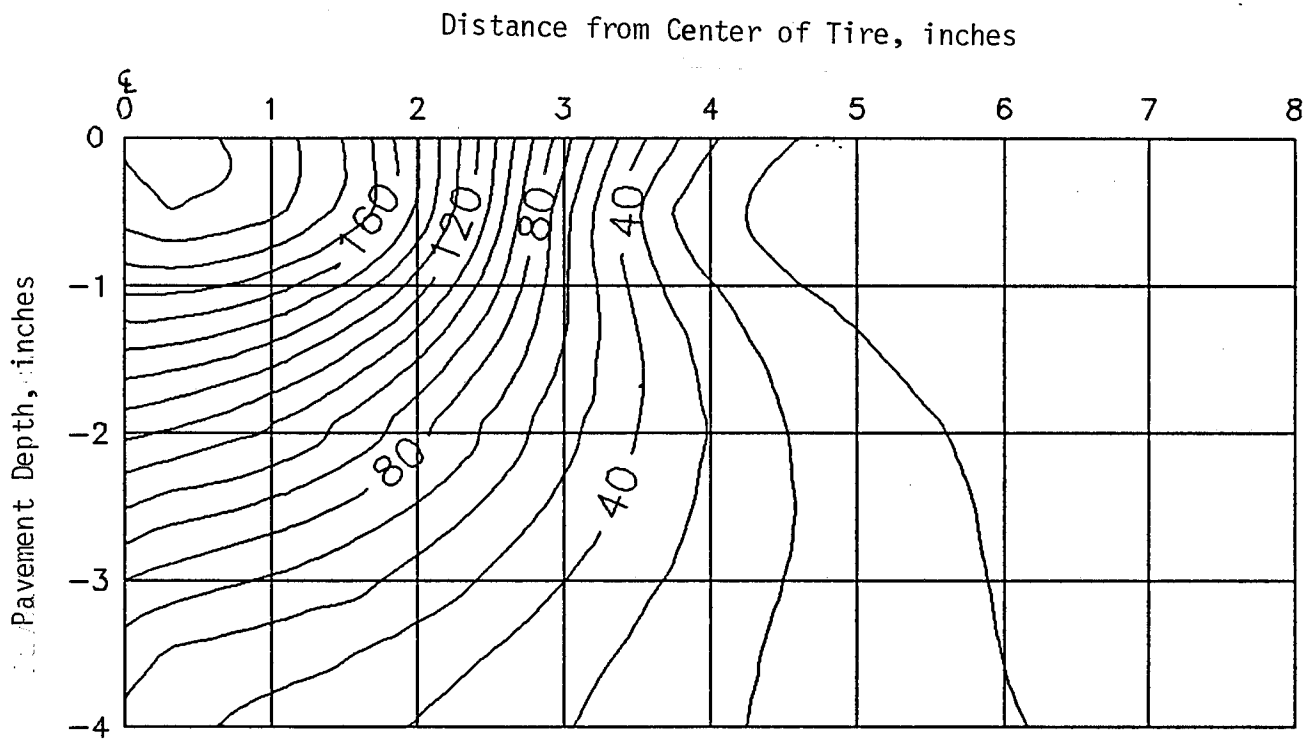

Figure 7.5. Octahedral normal stress contours for 40 percent natural sand mix surface layer in traditional pavement structure under single tire loading, and for hottest season (season 1).

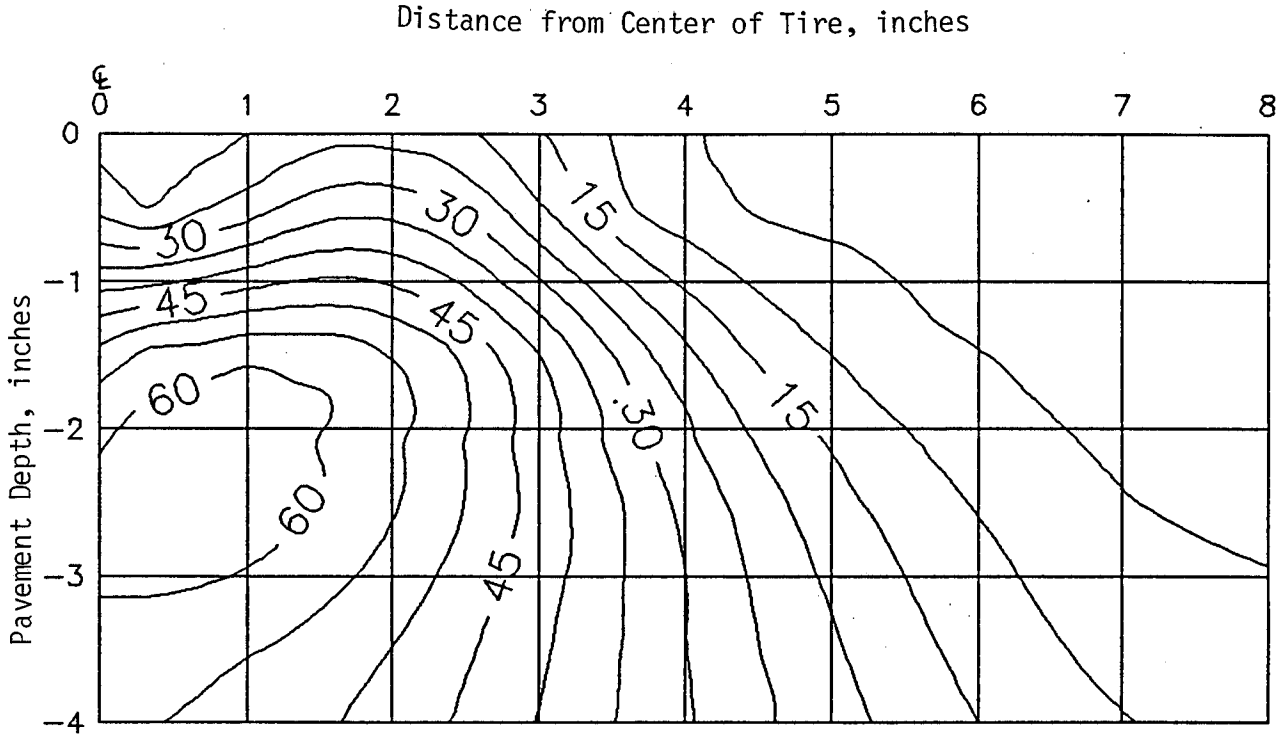

Figure 7.6. Octahedral shear stress contours for 40 percent natural sand mix surface layer in traditional pavement structure under single tire loading, and for hottest season (season 1).

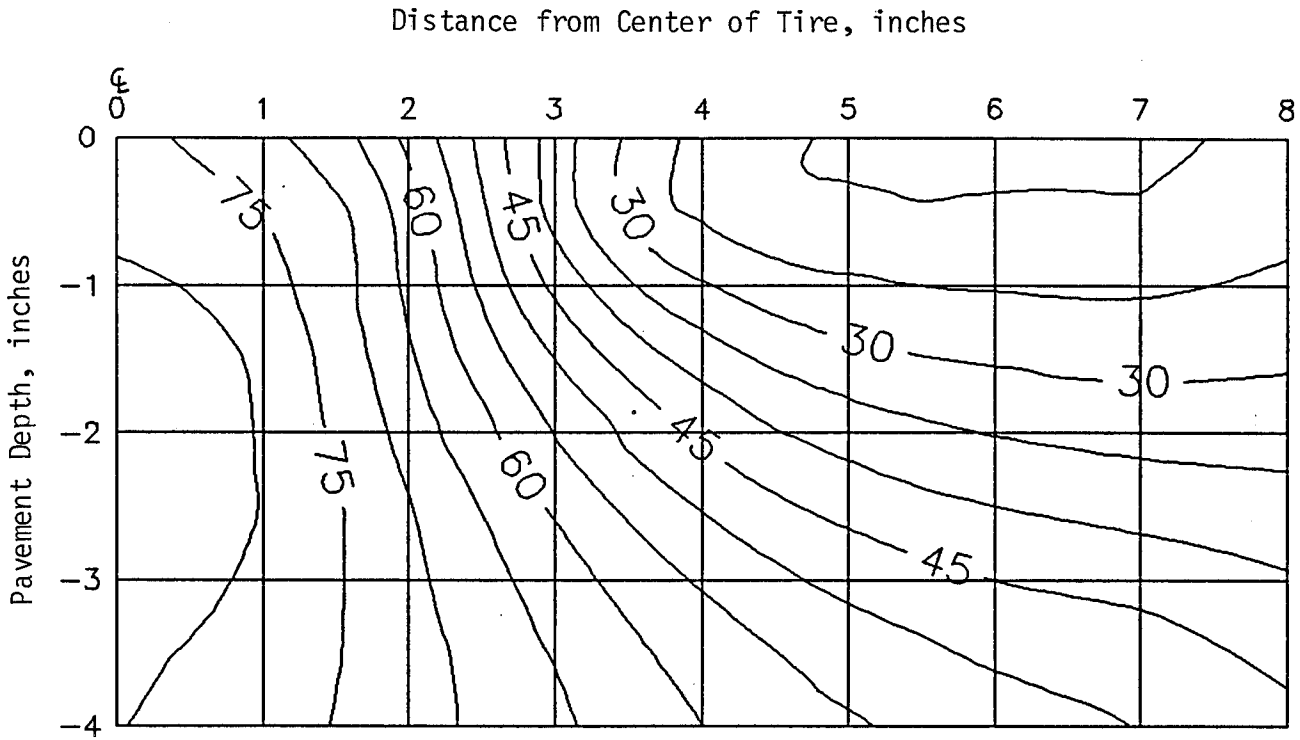

Figure 7.7. Octahedral shear strength contours for 40 percent natural sand mix surface layer in traditional pavement structure under single tire loading, and for hottest season (season 1).

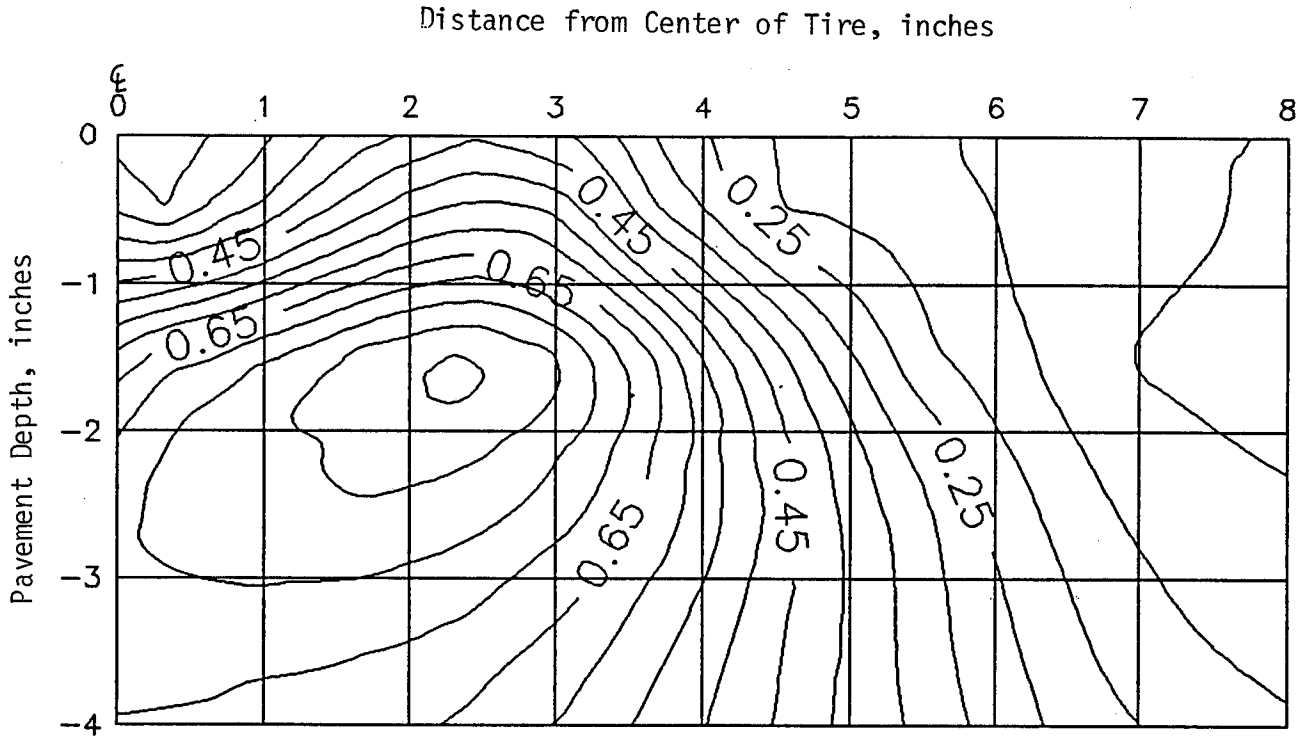

Figure 7.8. Octahedral shear stress ratio contours for 40 percent natural sand mix surface layer in traditional pavement structure under single tire loading, and for hottest season (season 1).

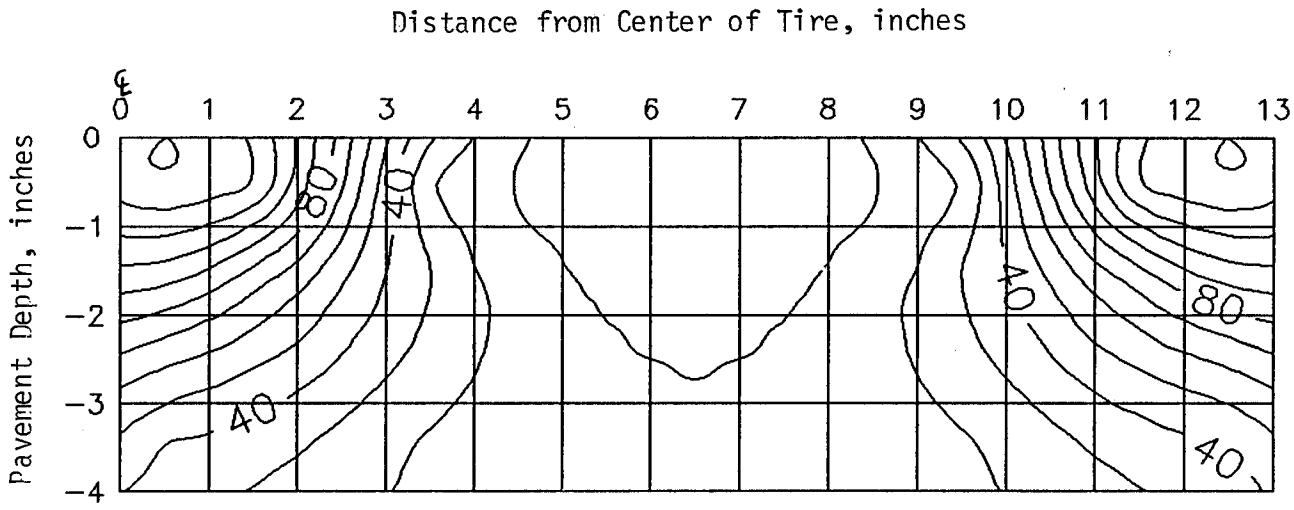

Figure 7.9. Octahedral normal stress contours for 40 percent natural sand mix surface layer in traditional pavement structure under DUAL tire loading, and for hottest season (season 1).

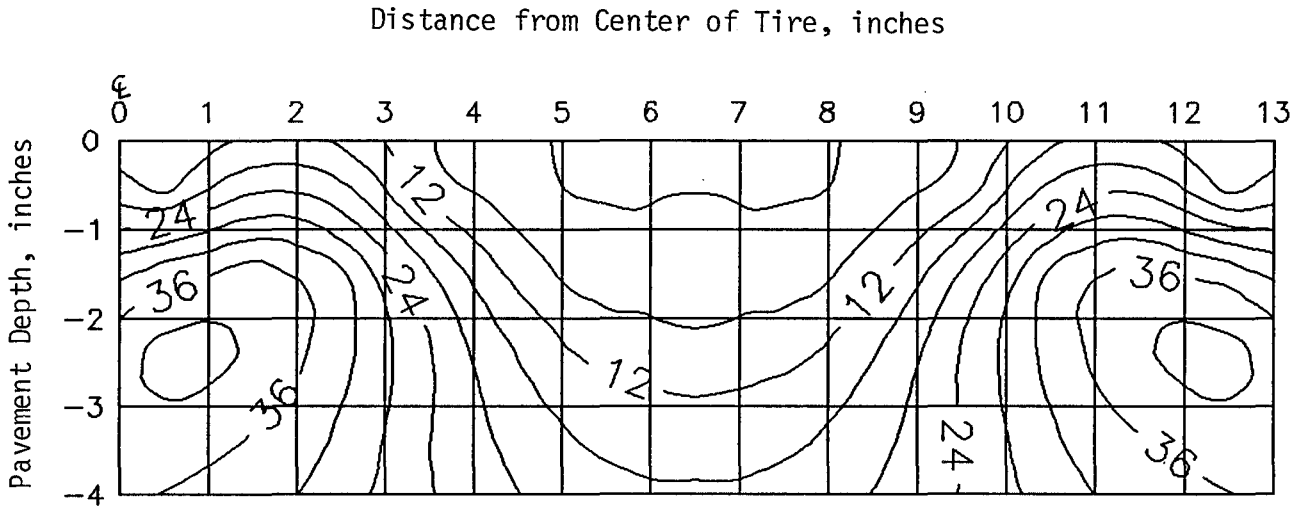

Figure 7.10. Octahedral shear stress contours for 40 percent natural sand mix surface layer in traditional pavement structure under DUAL tire loading, and for hottest season (season 1).

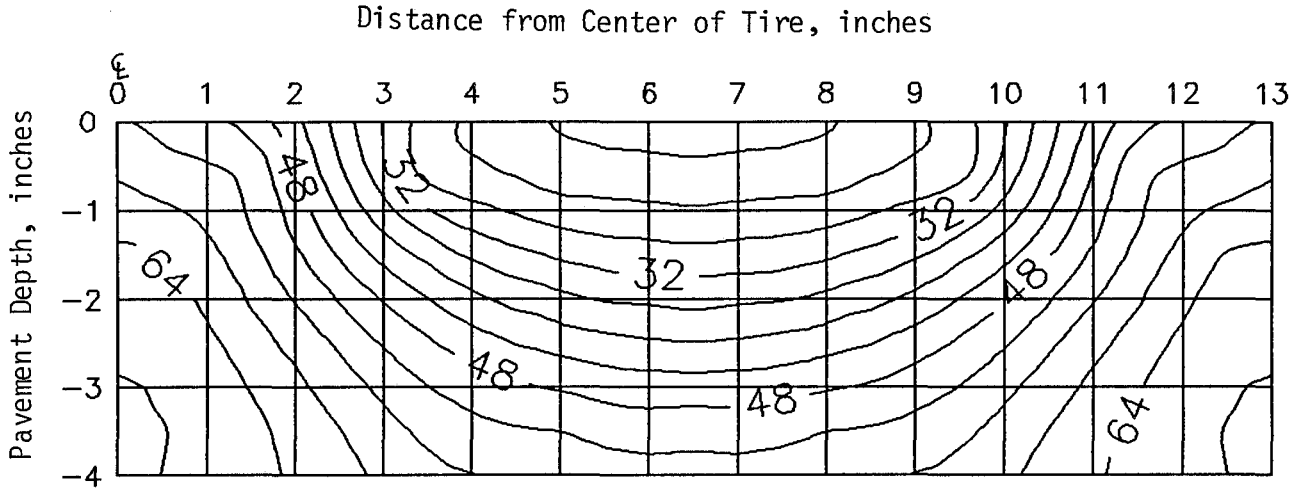

Figure 7.11. Octahedral shear strength contours for 40 percent natural sand mix surface layer in traditional pavement structure under DUAL tire loading, and for hottest season (season 1).

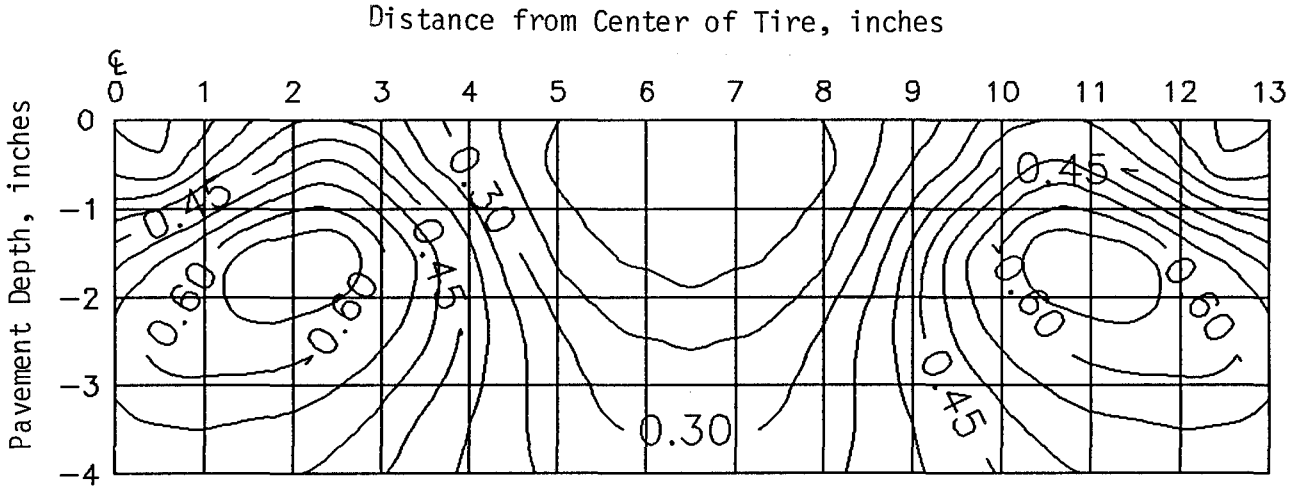

Figure 7.12. Octahedral shear stress ratio contours for 40 percent natural sand mix surface layer in traditional pavement structure under DUAL tire loading, and for hottest season (season 1).

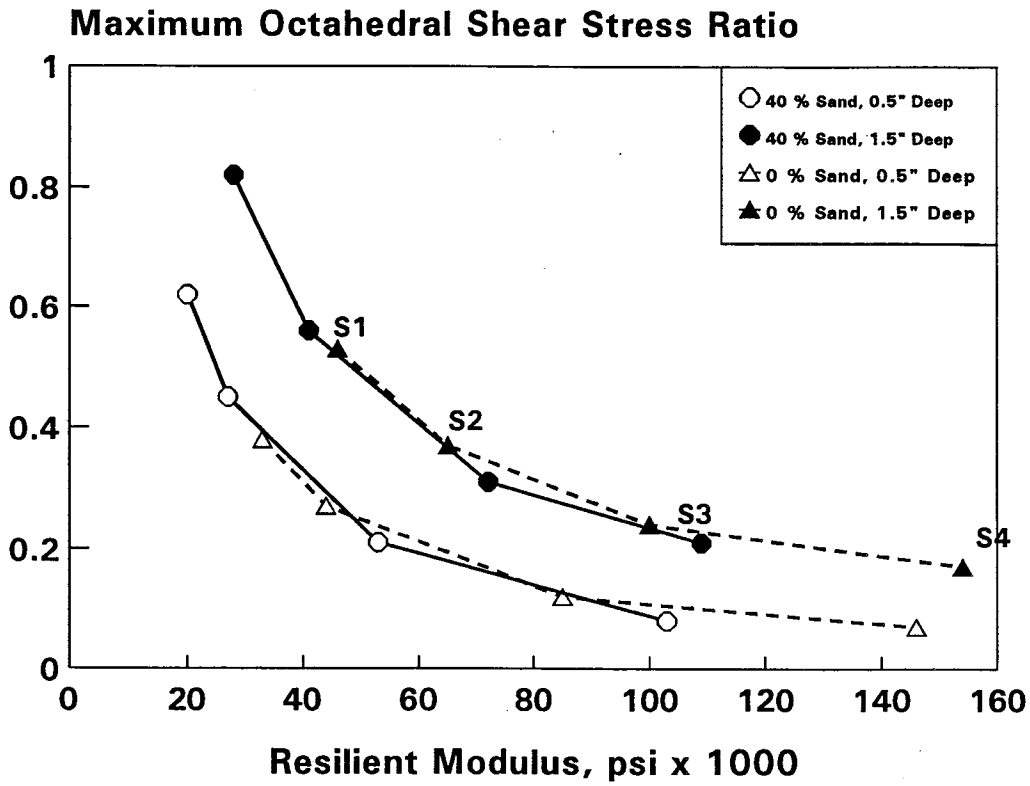

Figure 7.13. Maximum OSSR versus resilient modulus for first two inches of surface layer in traditional pavement structure under single tire loading.

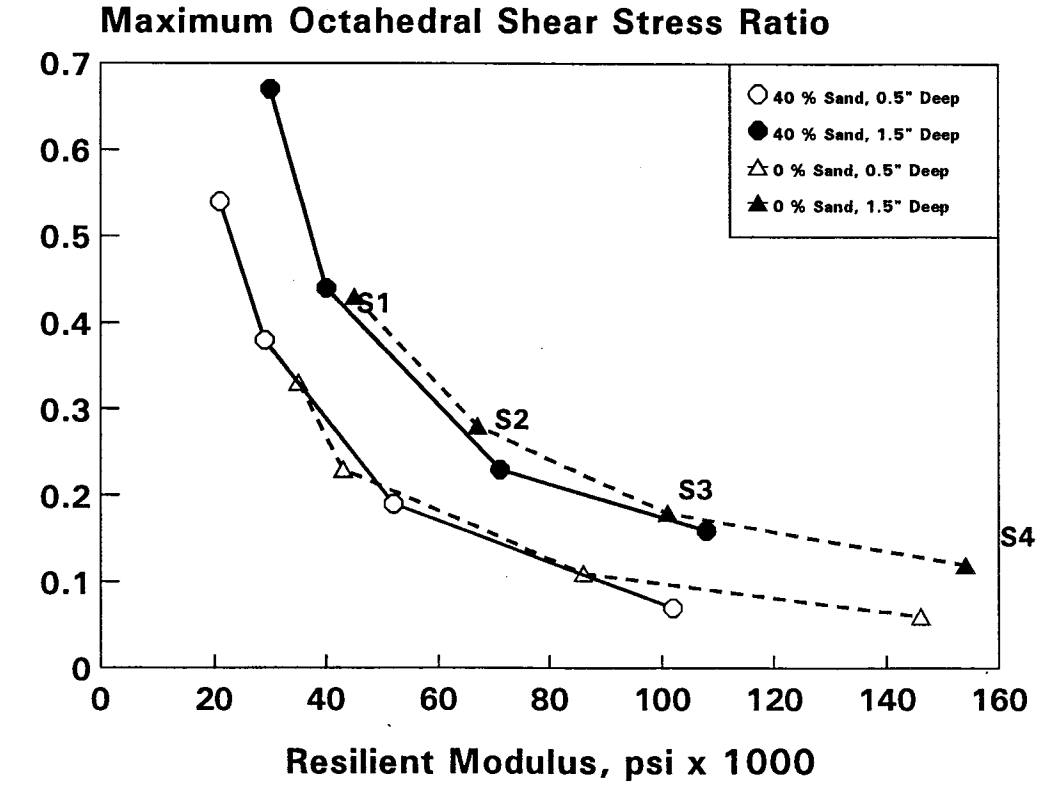

Figure 7.14. Maximum OSSR versus resilient modulus for first two inches of surface layer in traditional pavement structure under DUAL tire loading.

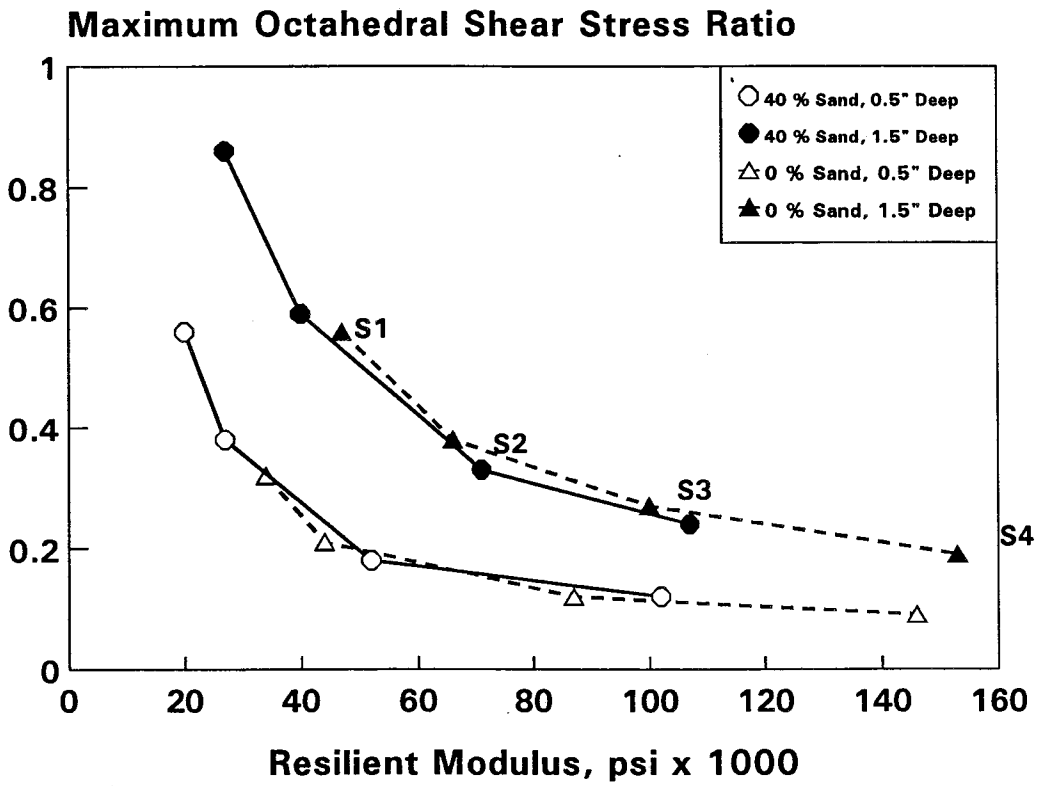

Figure 7.15. Maximum OSSR versus resilient modulus for first two inches of surface layer in asphalt treated base pavement structure under single tire loading.

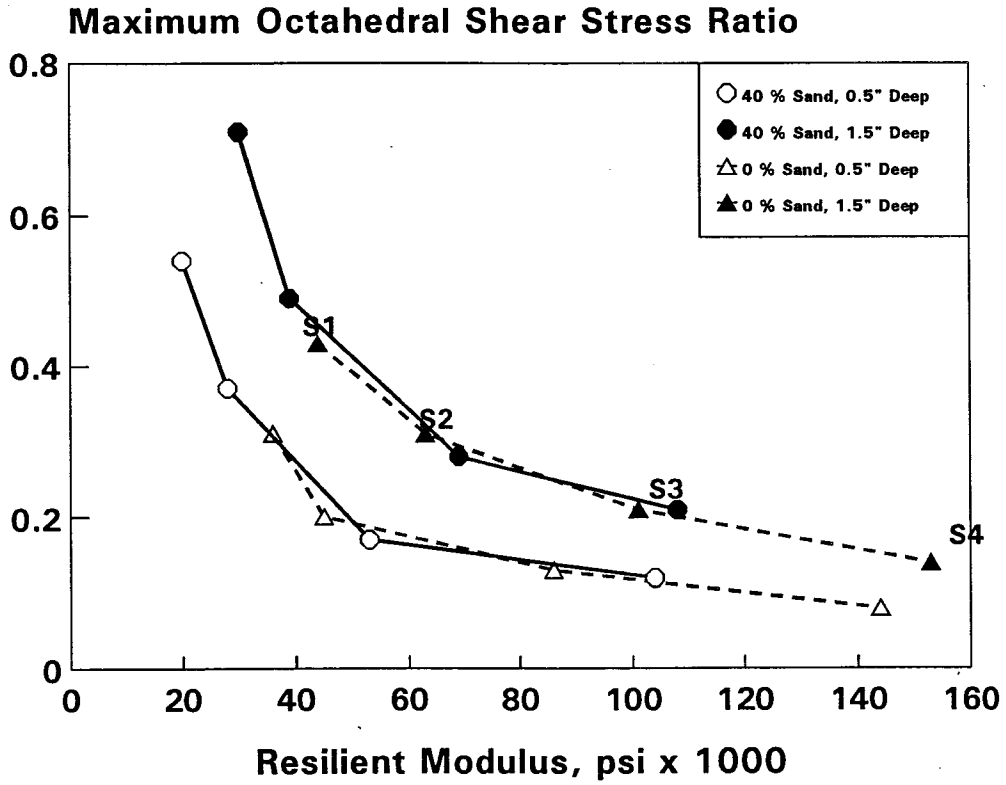

Figure 7.16. Maximum OSSR versus resilient modulus for first two inches of surface layer in asphalt treated base pavement structure under DUAL tire loading.

1. For both pavement structures (cases 1 and 2), under both single and dual tire loading conditions, there seems to be a critical modulus value. Above this critical value, variations in the mix characteristics have no major influence on the maximum octahedral shear stress ratio values for the first inch of the pavement structure. This fact may indicate that octahedral shear stress theory should be limited to the analysis of shear strength data collected at relatively high temperatures due to the overpowering influence (on shear strength) of the cohesive strength of the asphalt at low temperatures. Furthermore, it is well known that 80 percent (and more) of the permanent deformation in an asphalt concrete mixture occurs during the hottest periods of the year (modulus values are easily below 100,000 psi in the first sublayer). Permanent deformation and creep analysis can be considered as good complementary tools when using octahedral shear stress theory to analyze rutting potential.
2. If one concentrates solely on analyzing the first inch of the pavement structure, based on the fact that most of the rutting occurs in this first sublayer, one can tell from the figures that in all cases the potential for rutting, during the two hottest seasons (season 1 and 2), is 1.6 to 1.8 times greater for the 40 percent sand mix than it is for the 100 percent limestone mix.
3. Finally, the octahedral shear stress analysis results emphasize the fact that a mixture containing high percentages of natural sand is much more susceptible to rutting than a mixture that does not contain any natural sand (other variables being constant). It is important to stress this point because this study concentrates on analyzing the sensitivity of a mixture to natural sand content, using several theoretical and laboratory methods. Furthermore, it can be concluded that the maximum octahedral shear stress diagrams (Figures 7.13 to 7.16) represent a new and practical approach for evaluating the susceptibility to rutting of an asphalt concrete mixture.

CHAPTER VIII
OTHER FACTORS THAT AFFECT RUTTING

Other factors that may influence ruttin in Texas, but were not specifically addressed in this study are discussed below.

HOT MIX ASPHALT CONCRETE SPECIFICATIONS

Historically, Texas DOT specifications for Item 340, hot mix asphaltic concrete pavement, have allowed and possibly encouraged the use of gap-graded mixes (50). These mixtures are characterized by the "hump" in the gradation curve near the number 40 sieve and a relatively flat slope between the number 40 and the number 10 sieve. This indicates a deficiency of material in the number 40 to number 8 sieve size range and an excess of material passing the number 40 sieve (51). Mixtures of this type, particularly when the fines are composed primarily of natural sand, are termed "critical" in that they lack resistance to plastic deformation, tend to rapidly loose stability if the asphalt content exceeds optimum, and become tender and shove during periods of hot weather. One method of improving the aggregate grading specification to yield tough paving mixes would be to lower the upper limit of the total percentage of material allowed to pass the number 40 and 80 sieves. According to Chastain and Burke (52), in 1957, less than 20 percent of highway agencies allowed more than 37 percent passing the number 40 sieve and more than 40 percent of them required less than 32 percent passing the number 40 sieve. Additionally, the Type C specification does not allow a sufficient quantity of the largest size aggregates to effect their mutual interlock; the percentage of material passing the No. 5/8 sieve should be approximately 80 percent to 100 percent.

The 0.45 power gradation chart is particularly useful in evaluating aggregate gradations. A straight line, plotted from the origin of the chart to the percentage point plotted for the largest sieve with material retained, approximates the gradation of maximum density. Aggregate gradation should be examined on the 0.45 power chart as a routine procedure during mixture design. When a plant inspector becomes accustomed to using this chart, it will help him to recognize gradation problems early and make the necessary adjustments before large quantities of the mix are placed.

Although it is well known that siliceous gravels and sands generally produce asphalt concrete mixtures subject to plastic deformation and

moisture damage, existing specifications for Item 340 do not limit the use of these natural aggregate particles. The specification requires that a minimum of 85 percent of the particles retained on the number 4 sieve have at least 2 crushed faces. This is certainly a positive move regarding the coarse aggregate, but there is currently no limitation placed on the fine aggregate (sand).

The type and quantity of fine aggregate is critical in that it greatly influences the shear strength of the mixture, the amount of asphalt a mixture can tolerate, and the volume of air in the compacted pavement (26, 53, 7). Use of excessive quantities of natural sand is indirectly addressed in the specification by the requirement of a minimum Hveem stability. Experience, however, has shown that mixtures with satisfactory Hveem stability often will not provide satisfactory performance as surface courses on pavements carrying more than 10,000 vehicles per day (50).

To meet gradation requirements with limited use of natural sand, it is usually required to replace these particles with "manufactured sand" (crusher screenings with limited minus number 200). There is currently no standard specification for washed screenings, this deficiency has caused difficulties on occasion. A reasonable specification for washed screenings should require near 100 percent passing the number 4 sieve and limit the amount passing the number 200 sieve to about to 6 percent. Special provisions should be considered for particular situations, depending on the character of the available screenings and sand and the other aggregates blended to produce the mix.

Current Texas SDHPT specifications for Item 340 do not require a minimum VMA. Minimum allowable VMA for various nominal maximum particle sizes are recommended by FHWA (51) and McLeod (54). These values are based on compaction using the Marshall hammer. Optimum values of VMA using the Texas gyratory compactor need to be established. Based on findings from a recent study sponsored by the National Cooperative Highway Research Program (NCHRP) (55), it is reasonable to expect that acceptable VMA requirements using the gyratory compactor may be about 0.5 percent lower than those developed using the Marshall hammer. Krugler (56) pointed out that the greater the VMA in the dry aggregate, the greater space which is available for asphalt to coat the aggregate particles, while still leaving room for the optimum percentage of air voids. The thicker the asphalt film (up to the point where film thickness begins to interfere with stability by

reducing the internal friction of aggregate interlock), the more protected the mix is from water damage and oxidative aging.

Finally, incorporation of some or all of the above recommended changes into the Item 340 specification will result in a substantial increase in the Hveem stability. As a measure to further ensure that the mixture will withstand the applied loads, the minimum required Hveem stability should be raised to a value between 37 and 40. A minimum value of 37 is recommended by the Asphalt Institute (28) and the FHWA (51) for traffic volumes exceeding one million equivalent single axle loads during the design life.

METHOD OF TESTING

In the search for possible reasons for excess asphalt in paving mixtures, standard Texas test methods were investigated. Design of hot bituminous mixtures in Texas requires the use of test methods Tex-205-F (mixing) and Tex-206-F (compaction) for specimen preparation. These test methods specify a mixing temperature of 275°F and a compaction temperature of 250°F, respectively, regardless of the grade or viscosity-temperature relationship of the asphalt cement. Examination of 1988 data for AC-20 asphalts used in Texas revealed that the viscosity may range from 6 to 14 stokes at 250°F and from 2.8 to 6.8 stokes at 275°F. Based on the experience of the authors, this range of viscosities will significantly affect density of the compacted specimens. Higher viscosity will, of course, result in higher air voids. Since optimum asphalt content has historically been selected at 97 percent density (or 3 percent air voids), it follows that the harder (at compaction temperature) asphalts will require higher asphalt contents. Now since the materials under discussion are all AC-20's, the viscosity range at high pavement service temperatures (say 140°F) is comparatively small (1610 to 2280 stokes, based on 1988 Texas DOT asphalt data). Therefore, in service, the higher asphalt content required by the design procedure may be detrimental regarding resistance to plastic deformation of the mix. Furthermore, when modified asphalts are used, which often have significantly lower than usual temperature susceptibilities (or higher viscosities at the compaction temperature), the standard design procedure may require binder contents in excess of that desirable for good rutting performance.

The potential for these standard test methods to produce mixes with

excess asphalt should be investigated. If it is determined that the risk is unacceptable, then the test methods should be modified to require mixing and compaction at some preselected viscosity rather than the constant temperatures. Guidelines for the Marshall mixture design procedure (28, 57, 58) recommend a mixing temperature that provides 170 centistokes and a compaction temperature that provides 280 centistokes. Asphalt viscosity at compaction temperatures using the Texas gyratory compactor may not be as critical as viscosity when using the Marshall hammer, but this supposition should be verified.

CONSTRUCTION CONSIDERATIONS

It is possible to substantially reduce plastic deformation of the pavement by using larger nominal maximum size aggregates, that are mixed with harder grade of asphalt (AC-30) or modified asphalt binder. Davis (59) states the largest stone size should be two-thirds the pavement thickness. Larger crushed stone mixes generally require less energy to produce and less asphalt and are, therefore, less expensive. Research (60, 61) has shown that certain polymer additives will produce a significant increase in asphalt viscosity at high pavement service temperatures while having little affect on viscosity at low pavement service temperatures.

Where rutting is the primary concern and low temperature cracking is of little concern, it may be possible to achieve positive results by incorporating a polymer additive into AC-20. The modified binder should exhibit little change in penetration at 39.2°F while exhibiting a substantial increase in viscosity at 140°F. Consequently, the use of Type C mixtures with modified asphalt in place of Type D mixtures for surface courses should substantially help to alleviate permanent deformation. Higher than usual compaction energy may be required for these mixtures.

Plant mix seals or open-graded friction courses (OGFC) are normally quite resistant to rutting. These mixtures may provide a viable alternative to the usual Type D dense-graded mixtures for surface courses and overlays. Additional benefits provided by plant mix seals include improved surface friction and resistance to hydroplaning and reduced glare at night. Mechanical properties of OGFC's can be further enhanced by use of asphalt rubber or polymer modified binders (62).

Stone filled mixtures (63), briefly described in Reference 25, should also provide excellent resistance to rutting. Stone filled mixtures

essentially consist of a small top-size, dense graded asphalt concrete mix combined with about 45 percent (by total weight of mix) of a larger single-size stone of about 3/4-inch diameter for surface courses. A stone matrix is formed by the large stones and the voids between are filled with the fine-grained asphalt "intermix." Recycled asphalt pavement (RAP) could be used as the intermix. The bridging effect of the large stones resist plastic deformation and further densification under traffic in a manner similar to the open-graded mixes.

A relatively new paving surface called micro-surfacing has been purported to offer good resistance to rutting. Micro-surfacing is a mixture of polymer modified emulsified asphalt, graded crushed mineral aggregate, mineral filler, water, and sometimes other additives. It is basically a type II or type III slurry seal with a polymer modified binder. Micro-surfacing over a large stone asphalt binder course may be an excellent combination to accommodate high-volume, heavy wheel load traffic.

CHAPTER IX

CONCLUSIONS AND RECOMMENDATIONS

Based on results from a comprehensive laboratory test program where permanent deformation was measured with respect to the characteristics of the fines fraction of asphalt concrete mixtures with limited field tests conducted to verify the findings, the following conclusions and recommendations are warranted.

Conclusions

1. The field investigation revealed the following items contributed substantially to permanent deformation of asphalt concrete pavements:
   a. Asphalt content in excess of the design value,
   b. Excessive fine aggregate (sand-size particles), and
   c. Round shape and smooth texture of fine aggregate.
2. Results of the laboratory investigation show that, as natural (uncrushed) sand-size aggregate particles are replaced with crushed particles of the same gradation, the resulting asphalt concrete mixture becomes significantly more resistant to permanent deformation. A substantial increase in deformation was observed as the percentage of natural sand the mixtures was increased from zero to 20 percent. This indicates that 20 percent natural sand by total weight in the mixture tested is an excessive quantity if substantial resistance to deformation is an objective of the mixture.
3. Deformation sensitivity of the mixture resulting from variations in temperature and asphalt content increases as the percentage of natural sand in the mix increases.
4. Compactive effort required to produce a given air void content increased significantly as natural sand was replaced with manufactured sand.
5. The long-term unconfined compression tests (static creep and cyclic), along with the triaxial cyclic test, proved to be very effective methods for identifying and quantifying permanent deformation susceptibility in mixtures containing natural sand.
6. The hyperbolic theoretical model was developed that provides a near perfect predictor of actual creep and recovery performance of

asphalt mixturs. The "p" value defined within the model showed strong correlation with the amount and character of the sand-size aggregate particles, hence, proving to be representative of the influence that these particles have on permanent deformation. From the state-of-the-art theoretical approach, a new permanent deformation prediction model was developed, which is believed to be more representative of actual field performance than other existing models.

7. Particle index (ASTM D3398) of the aggregate used in an asphalt concrete mixture provides a direct measure of mix quality, which is intrinsically related to permanent deformation behavior.
8. Fractal analysis proved to be a very practical way of providing objective measures of the shape and surface texture in coarse aggregates. Fine aggregate particles were also ranked according to the shape and texture, but differences in sand-size and smaller particles could not be identified with the same high level of significance as the coarse particles. It is believed that by using photomicrographs, the same level of sensitivity can be obtained for fine aggregate as for coarse aggregate.
9. Octahedral shear stress theory can be used effectively to evaluate the potential of asphalt mixtures under specific stress states to permanently deform. The procedure relates the induced octahedral shear stress to the octahedral shear strength (at failure). A graphical representation of these stress and strength contours was produced and proved to be a very revealing indicator of deformation susceptibility throughout the asphalt pavement layer in question.

Recommendations

1. To avoid excessive permanent deformation under heavy traffic, the use of natural sand with rounded particle shapes and smooth surface textures in asphalt concrete mixtures should be limited to an amount not greater than 10 percent to 15 percent.
2. Continue to support research needed to analyze the sensitivity of the "p" value to variations in asphalt binder characteristics (modified asphalts) and changes in the type and character of the coarse aggregate used in the mixture. Additional work is needed to establish criteria for rut-resistant mixtures.

3. Additional research is required to calibrate the hyperbolic models under different stress and temperature conditions. It is expected that one or more parameters will show stress and/or temperature dependency. A complete calibration of the permanent deformation model developed herein should also be performed, and comparisons with other currently used models should be accomplished.
4. Additional work is needed to establish a full range of fractal dimensions for mixtures containing different aggregate types and then perform correlations with pavement performance and permanent deformation testing results. Fractal analysis is a simple technique and of very practical value. Its use should be extended to the analysis and measurement of pavement skid resistance.
5. Do not arbitrarily increase asphalt content above optimum to facilitate compaction or achieve the required density or because the mixture "looks dry." Mixture design data should be carefully reviewed to estimate the consequences of increasing asphalt content or, if warranted, a new mixture design should be developed.

REFERENCES

1. Kalcheff, I.V. and Tunnicliff, D.G., "Effects of Crushed Stone Aggregate Size and Shape on Properties of Asphalt Concrete," Proceedings of the Association of Asphalt Paving Technologists, Volume 51, 1982.
2. Benson, F.J., "Effects of Aggregate Size, Shape, and Surface Texture on the Properties of Bituminous Mixtures-A Literature Survey," Highway Research Board, Special Report 109, 1968.
3. Monismith, C.L., "Influence of Shape, Size, and Surface Texture on the Stiffness and Fatigue Response of Asphalt Mixtures," Highway Research Board, Special Report 109, 1968.
4. Hargett, E.R., "Effects of Size, Surface Texture, and Shape of Aggregate Particles on the Properties of Bituminous Mixtures," Highway Research Board, Special Report 109, 1968.
5. Herrin, M. and Goetz, W.H., "Effect of Aggregate Shape on Stability of Bituminous Mixes," Proceedings, Highway Research Board, Vol. 33, 1954.
6. Moore, R.B., and Welke, R.A., "Effects of Fine Aggregate on Stability of Bituminous Mixes," Michigan Transportation Commission, Research Report No. 78 TB-34-79F, December, 1979.
7. Griffith, J.M. and Kallas, B.F., "Influence of Fine Aggregate on Asphalt Concrete Paving Mixtures," Proceedings of Highway Research Record, Vol. 37, 1958, pp 219-255.
8. Brown, E.R., "Practical Approaches to Minimize Rutting in Hot Mix Asphalt," New Mexico Paving Conference, Albuquerque, New Mexico, January, 1988.
9. Lai, J.S., "Evaluation of Rutting Characteristics of Asphalt Mixes Using Loaded Wheel Tester," Georgia Department of Transportation, Research Project No. 8609, December, 1986.
10. Hanson, D.I., "Asphalt Mix Control in New Mexico, Proceedings of FHWA Tri-Regional Pavement Rehabilitation Conference," Oklahoma City, Oklahoma, May, 1984.
11. Page, G.C., "Rutting - Causes and Prevention," Proceedings of FHWA Tri-Regional Pavement Rehabilitation Conference, Oklahoma City, Oklahoma, May, 1984.
12. "Rutting Investigation," Materials Laboratory, Wyoming State Highway Department, Cheyenne, Wyoming, April, 1982.

13. Tam, K.K. and Lynch, D.F., "Ontario Freeway Rutting Investigation," Engineering Materials Office, Ontario MTC, Road and Transportation Association of Canada, 1986.
14. Van de Loo, P.J., "The Creep Test: A Key Tool in Asphalt Mix Evaluation and in Prediction of Rutting," Proceedings of AAPT, 1978, pp.522-557.
15. Barksdale, R.D. and Miller, J.H., "Development of Equipment and Techniques for Evaluating Fatigue and Rutting Characteristics of Asphalt Concrete Mixes," Georgia Institute of Technology, SCEGIT-77-149, July, 1977.
16. Monismith, C.L. and Tayelabi, A.A., "Permanent Deformation (Rutting) Considerations in Asphalt Concrete Pavement Sections," Proceedings of AAPT, Vol 57, 1988, pp.414-463.
17. Lai, J.S. and Anderson, D., "Irrecoverable and Recoverable Nonlinear Viscoelastic Properties of Asphalt Concrete," Highway Research Record 468, 1973.
18. Freeman, T.J. and Carpenter, S.H., "Characterizing Permanent Deformation in Asphalt Concrete Placed over Portland Cement Concrete Pavements," Transportation Research Record 1070, Washington, D.C., 1986.
19. Ameri-Gaznon, M. and Little, D.N., "Permanent Deformation Potential in Asphalt Concrete Overlay Over Portland Cement Concrete Pavements," Research Report No. 452-3F, Texas Transportation Institute, Texas A&M University, College Station, Texas, November, 1988.
20. Brown, S.F. and Bell, C.A., "The Validity of Design Procedures for the Permanent Deformation of Asphalt Pavements," Proceedings, 4th International Conference on the Structural Design of Asphalt Pavements, Vol. 1, University of Michigan, Ann Arbor, Michigan, August, 1977.
21. Mahboub, K. and Little, D.N., "Improved Asphalt Concrete Mixture Design Procedure," Research Report No. 474-1F, TTI, College Station, Texas, July, 1988.
22. Haas, R.C.G. and Papagianakis, A.T., "Understanding Pavement Rutting," Roads and Transportation Association of Canada, Toronto, Ontario, September, 1986.
23. Monismith, C.L., "Rutting Predictions in Asphalt Concrete Pavements," Transportation Research Record 616, Washington, D.C., 1976.

24. Saraf, C.L., Smith, W.S., and Finn, F.N., "Rut Depth Prediction," Transportation Research Record 616, Washington, D.C., 1976.
25. Van de Loo, P.J., "Practical Approach to the Prediction of Rutting in Asphalt Pavements: The Shell Method," Transportation Research Record 616, Washington, D.C., 1976.
26. Button, J. and Perdomo, D., "Investigation of Rutting in Asphalt Concrete Pavements," Research Report No. 1121-1, Texas Transportation Institute, Texas A&M University, College Station, Texas, and Transportation Research Record 1259, March, 1989.
27. Button, J.W. and Epps, J.A., "Evaluation of Fabric Interlayers," Research Report 261-2, Texas Transportation Institute, Texas A&M University, College Station, Texas, 1982.
28. The Asphalt Institute, "Mix Design Methods for Asphalt Concrete and Other Hot-Mix Types," Manual Series No. 2, May, 1984.
29. "Standard Specifications for Construction of Highways, Streets, and Bridges," Texas State Department of Highways and Public Transportation, Austin, Texas, 1982.
30. Kennedy, T.W. and Hudson, W.R., "Application of the Indirect Tensile Test to Stabilized Materials," Highway Research Record 235, Highway Research Board, Washington, D.C., 1968.
31. "Manual of Testing Procedures," 200-F Series, Texas State Department of Highways and Public Transportation, Austin, Texas, 1985.
32. Huang, E.Y., "A Test for Evaluating the Geometric Characteristics of Coarse Aggregate Particles," Proceedings, American Society for Testing Materials, Vol. 62, 1962, pp. 1223-1242.
33. "Construction Bulletin C-14," State Department of Highways and Public Transportation, Construction Division, April, 1984.
34. Kenis, W. J., "Predictive Design Procedures," VESYS User's Manual, FHWA Report 77-154, 1978.
35. Perl, M., Uzan, J. and Sides, A., "Visco-Elasto-Plastic Constitutive Law for Bituminous Mixtures Under Repeated Loading," Transportation Research Record 911, Washington, D.C., 1984, pp. 20-27.
36. Tseng, K.H. and Lytton, R.L., "Prediction of Permanent Deformation in Flexible Pavement Materials," Presented at ASTM Symposium on Implication of Aggregate in the Design, Construction and Performance of Flexible Pavements, New Orleans, Louisiana, December, 1986.

37. Juarez-Badillo, E., "General Compressibility Equation for Soils," Tenth International Conference on Soil Mechanics and Foundation Engineering, Stockholm, Sweden, Vol. 1, pp. 171-178.
38. Hooke, R. and Jeeves, T.A., "Direct Search Solution of Numerical and Statistical Problems," J. Assn. Comp. Mach., 8, 2, April, 1961.
39. Kuester, J.L. and Mize, J.H., "Optimization Techniques with Fortran," McGraw Hill, 1973.
40. Uzan, J. and Smith, R.E., TFPS Technical Report, Texas Transportation Institute, Texas A&M University, College Station, Texas, August, 1988.
41. Mandelbrot, B.B., "Fractals: Form, Chance and Dimension," San Francisco, California, 1977.
42. Mandelbrot, B.B., "The Fractal Geometry of Nature," San Francisco, California, 1982.
43. Richardson, L.F., "The Problem of Contiguity: An Appendix of Statistics of Deadly Quarrels," General Systems Yearbook, Vol. 6, pp. 139-187, 1961.
44. Fournier, A., Fussel, D., and Carpenter, L., "Computer Rendering of Stochastic Models," Commun. ACM, Vol. 25, No. 6, 1982, pp. 371-384.
45. Gagalowicz, A., "A New Method for Texture Fields Synthesis: Some Applications to the Study of Human Vision," IEEE Trans. Pattern Anal. Machine Intell., Vol PAMI-3, September, 1981, pp. 520-533.
46. Gonzales, R.C., "Digital Image Processing," Advanced Book Program, 1977.
47. Duncan, J.M., Monismith, C.L., and Wilson, E.L., "Finite Element Analysis of Pavements," Highway Research Record 28, 1968, pp. 18-33.
48. Roberts, F.L., Tielking, J.T., Middleton, D., Lytton, R.L. and Tseng, K.H., "Effects of Tire Pressure on Flexible Pavements," Report No. 372-1F, Texas Transportation Institute, Texas A&M University, College Station, Texas, August, 1986, pp. 223-235.
49. Li, J., "Use of Climatic Data for the Prediction of Permanent Deformation in Flexible Pavements," Masters of Engineering Report, Texas A&M University, College Station, Texas, June, 1987.
50. Button, J.W., M. Ameri-Gaznon, D. Perdomo, D.N. Little, and D.G. Zollinger, "Avoiding Early Failure of Intersection Pavements", Report 1172-1F, Texas Transportation Institute, Texas A&M University, November 1989.

51. FHWA Technical Advisory T5040.27, "Asphalt Concrete Mix Design and Field Control," Federal Highway Administration, U.S. Department of Transportation, Washington, D.C., March 1988.
52. Chastain, W.E., and J.E. Burke, "State Practices in the Use of Bituminous Concrete," HRB Bulletin No. 60, Highway Research Board, Washington, D.C., 1957, pp. 1-107.
53. Foster, C.R., "Dominant Effect of Fine Aggregate on Strength of Dense-Graded Asphalt Mixes," Special Report 109, Highway Research Board, Washington, D.C., 1970.
54. McLeod, N.W., "Designing Standard Asphalt Paving Mixtures for Greater Durability," Proceedings, Canadian Technical Asphalt Association, Volume 16, 1971.
55. Von Quintus, H.L., J.A. Scherocman, C.S. Hughes, and T.W. Kennedy, "Development of Asphalt-Aggregate Mixture Analysis Sytem: AAMAS," National Cooperative Highway Research Program, Washington, D.C., September 1988.
56. Krugler, P.E., "Voids in the Mineral Aggregate," Technical Quarterly, Volume 5, Issue 1, Texas State Department of Highways and Public Transportation, Austin, Texas, June 1989.
57. AASHTO Designation: T245-82, "Resistance to Plastic Flow of Bituminous Mixtures Using the Marshall Apparatus," Standard Specifications for Transportation Materials and Methods of Sampling and Testing, Part II, 14th Edition, August 1988.
58. ASTM Designation: D1559-82, Resistance to Plastic Flow of Bituminous Materials Using the Marshall Apparatus, Annual Book of Standards, Volume 04.03, Road and Paving Materials; Traveled Surface Characteristics, 1989.
59. Davis, R.L., "large Stone Mixes: A Historical Insight," IS103/88, National Asphalt Pavement Association, Riverdale, Maryland, 1989.
60. Button, J.W. and D.N. Little, "Asphalt Additives for Increased Pavement Flexibility," Report No. FHWA/TX-87/471-2F, Texas Transportation Institute, Texas A&M University, November 1987.
61. Little, D.N., J.W. Button, R.M. White, E.K. Ensley, Y. Kim, and S.J. Ahmed, "Investigation of Asphalt Additives," Report No. FHWA/RD-87/001, Texas Transportation Institute, Texas A&M University, November 1986.

62. Sainton, A., "Advantages of Asphalt Rubber Binder for Porous Asphalt Concrete," Beugnet Group, France, Paper submitted for presentation at 69th Annual Transportation Research Board, January 1990.
63. Acott, M., "Today's Traffic Calls for Heavy Duty Asphalt Mixes," Roads and Bridges, Volume 26, No. 1, January 1988, pp. 39-45.

APPENDIX A

SAMPLE PREPARATION AND TESTING TECHNIQUES

APPENDIX A
SAMPLE PREPARATION AND TESTING TECHNIQUES

Mixing Method

The asphalt and the aggregate were mixed according to Texas SDHPT method TEX-205-F. After blending, the temperature of the asphalt concrete mixture was raised to 250°F-270°F for compaction.

Cylindrical Specimen Fabrication

Cylindrical specimens were compacted four inches in diameter by eight inches high, using a kneading compactor.

Each specimen was compacted in three lifts of approximately equal height. In order to reach a uniform density throughout the sample, various trial samples were produced using different compactive efforts. These samples were then sawed at each lift interface, and tested for density. The following compaction scheme provided uniform density distribution in the cylindrical specimens:

1. First layer: 30 tamps
2. Second layer: 60 tamps
3. Third layer: 140 tamps

The stress level used during compaction was the same for every layer, although it varied among low and high air void samples, and among the different mixtures being compacted. It is clear, for example, that a sample containing 40 percent natural sand needed less energy of compaction for a target level of air voids, than a sample containing zero percent natural sand (40 percent limestone screenings).

Each cylindrical sample was then subjected to a constant sustained load for a period of one minute. This load was generally 1000 lbs for high air void samples, and 1500 lbs for low air void samples.

Subsequently, the specimens were capped on each end with sulfur and stored in a 50°F environmental chamber to minimize any binder changes before the test was performed. All specimens were then tested between four days and 15 days after fabrication. Just prior to testing, the samples were conditioned in the test temperature environment for at least eight hours to achieve an homogeneous temperature distribution within the specimen. The test was conducted under the conditions required by each specific test, as briefly described in the next sections of this appendix.

Long-term Static Creep Testing

In this test, a constant static load was applied to the sample for a reasonable long-term period of time (the target value was eight hours) within which the specimen was expected to reach failure. After testing several trial samples, it was determined that 60 psi was the stress level to be used. All tests used linear variable differential transformers (LVDT) to measure axial deformation.

Long-term Cyclic Testing

During the long-term cyclic testing a repeated haversine load with a peak stress of 60 psi was applied to the specimen. The same stress was used in order to facilitate comparison of the specimens among the testing techniques.

Triaxial Cyclic Testing

The compression stress level used for triaxial testing was also 60 psi. The confining pressure applied was 15 psi. Preparation of the samples was much more complicated since they had to be mounted on a triaxial cell.

APPENDIX B
RESULTS FROM LABORATORY INVESTIGATION

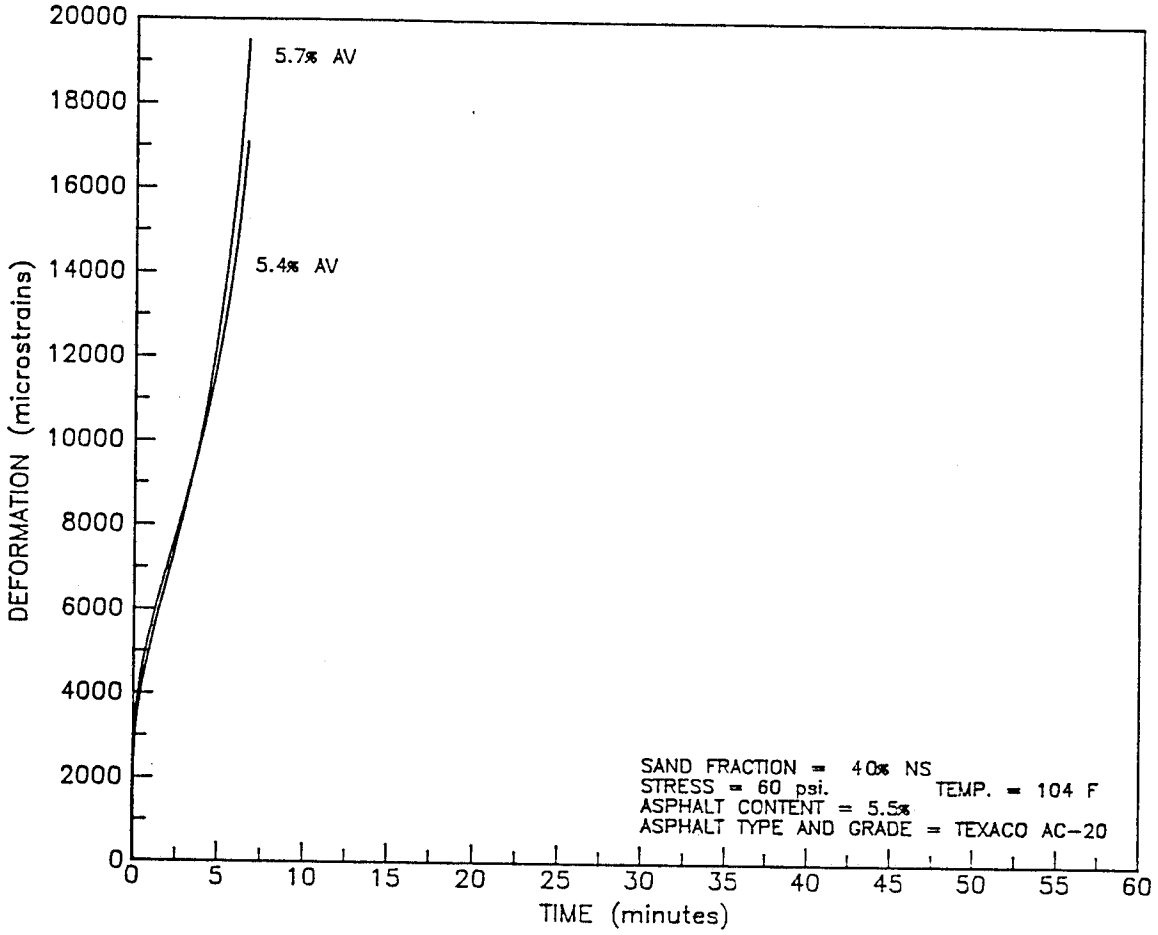

Figure B1. Total Deformation for Long-term Static Creep Tests at High Air Voids and 40% Natural Sand.

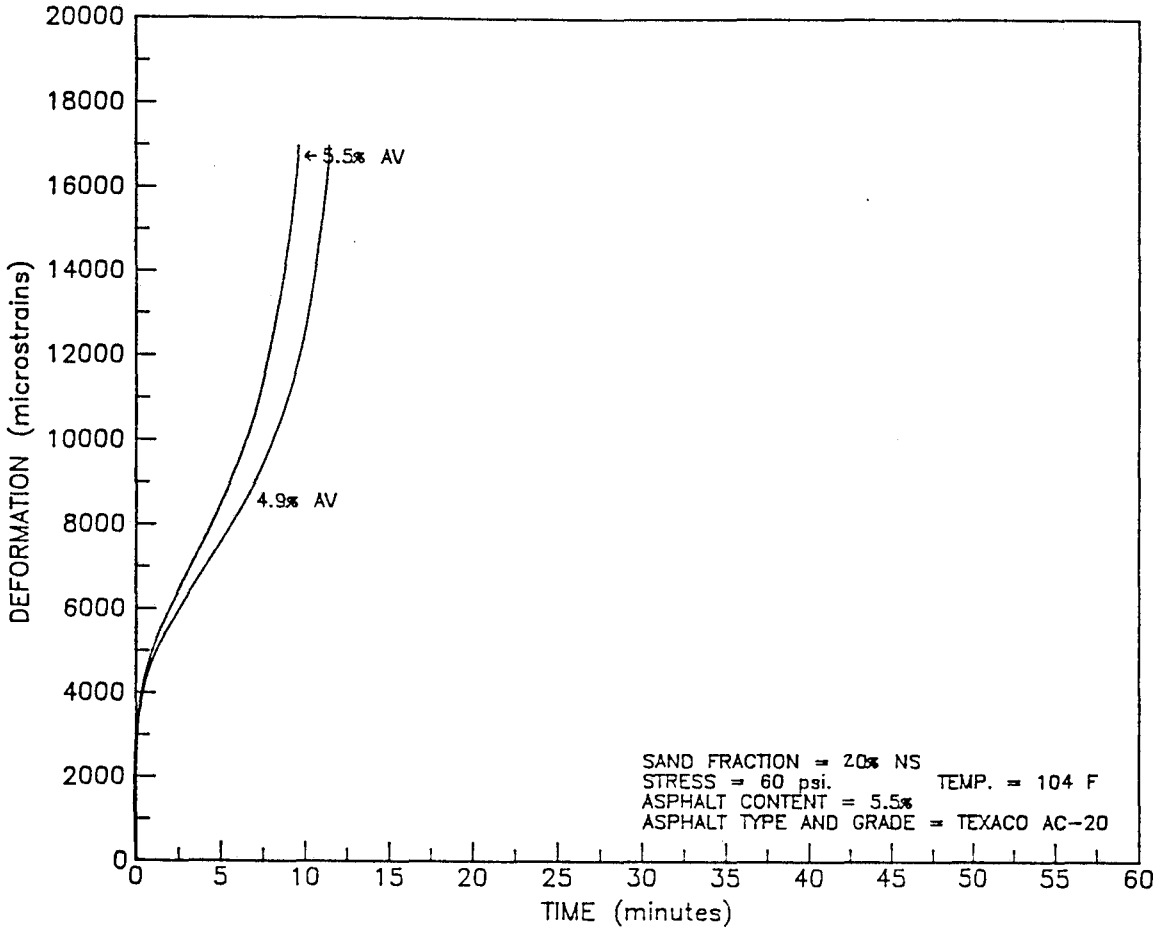

Figure B2. Total Deformation for Long-Term Static Creep Tests at High Air Voids and 20% Natural Sand.

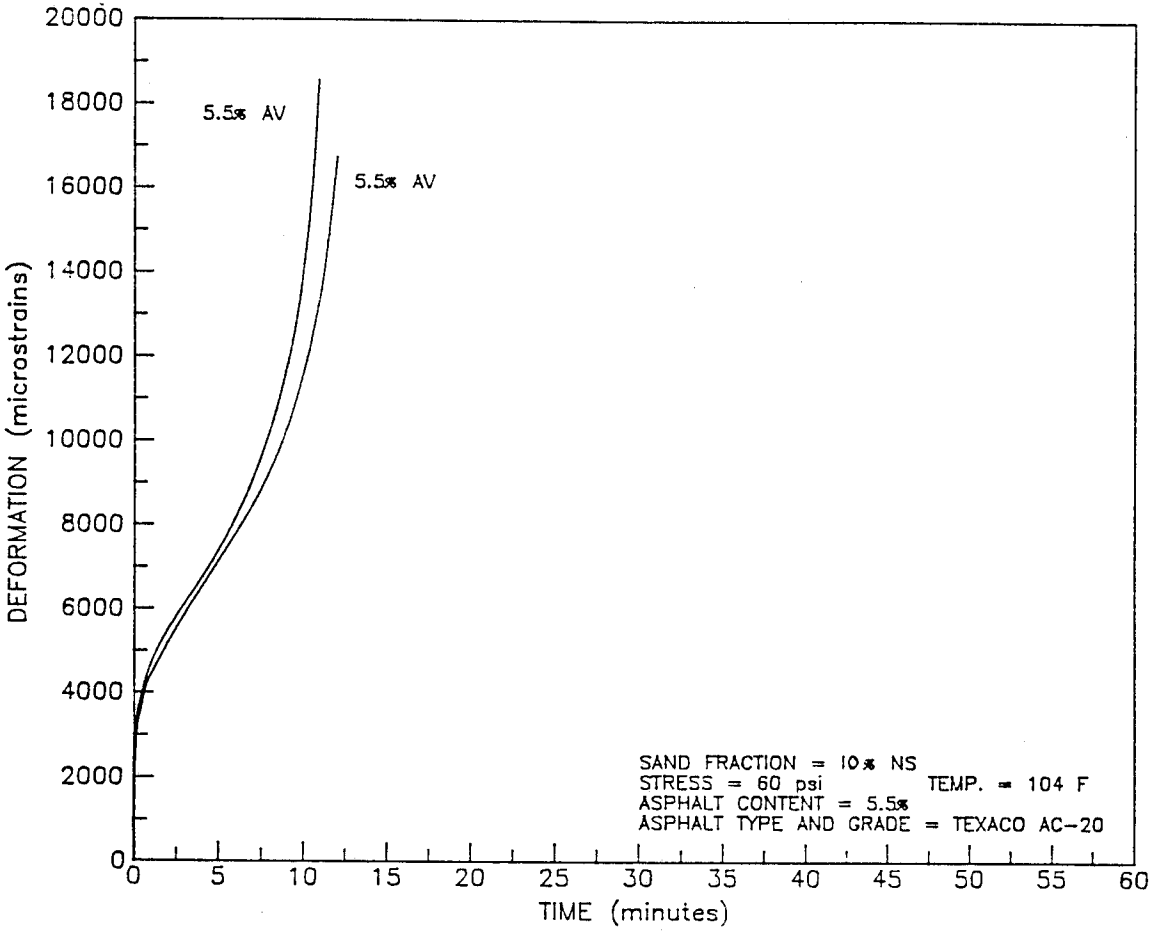

Figure B3. Total Deformation for Long-Term Static Creep Tests at High Air Voids and 10% Natural Sand.

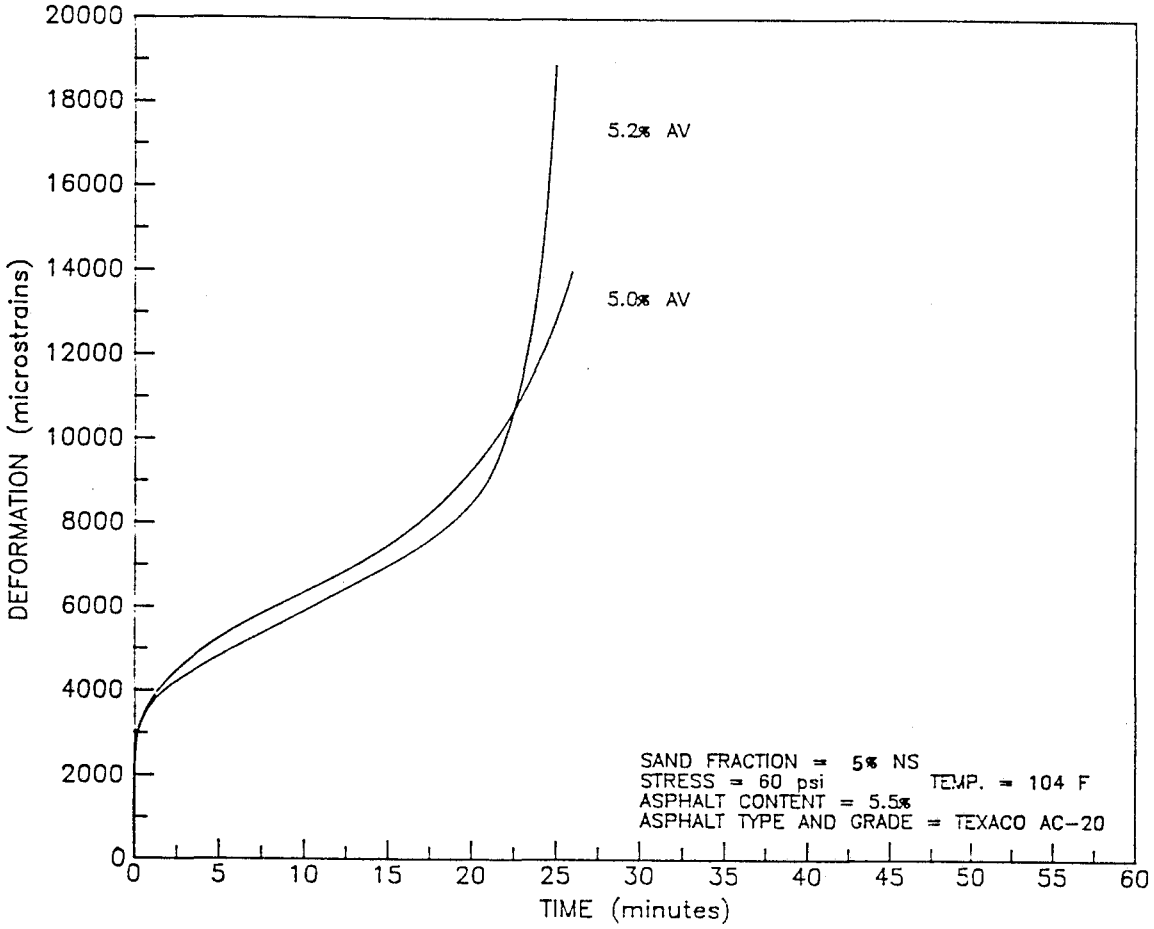

Figure B4. Total Deformation for Long-Term Static Creep Tests at High Air Voids and 5% Natural Sand.

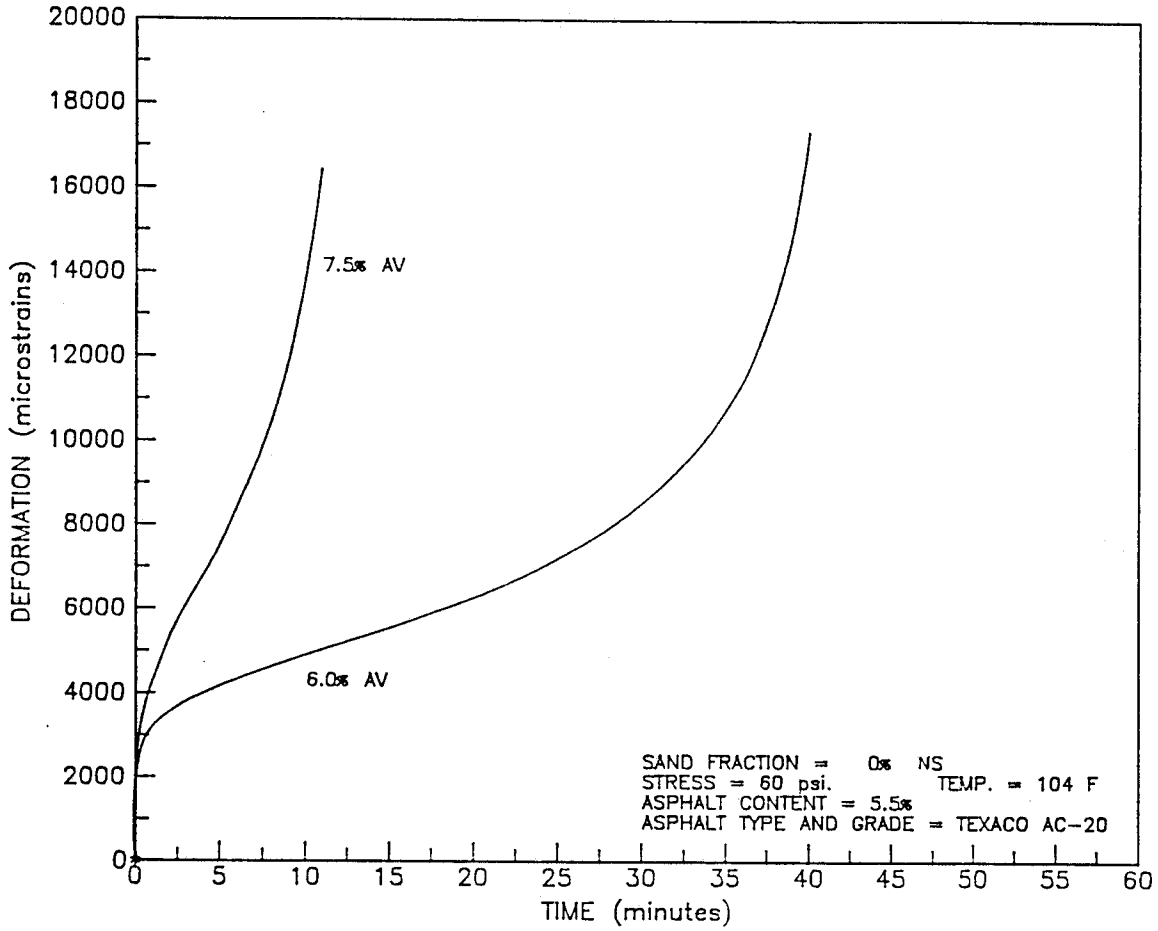

Figure B5. Total Deformation for Long-Term Static Creep Tests at High Air Voids and 0% Natural Sand.

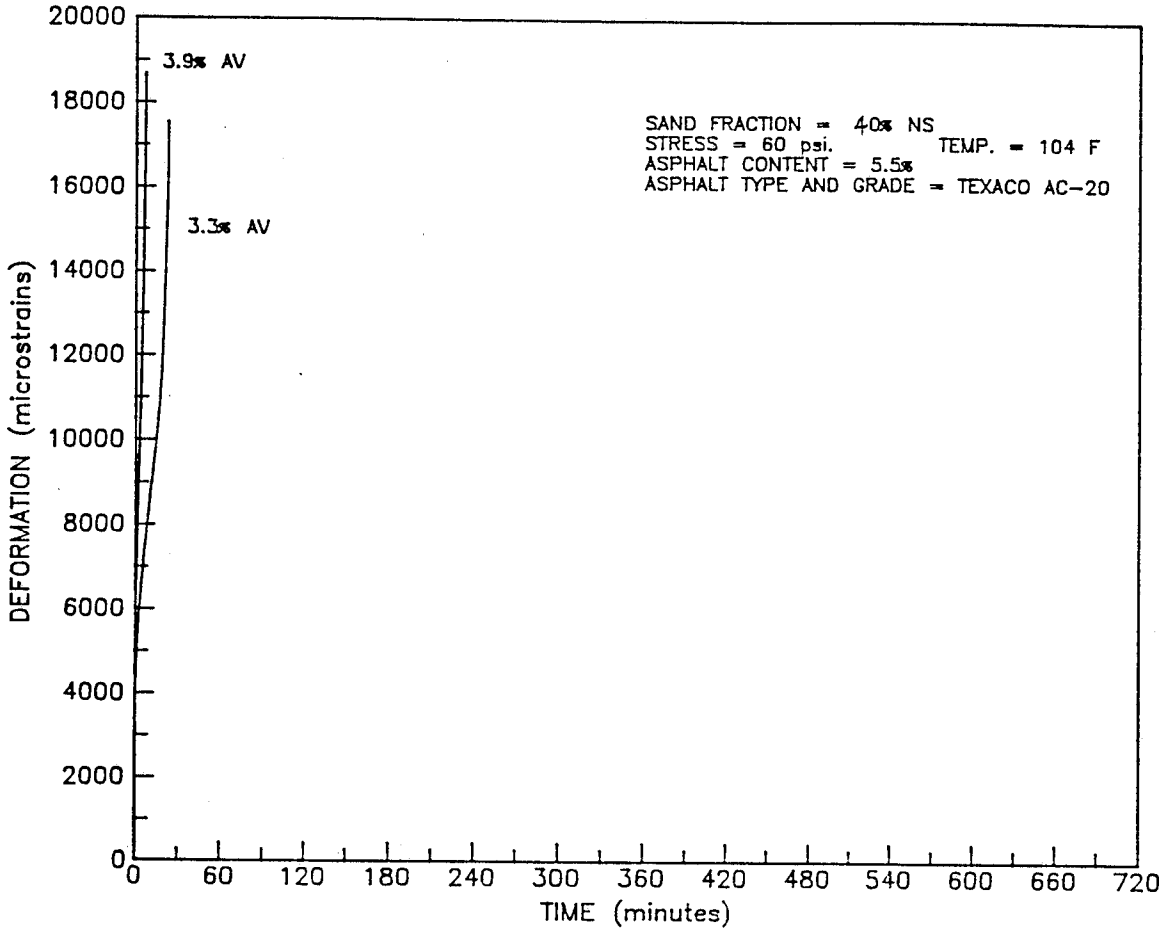

Figure B6. Total Deformation for Long-Term Static Creep Tests at Low Air Voids and 40% Natural Sand.

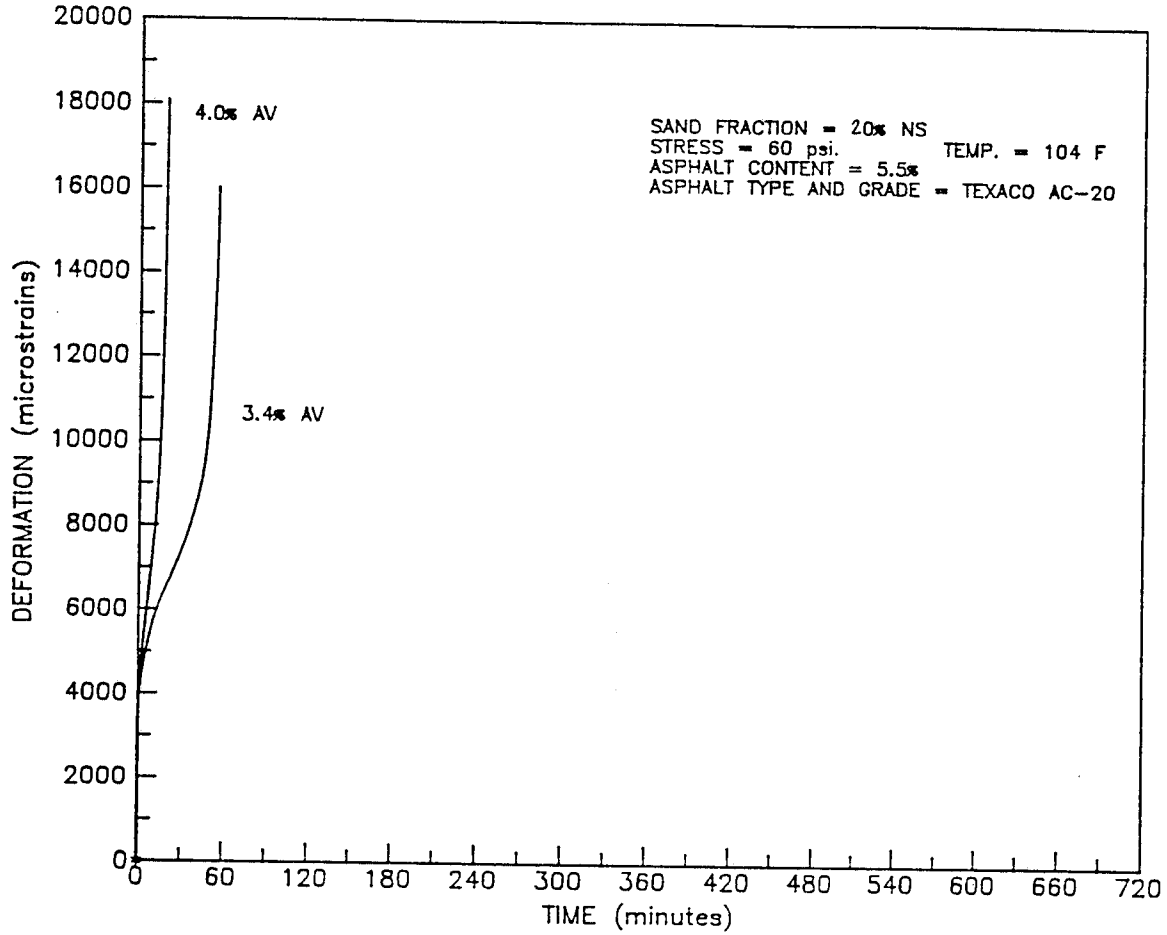

Figure B7. Total Deformation for Long-Term Static Creep Tests at Low Air Voids and 20% Natural Sand.

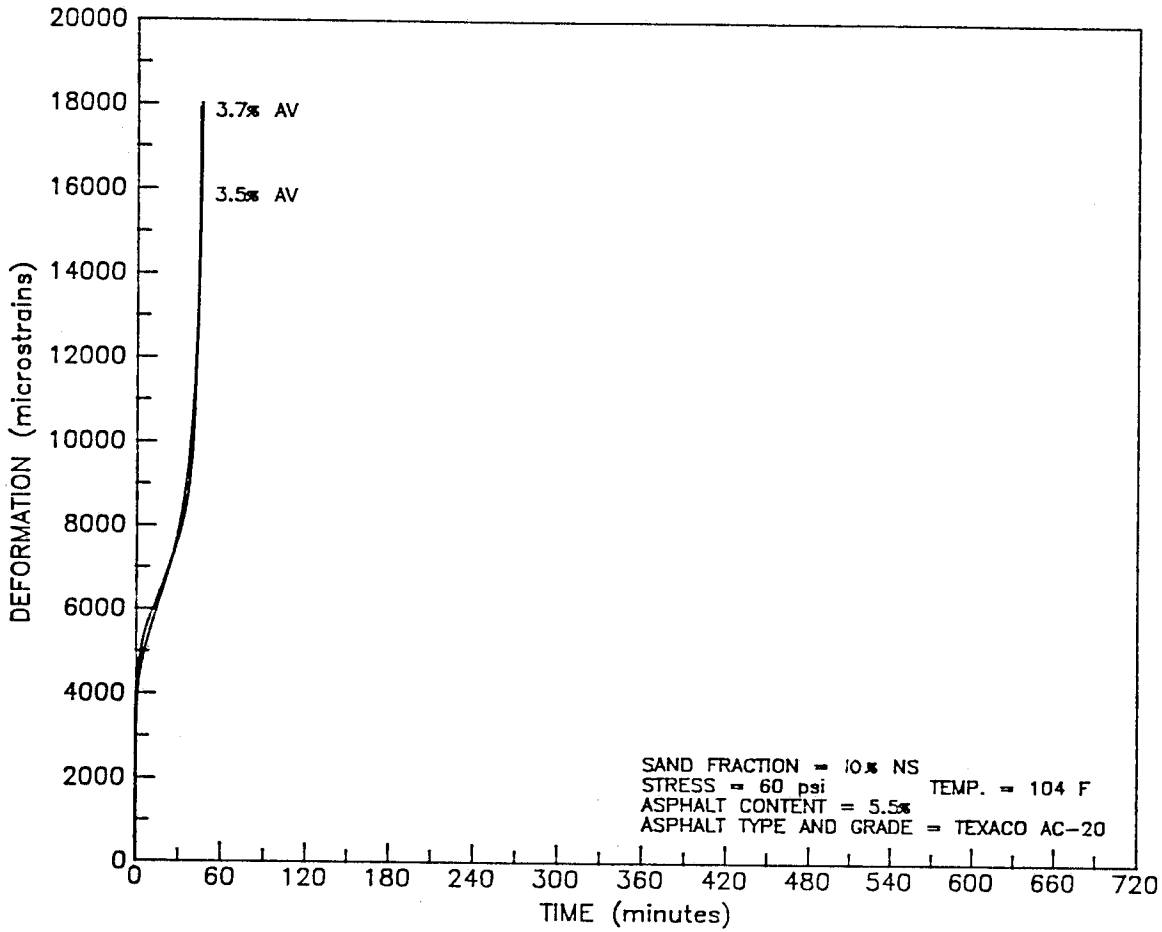

Figure B8. Total Deformation for Long-Term Static Creep Tests at Low Air Voids and 10% Natural Sand.

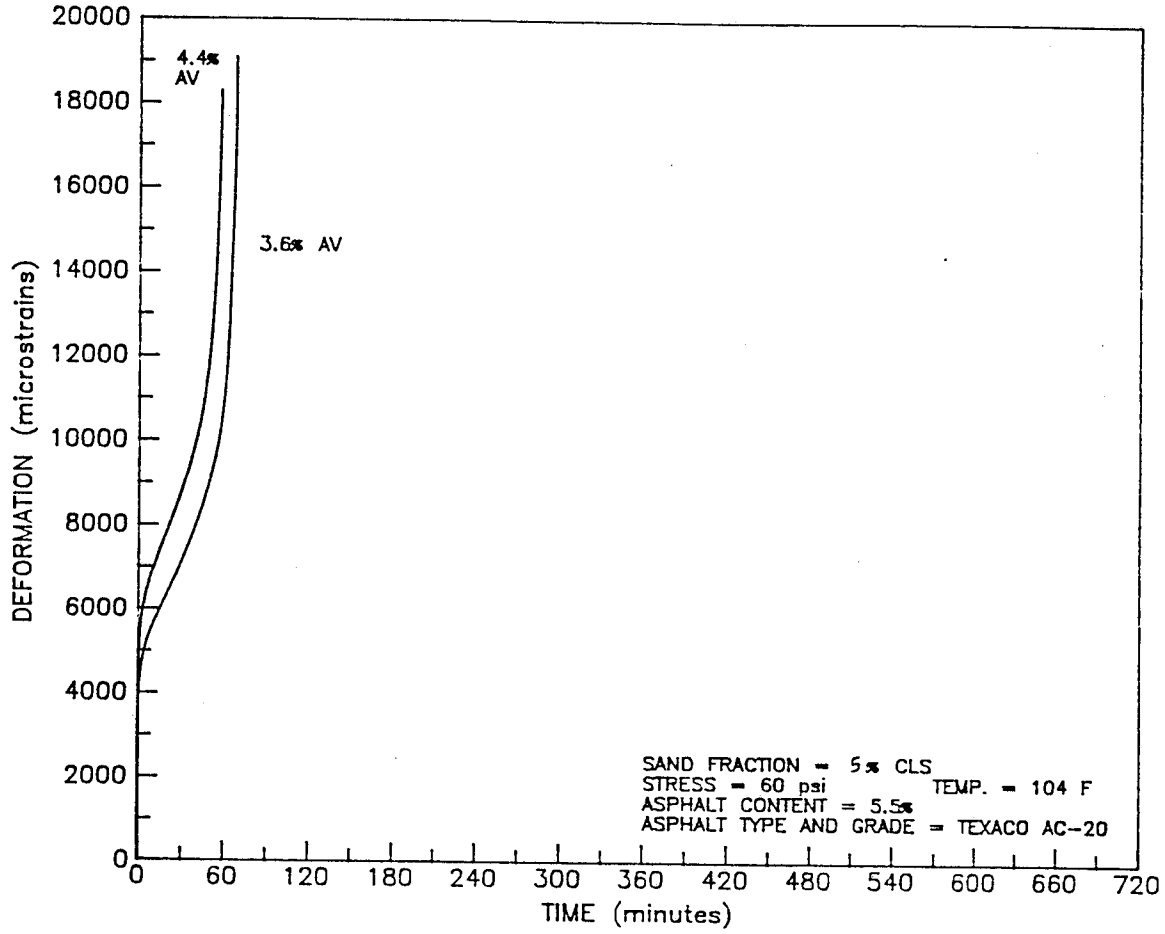

Figure B9. Total Deformation for Long-Term Static Creep Tests at Low Air Voids and 5% Natural Sand.

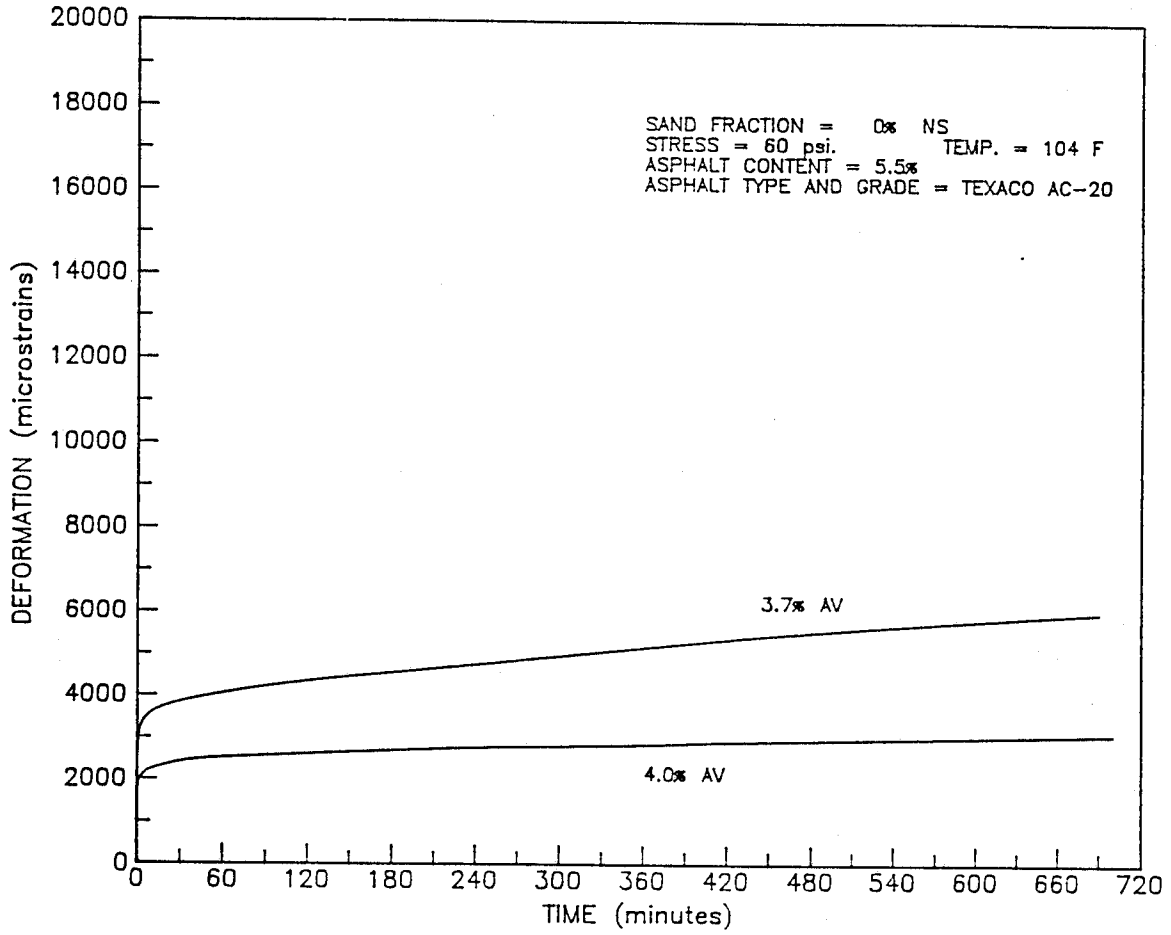

Figure B10. Total Deformation for Long-Term Static Creep Tests at Low Air Voids and 0% Natural Sand.

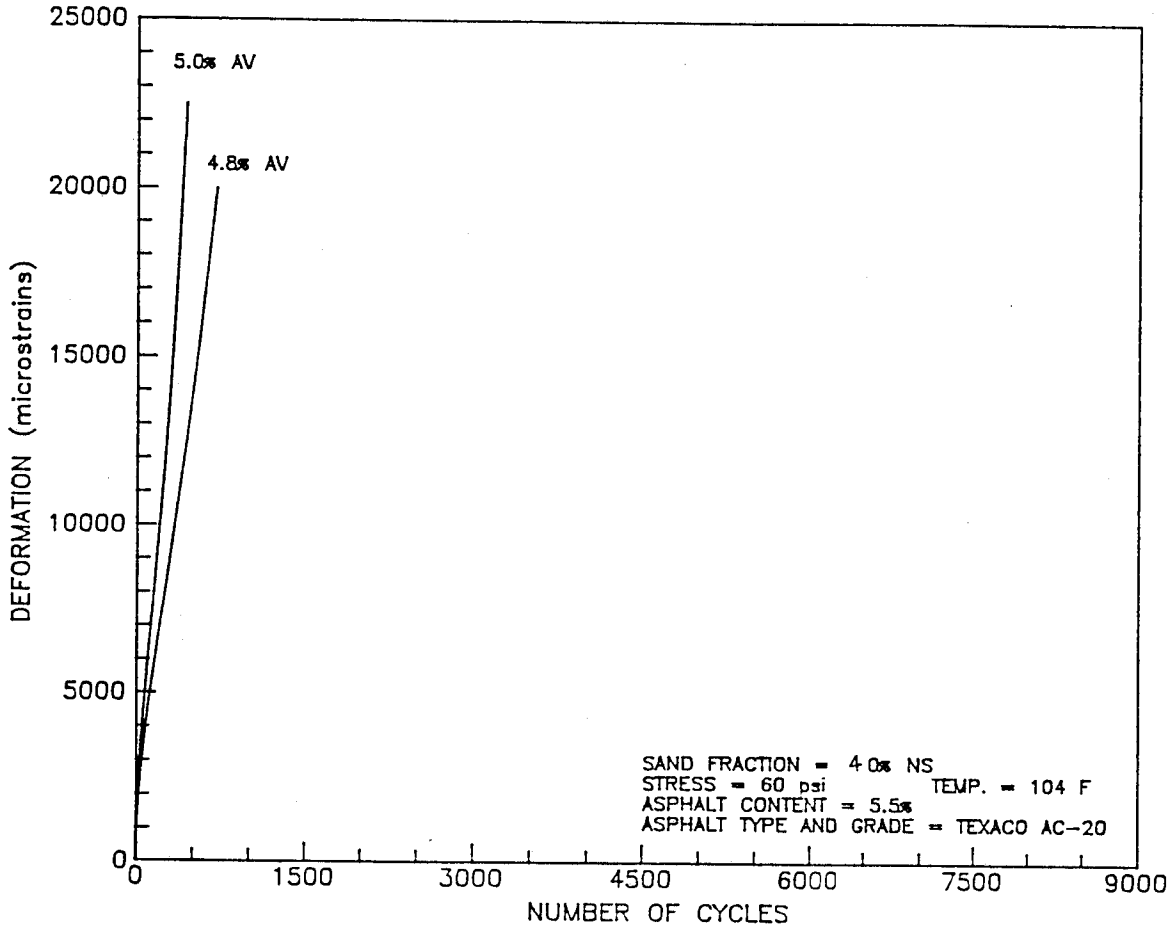

Figure B11. Permanent Deformation for Cyclic Tests at High Air Voids and 40% Natural Sand.

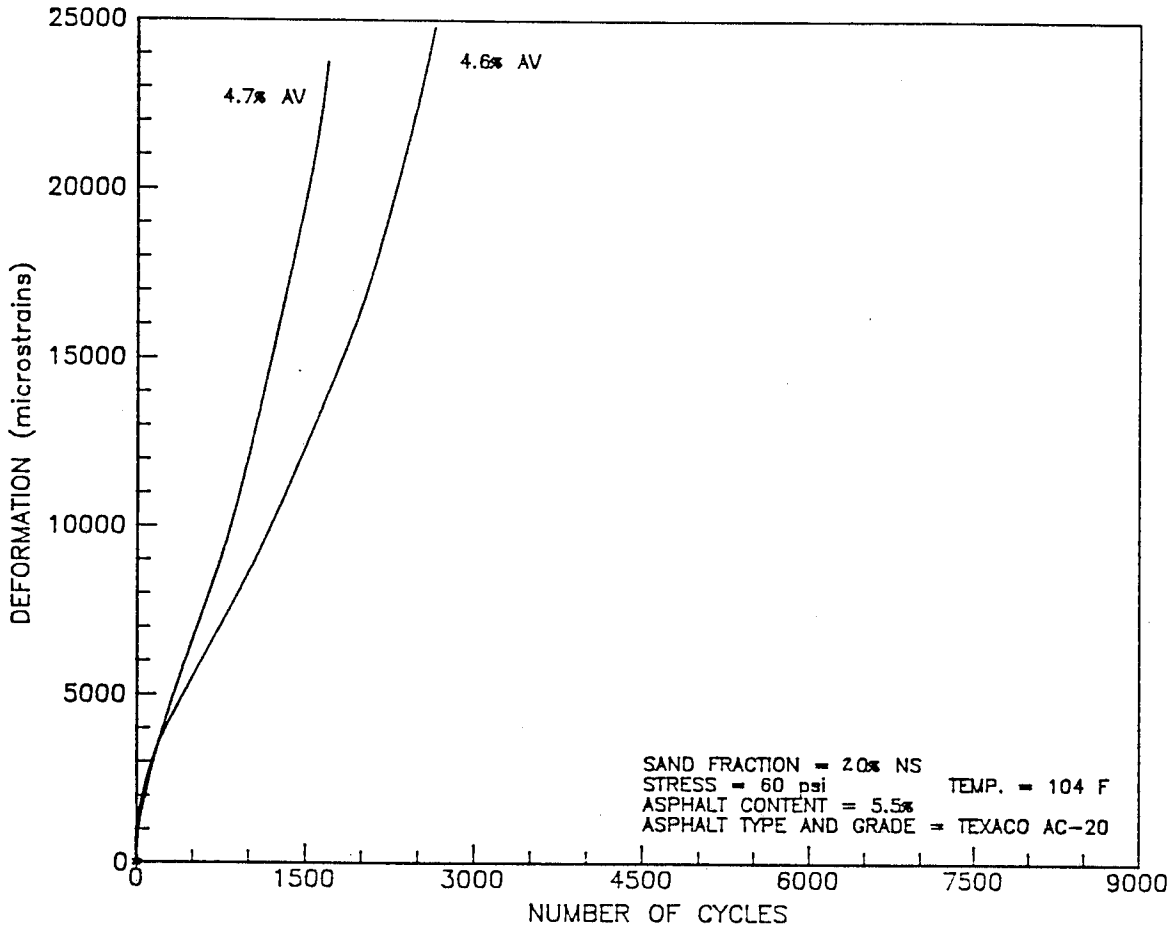

Figure B12. Permanent Deformation for Cyclic Tests at High Air Voids and 20% Natural Sand.

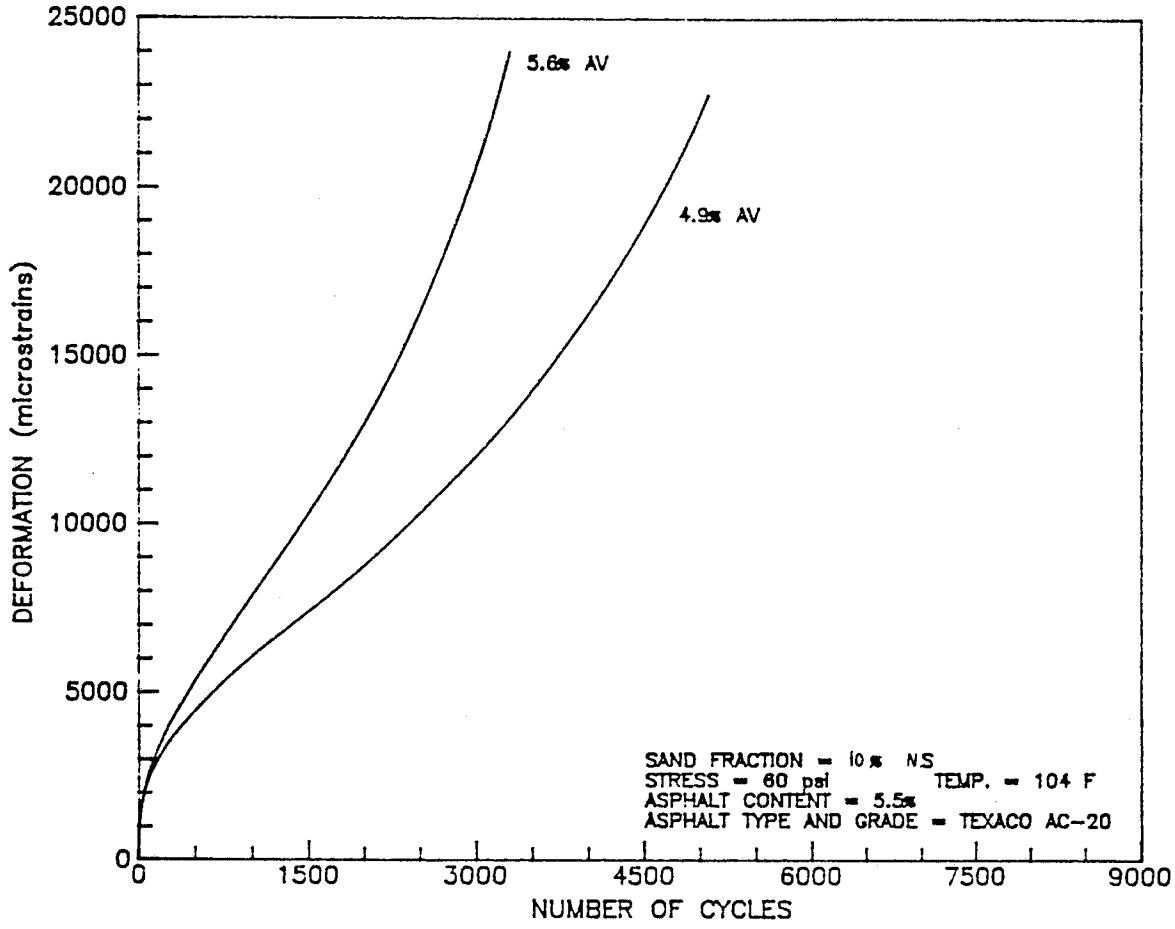

Figure B13. Permanent Deformation for Cyclic Tests at High Air Voids and 10% Natural Sand.

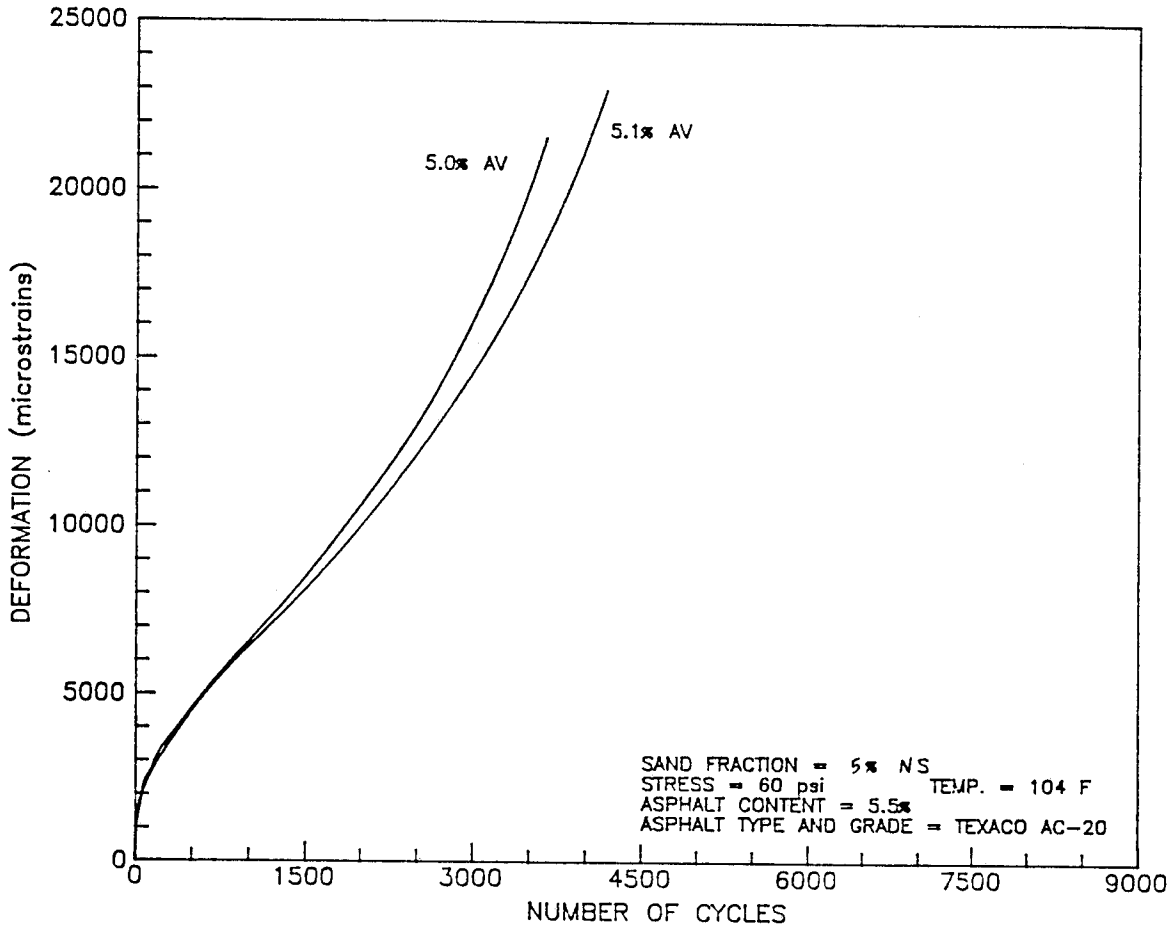

Figure B14. Permanent Deformation for Cyclic Tests at High Air Voids and 5% Natural Sand.

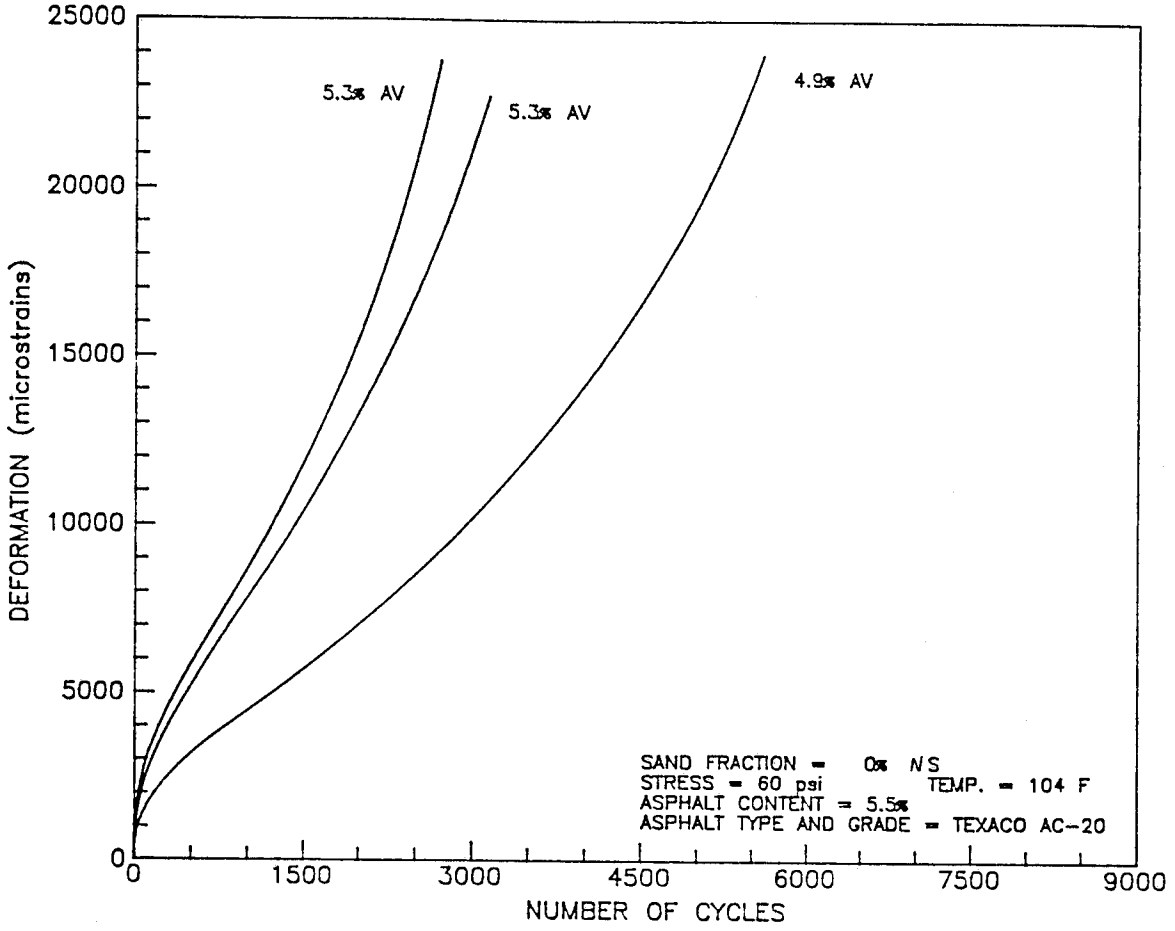

Figure B15. Permanent Deformation for Cyclic Tests at High Air Voids and 0% Natural Sand.

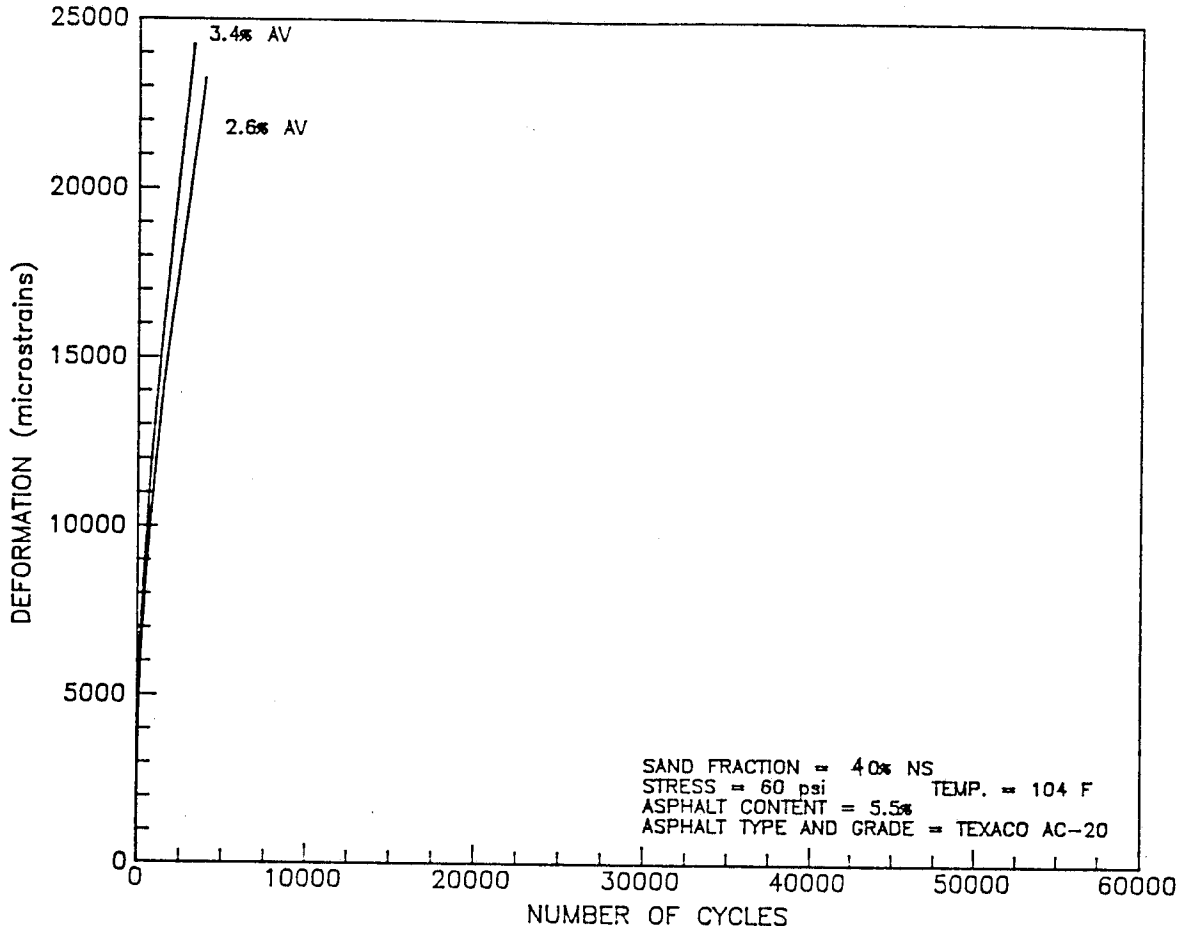

Figure B16. Permanent Deformation for Cyclic Tests at Low Air Voids and 40% Natural Sand.

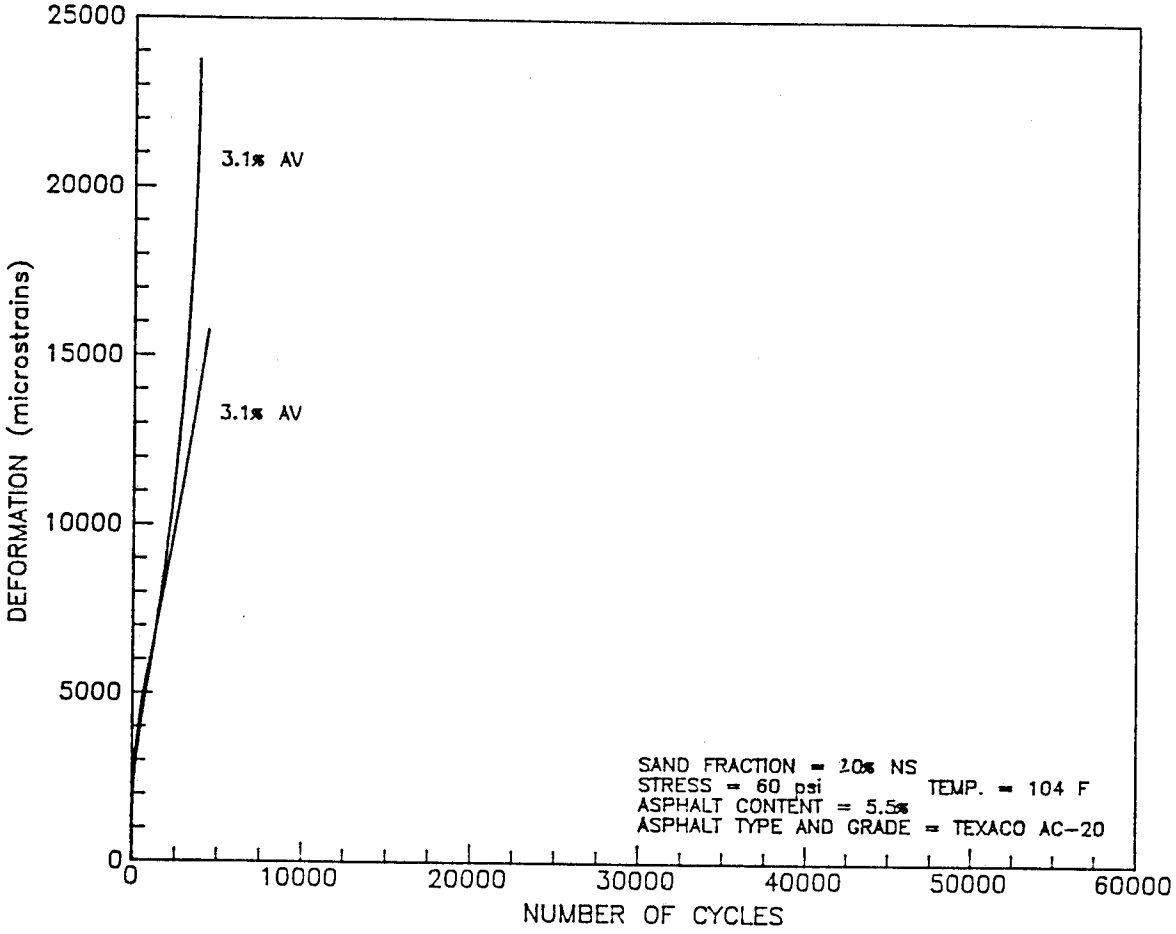

Figure B17. Permanent Deformation for Cyclic Tests at Low Air Voids and 20% Natural Sand.

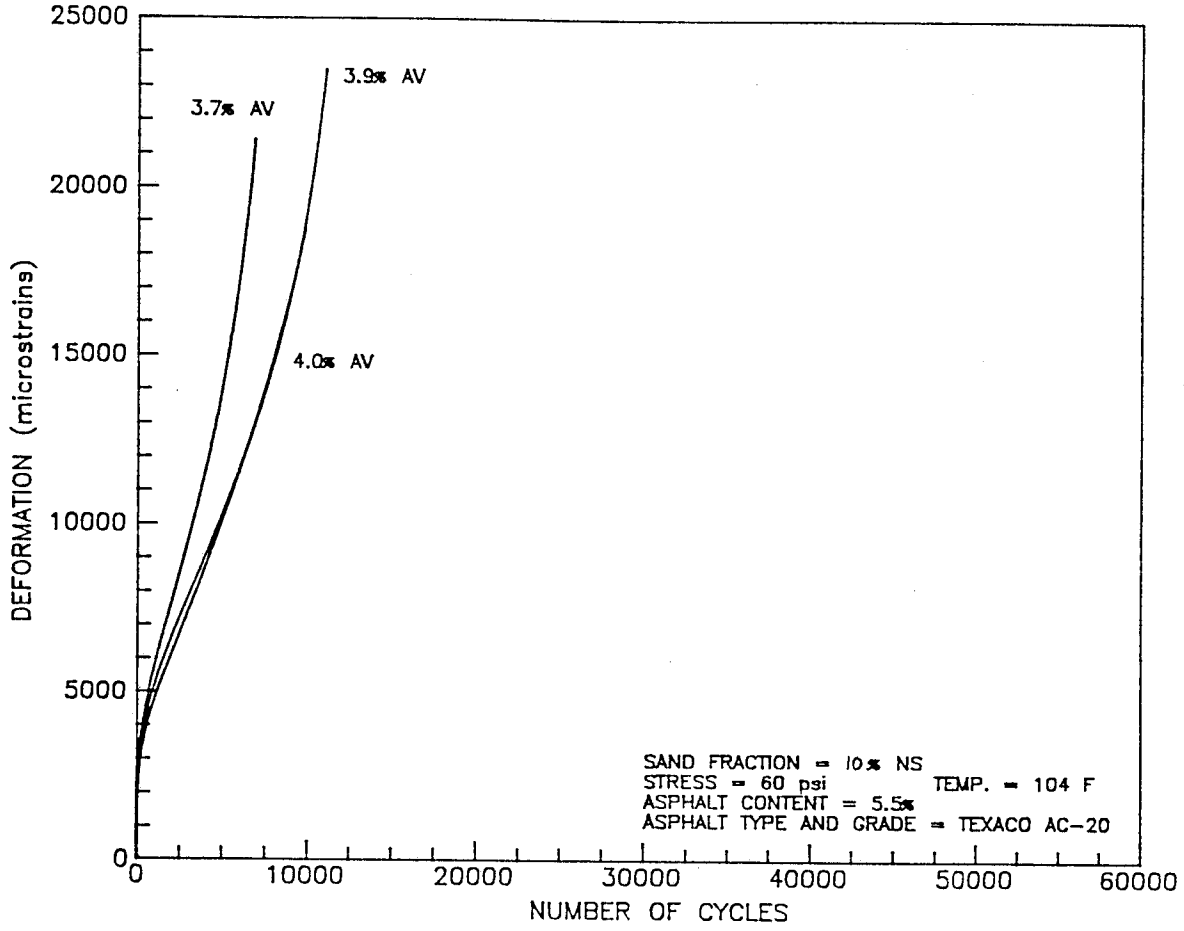

Figure B18. Permanent Deformation for Cyclic Tests at Low Air Voids and 10% Natural Sand.

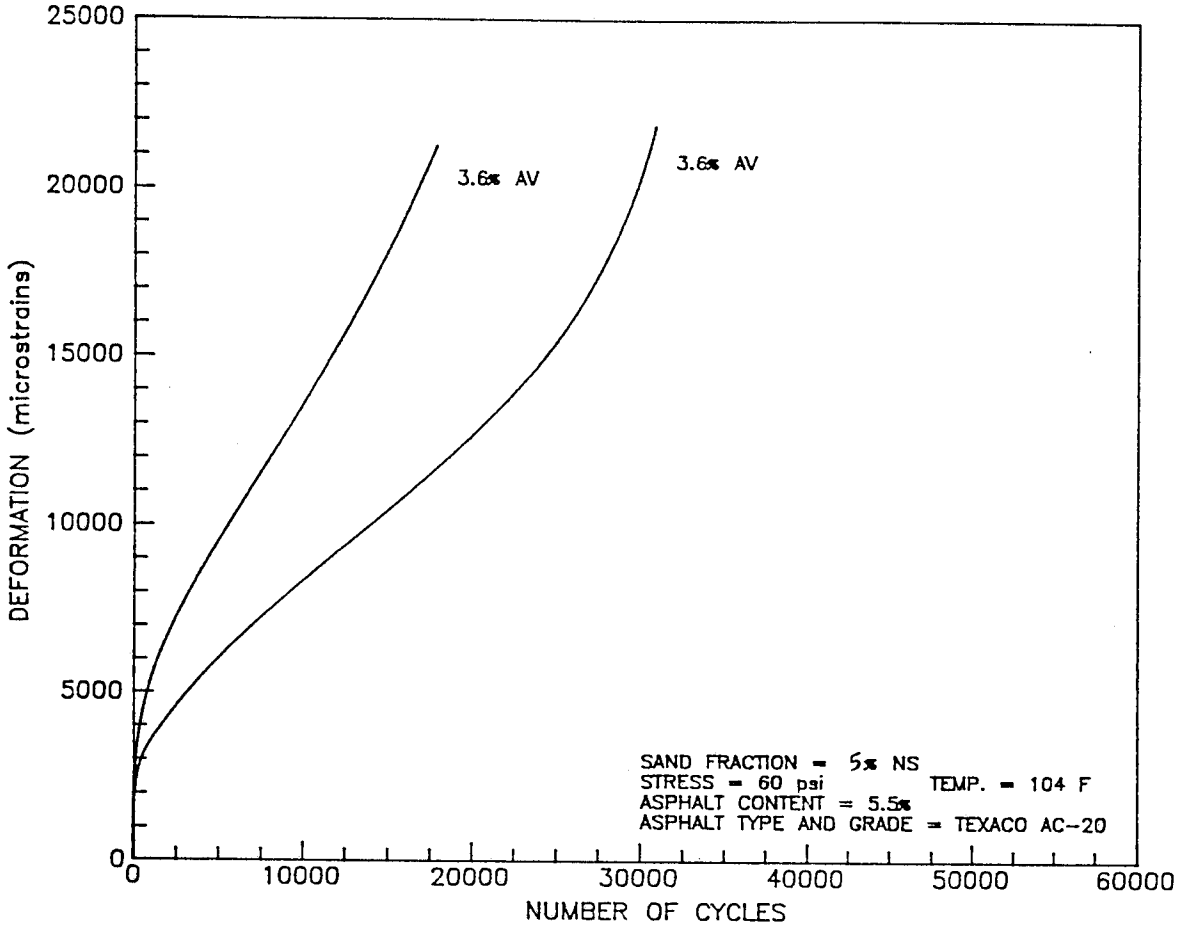

Figure B19. Permanent Deformation for Cyclic Tests at Low Air Voids and 5% Natural Sand.

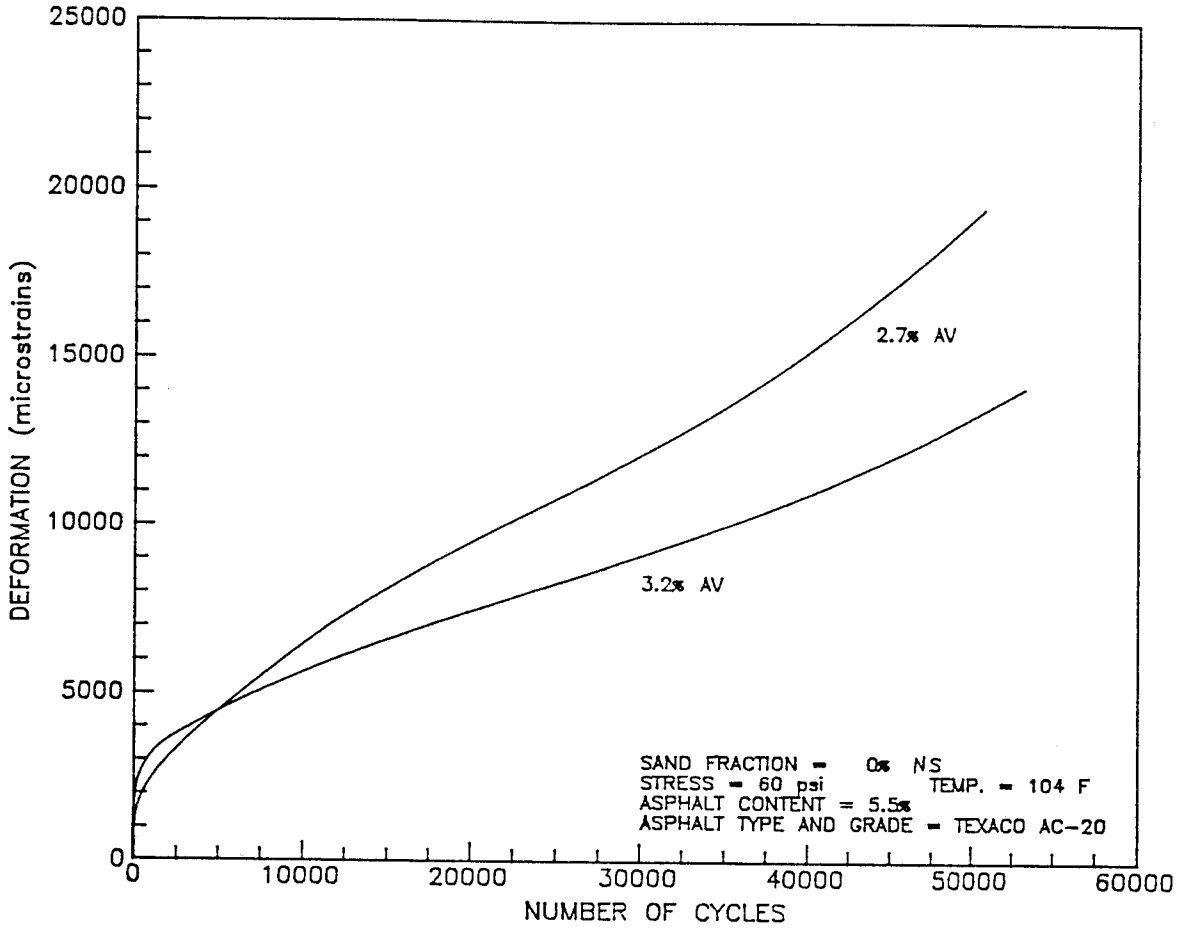

Figure B20. Deformation for Cyclic Tests at Low Air Voids and 0% Natural Sand.

APPENDIX C
RESULTS FROM THEORETICAL ANALYSIS

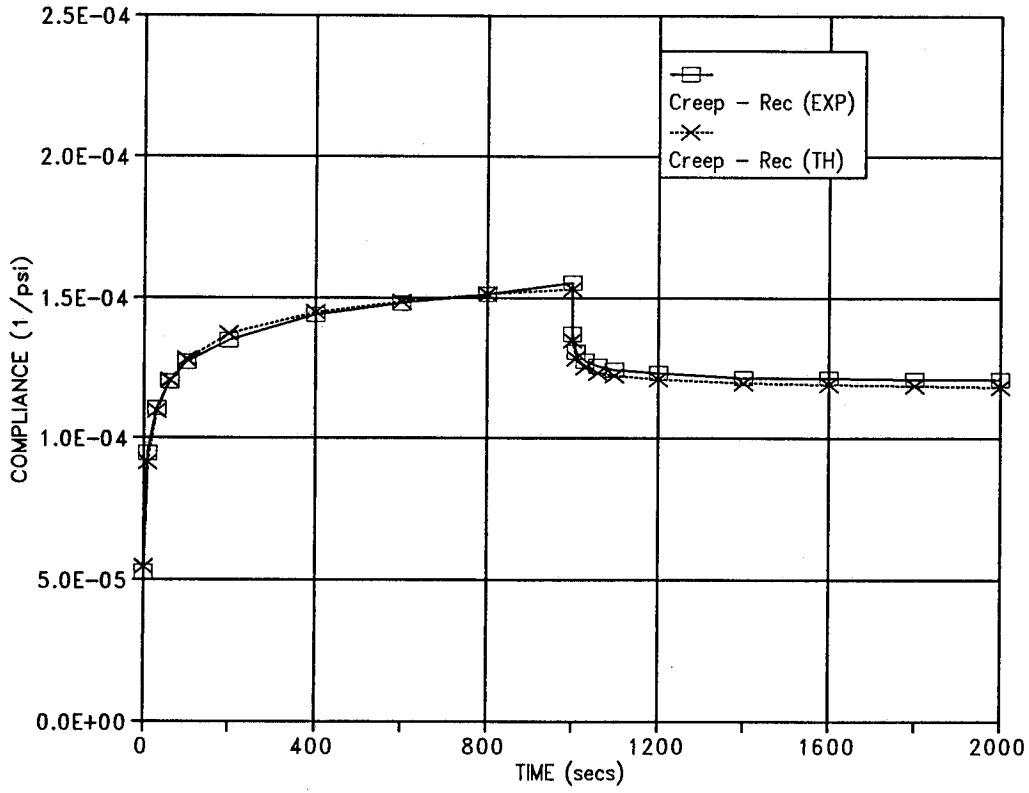

Figure C1. Typical Creep and Recovery Behavior for Mix with 0% Natural Sand, 7.1% Air Voids, and Optimum Asphalt Content.

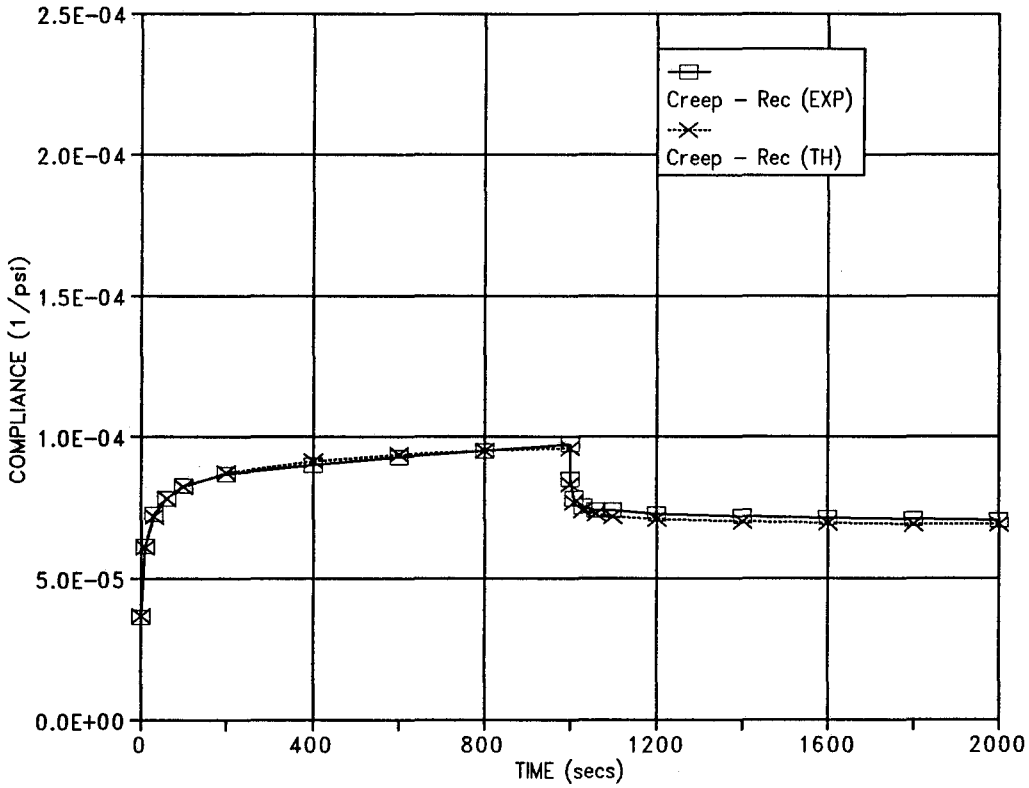

Figure C2. Typical Creep and Recovery Behavior for Mix with 0% Natural Sand, 5.1% Air Voids, and Optimum Asphalt Content.

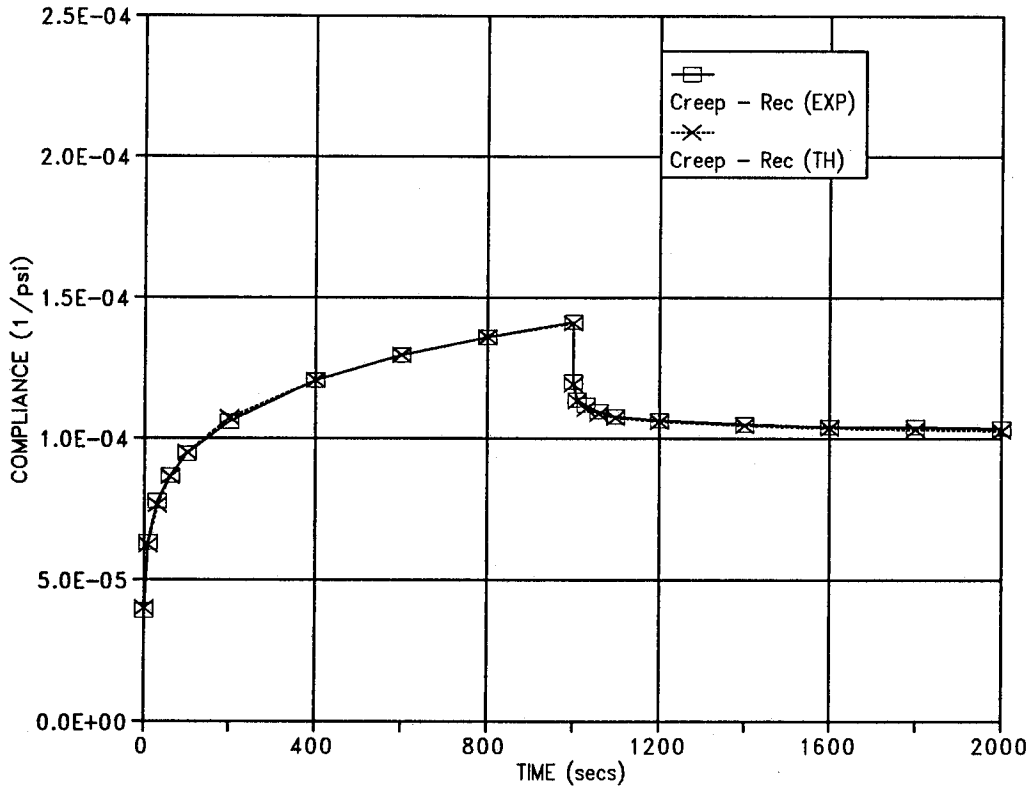

Figure C3. Typical Creep and Recovery Behavior of a Mix with 20% Natural Sand, 6.5% Air Voids, and Optimum Asphalt Content.

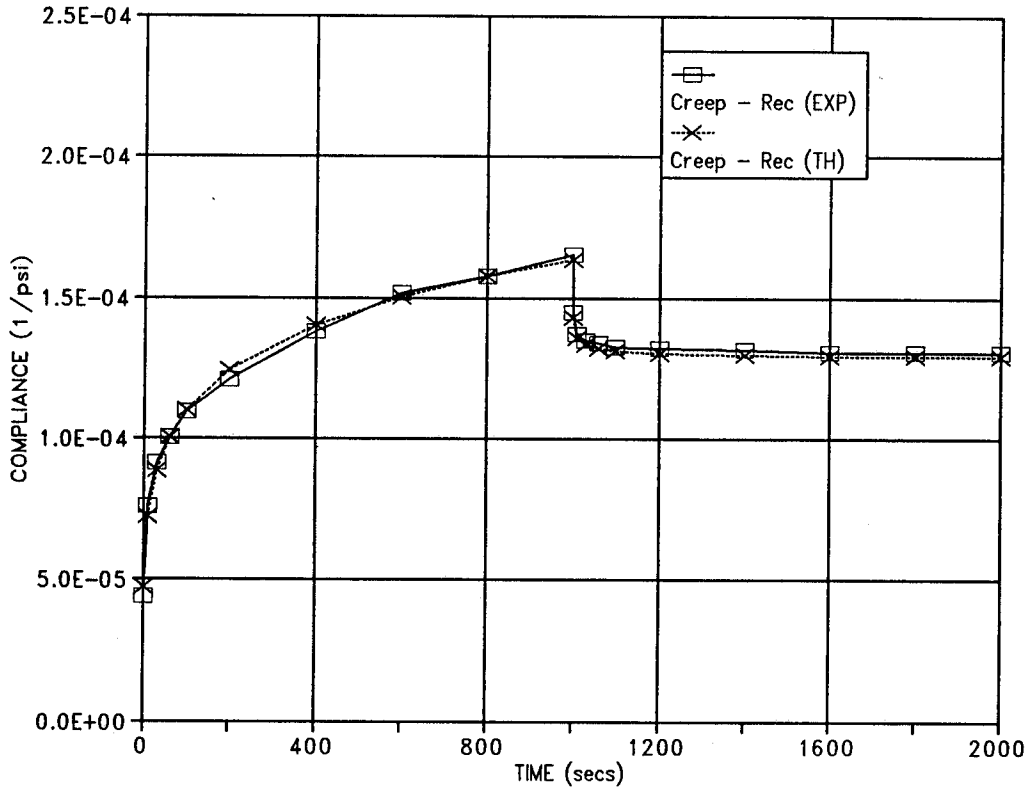

Figure C4. Typical Creep and Recovery Behavior of a Mix with 40% Natural Sand, 4.5% Air Voids, and Optimum Asphalt Content.